UNIVERSITY OF HAWAII
LIBRARY
APR 23 '52

The PHILOSOPHICAL MAGAZINE

FIRST PUBLISHED IN 1798

. 43 SEVENTH SERIES No. 338 March, 1952

A Journal of Theoretical Experimental and Applied Physics

EDITOR
PROFESSOR N. F. MOTT, M.A., D.Sc., F.R.S.

EDITORIAL BOARD
SIR LAWRENCE BRAGG, O.B.E., M.C., M.A., D.Sc., F.R.S.
SIR GEORGE THOMSON, M.A., D.Sc., F.R.S.
PROFESSOR A. M. TYNDALL, C.B.E., D.Sc., F.R.S.

PRICE 15s. 0d.
Annual Subscription £8 0s. 0d. payable in advance

AND PUBLISHED BY TAYLOR & FRANCIS LTD., RED LION COURT, FLEET ST., LONDON, E.C.4.

ADVANCES IN PHYSICS

A QUARTERLY SUPPLEMENT OF THE PHILOSOPHICAL MAGAZINE

On 1st January, 1952, the first number of this new Quarterly Supplement to the Philosophical Magazine was published. The aim of this Supplement will be to give those interested in physics comprehensive and authoritative accounts of recent important developments. It is felt by the Editor that in view of the rapid advances in many branches of physics, scientists will welcome a journal devoted to articles of this type.

VOLUME 1 APRIL 1952 NUMBER 2

Theories of Helium II. By Dr. R. B. Dingle (Cambridge University).

Wave Propagation and Flow in Liquid Helium II.
By Professor K. R. Atkins (University of Toronto, Canada).

Properties of Helium Three at Low Temperatures.
By Dr. J. G. Daunt (Ohio State University, U.S.A.).

Subject to alteration up to the time of going to Press

PRICE *per part* 15/- *plus postage* PRICE *per annum* £2 15s. 0d. *post free*

Editor: PROFESSOR N. F. MOTT, M.A., D.Sc., F.R.S.
Editorial Board: SIR GEORGE THOMSON, M.A., D.Sc., F.R.S.
PROFESSOR A. M. TYNDALL, C.B.E., D.Sc., F.R.S.
SIR LAWRENCE BRAGG, O.B.E., M.C., M.A., D.Sc., F.R.S.

Printed and Published by
TAYLOR & FRANCIS, LTD., RED LION COURT, FLEET ST., LONDON, E.C.4

XXI. *Magnetic Hysteresis in Superconducting Colloids*

By A. B. Pippard
Royal Society Mond Laboratory, Cambridge*

[Received November 2, 1951]

Abstract

The irreversible effects exhibited in the magnetization cycle of a superconducting colloid are analysed in terms of a simple model of a superconductor. Expressions are derived relating various critical field strengths to temperature and radius of the particle ; there is fair agreement between experiment and theory.

§1

Superconductors display under different conditions a somewhat bewildering variety of irreversible effects when subjected to cycles of magnetization and demagnetization. These may be classified into two main groups, those in which the Meissner effect is exhibited (i.e. complete expulsion of magnetic flux from the superconducting phase) and those in which it is not, and it is with the former group, the types of irreversibility characteristic of pure superconductors, that we shall be concerned here. These may be most simply described with reference to a long rod, of effectively zero demagnetizing coefficient, in a magnetic field parallel to its axis. Under ideal conditions, if the magnetic field H is increased from zero the rod remains superconducting, with the induction $B=0$, until the critical field H_c is attained, when it becomes normal and thereafter $B=H$; on lowering the field the Meissner effect occurs at the critical field and B once more becomes zero. The process of magnetization is then completely reversible, but in practice this ideal behaviour is rarely observed. The most striking, and most easily demonstrated, difference between real and ideal behaviour is the effect usually referred to as ‘ supercooling ’ ; if the field is lowered slowly from a value greater than H_c the normal state persists to fields less then H_c, and it is only at some lower field strength, which is critically dependent on the nature of the specimen, that the transition to the superconducting state occurs. The converse phenomenon of ‘ superheating ’, i.e. the persistence of the superconducting state in fields greater than H_c, is more difficult to demonstrate, and it is only recently that it has been shown unambiguously to occur in macroscopic samples (Garfunkel 1951). If the sample is not in the form of a long cylinder and has a non-vanishing demagnetizing coefficient the ideal reversible transition begins at a field less than H_c and proceeds through the intermediate state over a

---

* Communicated by the Author.

range of field strengths. It is now more difficult to discern whether superheating occurs, but it is probably observable in fairly thin cylinders in a transverse field under favourable conditions (Pippard 1950). On the other hand supercooling is still readily detectable, and is almost invariably observed in experiments on pure superconductors (e.g. Désirant and Shoenberg 1948).

If we turn now to much smaller samples, such as spherical colloidal particles, we find under certain circumstances much more pronounced irreversible effects, as is shown by Shoenberg's (1940) study of mercury colloids. The larger particles, of radius about 10^{-4} cm, show considerable supercooling, and probably superheating as well, for the area under the magnetization curve is somewhat larger than is to be expected (Pippard 1951). On the other hand, no hysteresis was observed with much smaller particles, of radius probably little more than 10^{-6} cm.

There is not really enough experimental evidence to allow the size-dependence of the irreversible effects to be described with certainty, but so far as can be seen the general features appear to be as follows. Spheres of radius less than about 5×10^{-6} cm show very little hysteresis ; as the size is increased hysteresis appears and becomes more and more marked until the radius is a few times 10^{-5} cm ; in this range of sizes the hysteresis is less near the transition temperature than at lower temperatures ; for larger particles and macroscopic samples the hysteresis is less, and at the same time becomes smaller at low temperatures than near the transition temperature. In the following sections we shall investigate the extent to which these observations are consistent with current views of the nature of the superconducting state.

§2

The extensive study by Faber (1952) of supercooling in macroscopic superconductors has elucidated the general features of the way in which the supercooled normal state breaks down. The superconducting phase is always initiated at one or more centres, where apparently superconducting nuclei are more readily formed, and the existence of super cooling argues the existence of a potential barrier which must be overcome before the nucleus can be created. Once a nucleus has been formed it may expand without further hindrance to convert the whole sample into the superconducting state. According to Faber the surface energy at the interface of normal and superconducting regions is largely responsible for the potential barrier, and his observation that super cooling is most pronounced near the transition temperature is consistent with the temperature variation of the surface energy, as deduced from studies of the intermediate state in small superconductors (Désirant and Shoenberg 1948).

Now it is likely (Ginsburg and Landau 1950 ; Pippard 1951) that this interphase surface energy is a consequence of the impossibility of a sharp phase-boundary ; in pure metals the transition layer between the two phases may be as wide as 10^{-4} cm. According to the views of the present author (Pippard 1951) this is a consequence of the long-range order exhibited by superconductors, which may be expressed in the following way. If we suppose the superconducting phase to be characterized by an internal parameter ω, the degree of order, which takes a non-vanishing value in the superconducting phase and is zero in the normal phase, then ω cannot vary at will from point to point, but only slowly, so that, for example, at a phase boundary in a pure superconductor it cannot drop to zero in a distance less than about 10^{-4} cm.

On this view it is clear that in a colloidal particle of diameter less than 10^{-4} cm the transition from one phase to the other cannot occur by the creation of a phase boundary, but must affect the whole particle at once. There is no very definite experimental evidence on this point since the measurements have necessarily been performed with an enormous number of particles simultaneously, and on account of the size-variation of the particles, if for no other reason, the measured transitions into the normal state are spread out. However the series of measurements by Shoenberg (1940) on mercury colloids of progressively greater uniformity lend some support to the hypothesis that the transition of a single particle is accomplished suddenly, without the appearance of the intermediate state. We therefore interpret the change in hysteresis behaviour which sets in at a particle size around 10^{-4} cm as associated with the possibility in larger particles of an appreciable variation of ω over the particle, or even the creation of a phase-boundary. No attempt will be made here to discuss magnetic hysteresis in the larger particles, and we shall confine the discussion to particles sufficiently small that it is reasonable to suppose ω to take the same value at all points.

§3

It is not difficult to see how hysteresis arises in the magnetic behaviour of these colloidal particles. In the absence of a magnetic field the Gibbs function, G, (which in this case is the same as the Helmholtz free energy) of such a particle may be supposed to depend, among other parameters, on ω and the temperature. For example, the dependence on ω at some given temperature may take the form of curve (*a*) in fig. 1, and the equilibrium value of ω is that corresponding to the minimum of G. Now in a magnetic field there will be a positive magnetic contribution to G, which will depend on the extent to which the magnetic field is excluded from the particle. Since we may expect that the penetration depth, λ, will be closely linked with ω, becoming infinite as ω tends to zero, the magnetic contribution to G will vary with ω somewhat as shown in curve (*b*) ; the larger the particle the steeper will be the initial rise, and the curve will flatten off as λ becomes small relative to the size of the particle. The Gibbs function itself is the sum of the two contributions, as shown in curve (*c*). The curves have been drawn to represent the state of affairs for such an applied field that the minimum of curve (*c*) at ω' has the same value as at the origin, that is, the superconducting state ($\omega' \neq 0$) is in thermodynamical equilibrium with the normal state ($\omega = 0$). However, under these conditions no transition between the states can occur, if we ignore the possibility of thermodynamical fluctuations, on account of the maximum of G between the minimum and the origin. In order to allow a transition from the superconducting into the normal state, the magnetic field must be increased, i.e. curve (b) must be scaled up in proportion to H^2, until the potential barrier disappears. Conversely, in order to allow a transition from the normal into the superconducting state the magnetic field must be reduced below the value corresponding to thermodynamical equilibrium. Thus under the conditions for which the diagrams have been drawn we should expect both superheating and supercooling to occur. This is exhibited diagrammatically in fig. 2, which shows the variation of G with ω for various values of H. The top curve is that which just allows a transition from superconducting to normal, and the bottom curve that which just allows the transition from normal to superconducting. From this diagram we can construct a curve showing how ω', the equilibrium value of ω in the superconducting state, varies with H. Such a curve is shown in fig. 3 in which the arrows distinguish the branches corresponding to increasing and decreasing fields. It is clear from this figure that there is a discontinuity in ω at both the superheated and the supercooled transitions.

Fig. 1

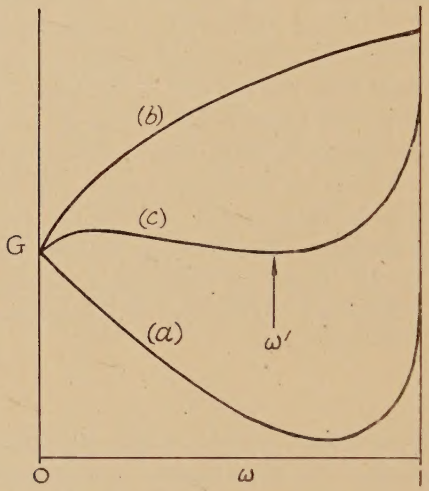

Gibbs function of small particle :
(a) in absence of field,
(b) field contribution,
(c) resultant curve for G.

If the particle is rather smaller, having dimensions comparable to λ_0, the penetration depth at 0° K, the field is only partially excluded for all values of ω, and the magnetic contribution to G follows a curve which rises much less steeply than fig. 1 (*b*). Under these conditions there may be no potential barrier to give rise to superheating and supercooling. This is illustrated in figs. 4 and 5, which are analogous to figs. 2 and 3, respectively.

Fig. 2

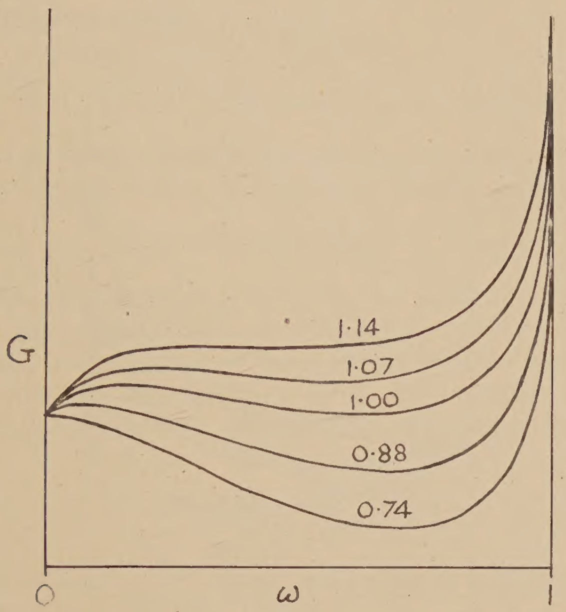

G versus ω for different values of H. The numbers attached to each curve are relative values of H.

Fig. 3

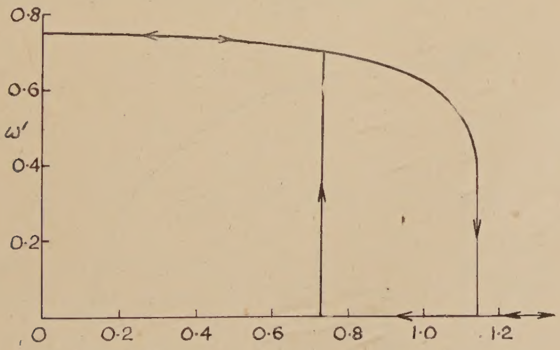

H (arbitrary units)
Variation of ω' with H, from fig. 2.

The equilibrium value ω' now is a continuous function of H, and no hysteresis is to be expected. Thus at any given temperature we should expect to find a critical size of particle below which no hysteresis is observed.

§ 4

After this qualitative discussion it is a simple matter to formulate the problem quantitatively. We shall suppose that for a given colloidal particle at a given temperature the free energy in zero field is a function of ω only ; i.e. $F=F(\omega)$, and that the magnetic susceptibility of the particle is also dependent only on ω. We may therefore write for the magnetic moment in a field H, $M=-2K(\omega)H$. The Gibbs function, $G(=F-MH)$, then takes the form

Fig. 4

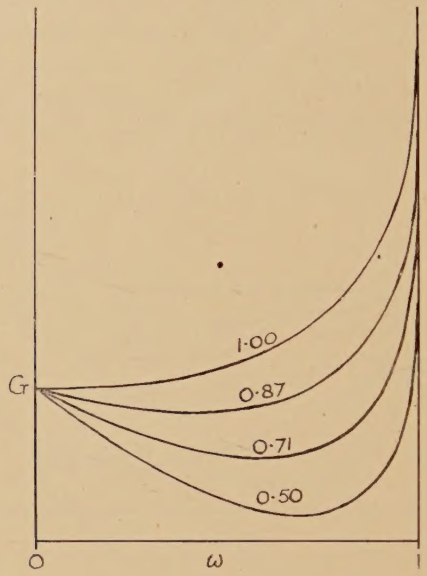

G versus ω for different values of H. The particle size is smaller than in fig. 2.

Fig. 5

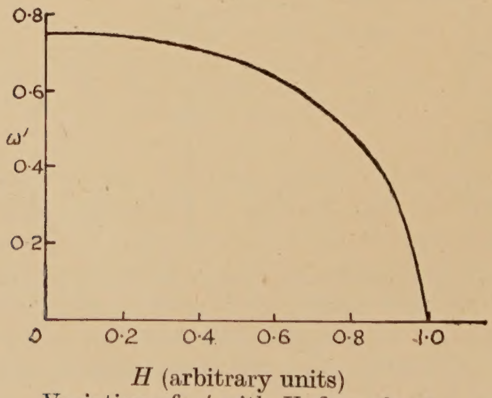

Variation of ω' with H, from fig. 4.

$$G(\omega,H)=F(\omega)+H^2K(\omega)\,. \qquad \qquad (1)$$

As stated before, ω' is determined by the condition $(\partial G/\partial\omega)_H=0$. We shall now derive expressions, in terms of F and K, for the three fields of particular interest, H_e the field at which the superconducting and normal phases are in equilibrium with one another from a thermodynamical point of view, H_{sh} the field at which superheating ceases, and H_{sc} the field at which supercooling ceases.

The field H_e is determined by the condition

$$G(\omega', H_e)=G(0, H_e)=F(0), \quad \text{since} \quad K(0)=0.$$

Now it is clear from fig. 2 that if H is less than H_e it is possible to find a value of ω, not the equilibrium value ω', such that the equation

$$G(\omega, H)=F(0) \quad . \quad . \quad . \quad . \quad . \quad . \quad . \quad . \quad . \quad . \quad (2)$$

is satisfied. On the other hand, if $H>H_e$, no solution of the equation is possible, since the minimum at ω' corresponds to a higher value of G than $F(0)$. Thus H_e is the largest value of H for which a solution of (2) is possible, and consequently, from (1), H_e^2 is the maximum value that can be taken by the function $[F(0)-F(\omega)]/K(\omega)$. We may write this result in the form

$$H_e^2=\operatorname*{Max}_{0\leqslant\omega\leqslant1}\left\{\frac{F(0)-F(\omega)}{K(\omega)}\right\}. \quad . \quad . \quad . \quad . \quad . \quad (3)$$

If the analytical forms of F and K are known it is a simple matter to compute H_e from this formula.

A similar expression for H_{sh} may be obtained immediately, since it is clear from fig. 2 that H_{sh} is the greatest field for which the curve of G exhibits a horizontal gradient at any point. Thus H_{sh} is the largest field for which a solution is possible of the equation

$$\frac{dF}{d\omega}+H^2\frac{dK}{d\omega}=0,$$

and consequently

$$H_{sh}^2=\operatorname*{Max}_{0\leqslant\omega\leqslant1}\left\{-\left(\frac{dF}{d\omega}\right)\Big/\left(\frac{dK}{d\omega}\right)\right\}. \quad . \quad . \quad . \quad . \quad . \quad (4)$$

Finally we may observe from fig. 2 that H_{sc} is the field for which the curve of G exhibits a horizontal gradient when $\omega=0$. Hence, from (1),

$$H_{sc}^2=-\left[\left(\frac{dF}{d\omega}\right)\Big/\left(\frac{dK}{d\omega}\right)\right]_{\omega=0}. \quad . \quad . \quad . \quad . \quad . \quad (5)$$

It should be realized, of course, that the functions F and K in fact depend on temperature and on the size and shape of the particle as well as on ω, though only ω is variable in any given experiment. The relative values of H_e, H_{sh} and H_{sc} therefore depend on a variety of conditions, and in suitable circumstances they may coincide. No magnetic hysteresis would then be observed, and this is the case illustrated in fig. 4.

§5

In order to estimate the extent of the hysteresis to be expected under any given conditions it is necessary to choose suitable forms for the functions $F(\omega)$ and $K(\omega)$. At present the theory of superconductivity is not sufficiently advanced for it to be possible to say whether the general assumptions of § 4 are likely to be justified, so that there is no certainty that the problem can indeed be formulated in terms of these two functions. Still less is it possible to state the forms of F and K. However, one phenomenological theory has been proposed by Gorter and Casimir (1934), which exhibits some of the thermodynamical properties of superconductors in an idealized form. In this theory, ω is interpreted as the fraction of electrons which are in a superconducting condition, and the free energy per unit volume, in the absence of a field, is written in the form

$$f=-\frac{H_0^2}{8\pi}[\omega+2t^2\sqrt{(1-\omega)}],$$

where H_0 is the critical field at 0° K of a massive specimen, and t is the reduced temperature, T/T_c. Thus for a spherical specimen of radius a,

$$F=-\tfrac{1}{6}a^3H_0^2[\omega+2t^2\sqrt{(1-\omega)}]. \qquad (6)$$

It has been found (Daunt, Miller, Pippard and Shoenberg 1948) that if the interpretation of ω as the fraction of superconducting electrons be used to predict the temperature variation of the penetration depth λ, by writing $\lambda=\lambda_0/\sqrt{\omega}$, λ_0 being the penetration depth at 0° K, then the prediction is in good accord with experimental data so far as the latter go. If then we assume the London penetration law the form of $K(\omega)$ may be derived immediately. For example, for a sphere of radius a (London 1936)

$$K=\frac{a^3}{4}\left(1-\frac{3}{\alpha\sqrt{\omega}}\coth(\alpha\sqrt{\omega})+\frac{3}{\alpha^2\omega}\right), \qquad (7)$$

where $\alpha=a/\lambda_0$.

Using eqns. (6) and (7) we may now give analytical form to the expressions (3), (4) and (5) for the characteristic field strengths, H_e, H_{sh} and H_{sc} :

$$\left(\frac{H_e}{H_0}\right)^2=\frac{2}{3}\operatorname*{Max}_{0\leqslant\omega\leqslant1}\left\{\frac{\omega-2t^2[1-\sqrt{(1-\omega)}]}{1-(3/\alpha\sqrt{\omega})\coth(\alpha\sqrt{\omega})+(3/\alpha^2\omega)}\right\}, \qquad (8)$$

$$\left(\frac{H_{sh}}{H_0}\right)^2=\frac{4\alpha^2}{9}\operatorname*{Max}_{0\leqslant\omega\leqslant1}\left\{\omega^2\frac{1-t^2/\sqrt{(1-\omega)}}{\alpha\sqrt{\omega}\coth(\alpha\sqrt{\omega})+\alpha^2\omega\,\mathrm{cosech}^2(\alpha\sqrt{\omega})-2}\right\}, \qquad (9)$$

$$\left(\frac{H_{sc}}{H_0}\right)^2=\frac{10}{\alpha^2}(1-t^2). \qquad (10)$$

A typical example of the variation with temperature of these characteristic fields is shown in fig. 6, which has been computed for α equal to 3, i.e. a spherical particle whose radius is $3\lambda_0$. It will be seen that the hysteresis becomes less marked as the temperature is raised, and that for values of t greater than 0·88 the transition is reversible. The variation with α of the temperature, t', above which no hysteresis should be observed, may be deduced explicitly from (8), since, according to § 2, it is only below t' that ω', the equilibrium value of ω, is different from zero in a field H_e. Hence if we put $t=t'$ in (8) and expand the quantity in brackets as a series in ω, the desired relation between t' and α is obtained by equating to zero the coefficient of the term in ω, since this ensures that the right hand side just achieves its maximum value when $\omega=0$. Performing this expansion we find that (8) takes the form

$$\left(\frac{H_e}{H_0}\right)^2=\frac{10(1-t^2)}{\alpha^2}\operatorname*{Max}_{0\leqslant\omega\leqslant1}\left\{1-\left(\frac{t^2}{4(1-t^2)}-\frac{2\alpha^2}{21}\right)\omega-\dots\right\}.$$

Fig. 6

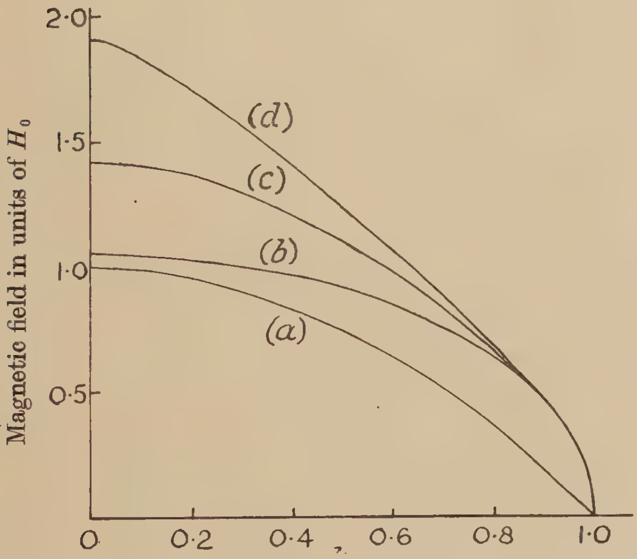

Critical fields versus reduced temperature :
(*a*) H_c for bulk material,
(*b*) H_{sc} for colloidal sphere of radius $3\lambda_0$,
(*c*) H_e for colloidal sphere of radius $3\lambda_0$,
(*d*) H_{sh} for colloidal sphere of radius $3\lambda_0$.

Hence

$$\frac{t'^2}{4(1-t'^2)}-\frac{2\alpha^2}{21}=0,$$

or

$$\alpha^2=\frac{21t'^2}{8(1-t'^2)}. \qquad \qquad (11)$$

Under these conditions $(H_e/H_0)^2=[10(1-t'^2)]/\alpha^2$, which has the same form as (10), so that, as expected, there is no supercooling. A similar expansion of (9) yields the result that the superheating also just vanishes at this temperature.

Inspection of (11) shows at once that there is no size of particle, however small, for which some hysteresis should not be observed at a sufficiently low temperature. This temperature may, however, be so low as to lie outside the convenient experimental range. For example, the value of α for Shoenberg's (1940) smallest colloid preparation was about 0·35, so that, from (11), we should expect t' to be about 0·21, corresponding to a temperature of 0·87° K. It is therefore not surprising that no hysteresis was observed at temperatures above 1° K.

§6

The experiments of Shoenberg are the only ones so far performed on spherical particles, and therefore susceptible of comparison with the above results. It is a simple matter to modify the theory to apply to thin films, for which there is more information, but it is unlikely that any films have yet been studied which have been so uniform as to make detailed comparison with theory worth while, and, as has been discussed elsewhere (Pippard 1951), it is possible that the magnetic behaviour of films is explicable in terms of phase-boundary formation rather than a homogeneous transition of the type dealt with here. We shall therefore attempt a comparison of theory and experiment only for spherical particles.

The smallest colloidal particles studied by Shoenberg had diameters less than λ_0 and showed no hysteresis. This we found in the last section to be in accordance with the theory. It is not, however, a very convincing test of the theory, which can be more critically assessed on its predictions concerning the hysteresis of larger spheres. Unfortunately no detailed data are available for Shoenberg's preparation Hg B, which showed greater hysteresis at lower than at higher temperatures, as the theory predicts, while Hg C, in which the particles were probably rather larger, shows the greatest hysteresis at the higher temperatures. This suggests that the particles are now large enough to allow ω to vary from point to point, and their behaviour is therefore not directly comparable with our theory. Nevertheless a rough comparison is possible ; for the condition we have laid down, that ω shall be constant, is an extreme condition, and the hysteresis observed should not exceed that predicted by theory if an alternative mechanism for the transition exists.

We may estimate the mean value of α for the preparation Hg C4 from the fact that at the lowest temperatures the ratio χ/χ_0 of the measured susceptibility to that appropriate to perfect diamagnetism was 0·50. This means that

$$1-\frac{3}{\alpha}\coth\alpha+\frac{3}{\alpha^2}=0{\cdot}50,$$

or

$$\alpha=4{\cdot}75.$$

According to (11), then, we should expect no hysteresis for values of t greater than 0·945, that is, at temperatures above 3·94° K. Yet experimentally it was found that at 3·883° K the hysteresis was very great, the ratio H_{sh}/H_{sc} being nearly 3 ; at this temperature eqns. (9) and (10) predict a ratio of only 1·03.

This striking discrepancy may reveal the inadequacy of the theoretical model, but another interpretation is conceivable, namely, that the estimate of the amount of mercury present in the preparation Hg C4 was seriously in error, and that in fact χ/χ_0 was considerably greater than 0·50. There are two pieces of evidence which favour this view. First, if we take $\alpha=4{\cdot}65$ and $\lambda_0=4{\cdot}3\times10^{-6}$ cm, the value determined by Laurmann and Shoenberg (1949), the mean radius of the particles becomes 2×10^{-5} cm, while a microscopic examination of the preparation suggested that it was about 10^{-4} cm. Secondly, if the penetration depth varies with temperature according to the law,

$$\lambda=\lambda_0(1-t^4)^{-\frac{1}{2}}, \qquad \ldots\ldots\ldots \qquad (12)$$

which describes the experimental results both for macroscopic specimens and for the smallest colloid preparation (*see* Laurmann and Shoenberg 1949 ; Daunt, Miller, Pippard and Shoenberg 1948), the susceptibility of a preparation for which $\alpha=4{\cdot}65$ should decrease by a factor 2·1 between 0° K and 3·883° K, while the measured decrease was only by a factor 1·24. This discrepancy may be accounted for if we assume that the mercury present in the preparation was only about 0·62 of the estimated amount, and that in consequence χ/χ_0 at 0° K was 0·8 rather than 0·5. The drop by a factor 1·24 between 0° K and 3·883° K is then consistent with (12). Moreover, the value of α is now raised to 15, corresponding to a mean radius of $6{\cdot}5\times10^{-5}$ cm, which is much closer to the microscopic estimate. It is not immediately obvious that such a gross error in the chemical estimation of the mercury content of the preparation could have arisen. Perhaps a substantial proportion was present not in the form of metallic mercury but as oxide, either on the surface of the particles or as detached fragments, which would not become superconducting but would be estimated in the chemical analysis.

If this interpretation is correct, the discrepancy between experiment and theory is much less, as is shown by the comparison in the table, for which H_{sh} and H_{sc} were calculated taking $\alpha=15$ and $H_0=410$ gauss.

T°K	H_{sh} calc.	H_{sh} obs.	H_{sc} calc.	H_{sc} obs.
1·935	690	410	77	210
3·883	75	75	31	28

The observed values of H_{sh} and H_{sc} have been taken as those field strengths at which about one half of the material had made the transition. The good agreement between theory and experiment at the higher temperature is probably largely fortuitous, in view of the doubtful interpretation of the experimental results. At the lower temperature agreement is not nearly so good, but at least the disagreement is in the right direction, the observed hysteresis being less than the predicted. It is quite possible that the hypothesis made in § 2, that ω is constant over the particle, begins, as the particle size is increased, to break down at the lower temperatures first, since the observed temperature variation of the interphase surface energy indicates that the range of order is smaller at lower temperatures. Thus one might expect the comparison of theory and experiment to give results similar to those in the table.

It would be unwise, however, on the basis of so little experimental material to claim more than qualitative validity for the theory. A much better check could be obtained from experiments with particles for which α was about 3, so that hysteresis should, according to (11), be observed at the lower but not at the higher temperatures, as illustrated in fig. 6. Such experiments, if they gave results in conflict with the theory, might serve a useful purpose in suggesting a possible form for the dependence of the free energy on the degree of order, ω, if indeed the thermodynamics of a superconductor may be formulated in so simple a way.

REFERENCES

DAUNT, J. G., MILLER, A. R., PIPPARD, A. B., and SHOENBERG, D., 1948, *Phys. Rev.*, **74**, 892.

DÉSIRANT, M., and SHOENBERG, D., 1948, *Proc. Roy. Soc.* A, **194**, 63.

FABER, T. E., 1952, to be published shortly.

GARFUNKEL, 1951, see *Proc. International Conf. on Low Temperature Phys.* (Oxford 1951), p. 117.

GINSBURG, V. L., and LANDAU, L., 1950, *J. Exp. & Theor. Phys.*, **20**, 1064.

GORTER, C. J., and CASIMIR, H. B. G., 1934, *Z. Tech. Phys.*, **12**, 539.

LAURMANN, E., and SHOENBERG, D., 1949, *Proc. Roy. Soc.* A, **198**, 560.

LONDON, F., 1936, *Physica*, **3**, 450.

PIPPARD, A. B., 1950, *Proc. Roy. Soc.* A, **203**, 210 ; 1951, *Proc. Cam. Phil. Soc.* **47**, 617.

SHOENBERG, D., 1940, *Proc. Roy. Soc.* A, **175**, 49.

XXII. *The Angular Distribution of Neutrons produced in Beryllium by* 170 MEV *Protons*

By M. SNOWDEN
Atomic Energy Research Establishment, Harwell*

[Received November 15, 1951]

ABSTRACT

The angular distribution of high energy neutrons produced by bombarding a beryllium target with the 170 MEV proton beam of the Harwell cyclotron has been measured. The angular spread for neutrons with energies greater than 50 MEV was found to be 67° at half intensity and in this spread the higher energy neutrons were shown to be confined to the smaller angles. The total cross section for the production of neutrons with energies greater than 50 MEV was found to be $99 \pm 40 \times 10^{-27}$ cm^2, while the differential cross section at 4° was $69 \pm 30 \times 10^{-27}$ cm^2/steradian.

§1. INTRODUCTION

THE angular distribution of high energy neutrons produced by 340 MEV protons has been measured for angles up to 27° to the forward direction and for various target materials by Miller, Sewell and Wright (1951). In this work the relative numbers of neutrons were indicated by the ^{11}C positron activity induced in polythene discs exposed to the neutron beam. De Juren (1951) made similar measurements by recording fissions in bismuth. The excitation functions for these reactions are not exactly known but they certainly differ in shape; moreover, the threshold energy for the carbon reaction is about 20 MEV whereas the fission of bismuth is not detectable below 50 MEV. Consequently the very similar results obtained in the two experiments indicate that at 330 MEV the angular distribution is not strongly dependent upon neutron energy.

It was thought worthwhile to extend this work using the 170 MEV protons accelerated by the Harwell cyclotron. A beryllium target was used and the neutrons produced were detected with a recoil proton telescope (Hadley *et al.* 1949). An absorber was used to vary the threshold of detection and the response as a function of neutron energy calculated with the help of the Berkeley experimental data on n–p scattering (Christian and Hart 1950). Owing to the complication of this method of measurement it was only convenient to make measurements at a few different angles.

During this work the opportunity was taken to redetermine the cross section for neutron production in beryllium and the result is included.

---

* Communicated by the Author.

§2. Apparatus

The experimental arrangement of fig. 1 was used. There were six collimating holes in the main 6 ft. thick concrete shielding wall *W*. The axis of hole No. 6 was tangential to the orbit of radius 48·5 in., but the axes of holes 1–5 intersected such tangents at angles of 4°, 26°, 40°, 51° and 60° respectively. A monitor target *D* was aligned for hole No. 6 and the neutron intensity in the forward direction from this target was measured in the double coincidence telescope *M*. The beryllium target *B*, 0·352 in. thick, was aligned with one of the holes 1–5 while the other four were blocked with brass absorbers. The neutrons which emerged at this angle to the forward direction passed through a thin aluminium window *N* in the cyclotron tank and were then recorded in the triple coincidence telescope *T*. The front collimating block *F* was also aligned with the particular collimating hole in use.

Fig. 1

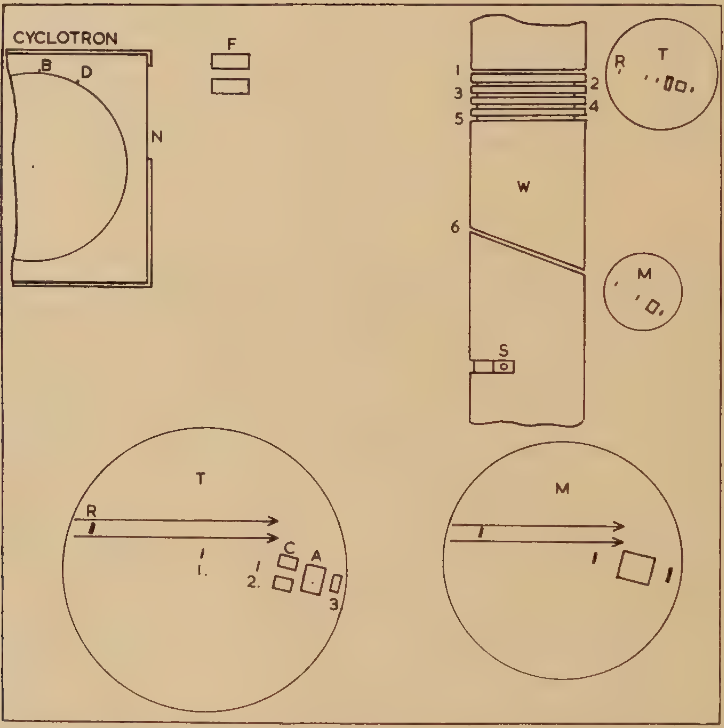

In addition a measure of the integrated neutron output from the cyclotron during any particular run was obtained from the counts recorded by a slow neutron counter placed in a recess in the shielding wall at *S*.

The neutrons emerging from the 5·3 cm diameter collimator hole were allowed to strike a polythene disc *R*, 9 mm thick and 5 cm diameter, which had been set up on the axis of the collimator. Three scintillation counters were used to detect the protons ejected from the polythene disc at an angle of 12° to the forward direction. Counters 1 and 2 were identical and used clear naphthalene crystals 3 cm square and 3·2 mm thick, whereas counter 3 used a larger crystal 4·8 cm diameter and 2·5 cm thick. A carbon absorber *A* could be placed between counters 2 and 3 to set the minimum energy of the protons detected. Taylor's (1950) results for the range energy relation in carbon were used. The solid angle subtended at the radiator by the telescope was defined by the 2·45 cm hole in a 4 cm long copper block *C* placed immediately after counter 2. Only protons traversing this hole reached the absorber *A* and counter 3. The monitor channel was similar but used only two scintillation counters and was set for a threshold proton energy of 90 MeV.

§ 3. EXPERIMENTAL METHOD

Tests were first performed to determine that every proton traversing the three counters of the measuring telescope was registered as a triple coincidence. Similar tests were made in the monitor channel. The measuring telescope was then set to a particular threshold energy and the counting rates obtained at each hole collated with the help of the monitor channel. This experiment was repeated for several threshold energies. In practice some of the recoil protons failed to reach the third counter due either to nuclear absorption or scattering in the absorber. The correction for this effect was determined by an experiment in the external proton beam of the cyclotron. It was found that the correction for a particular absorber depended on the incident proton energy. To apply the correction, therefore, a rough knowledge of the incident proton spectrum was required and this was obtained from the data already recorded for each neutron angle. The corrections varied from 10% for the lowest threshold energy to 40% for the highest threshold energy. The Berkeley results for *n–p* scattering were then applied to the corrected proton data to give the incident neutron intensities.

§ 4. RESULTS

In fig. 2 the angular distribution of neutrons is drawn for several different values of the threshold neutron energy. The curves are normalized to unity for the forward direction and the angles in the laboratory system are plotted as abscissae. For neutrons of energy greater than 50 MeV the full angular spread at half intensity is 67°. The higher energy neutrons are confined to the smaller angles, which is the result to be expected if they are produced by interaction of the incident proton with a single nucleon within the nucleus.

The curve for the lowest threshold neutron energy was integrated and the effective proton current estimated from the results of Cassels, Dickson and Howlett (1951). Hence the total cross section for the production in beryllium of neutrons with energies greater than 50 MeV was found to be $99 \pm 40 \times 10^{-27}$ cm^2. The differential cross section at 4° was found to be $69 \pm 30 \times 10^{-27}$ cm^2/steradian in reasonable agreement with the value of $99 \pm 19 \times 10^{-27}$ cm^2/steradian obtained earlier by Cassels, Randle, Pickavance, and Taylor (1951).

ACKNOWLEDGMENTS

The author wishes to thank the cyclotron operating crew for co-operation and Mr. D. Salter for his help in taking measurements. He is also indebted to Dr. T. G. Pickavance and other colleagues in the cyclotron group for their interest and advice. This paper is published by permission of the Director of the Atomic Energy Research Establishment.

Fig. 2

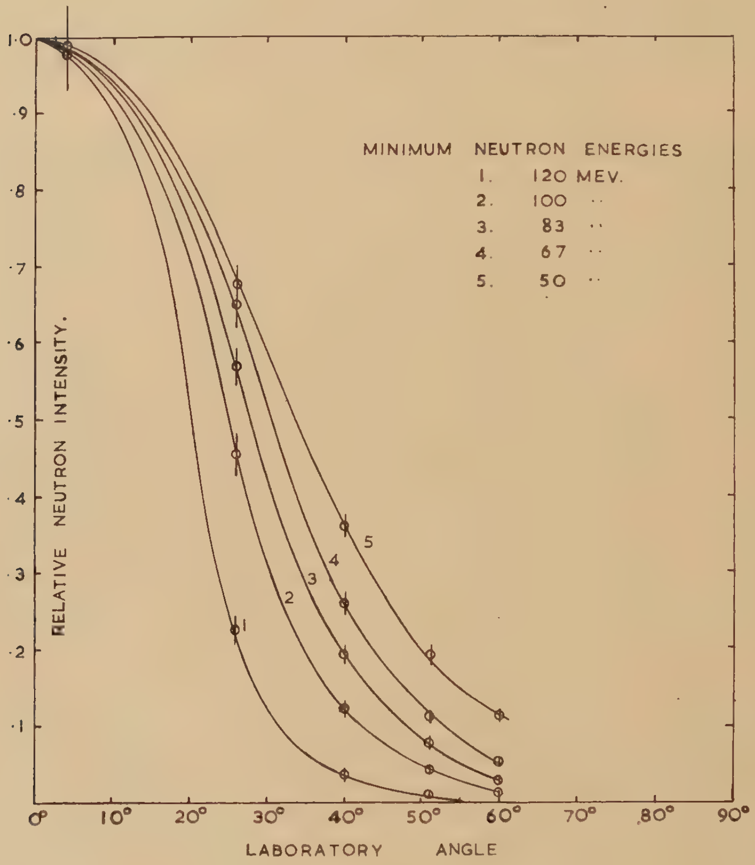

REFERENCES

CASSELS, J. M., DICKSON, J. M., and HOWLETT, J., 1951, *Proc. Phys. Soc.* B, **64**, 590.
CASSELS, J. M., RANDLE, T. C., PICKAVANCE, T. G., and TAYLOR, A. E., 1951, *Phil. Mag.*, **42**, 215.
CHRISTIAN, R. S., and HART, E. W., 1950, *Phys. Rev.*, **77**, 441.
DE JUREN, J., 1951, *Phys. Rev.*, **81**, 458.
HADLEY, J., KELLY, E., LEITH, C., SEGRÈ, E., WIEGAND, C., and YORK, H., *Phys. Rev.*, **75**, 351.
MILLER, R. D., SEWELL, D. C., and WRIGHT, R. W., 1951, *Phys. Rev.*, **81**, 374.
TAYLOR, A. E., 1950, *Phil. Mag.*, **41**, 966.

XXIII. *The Dependence of Photographic Sensitivity on Temperature*[*]

By G. C. FARNELL
Research Laboratories, Kodak Ltd., Wealdstone, Harrow, Middlesex[†]

[Received November 19, 1951]

ABSTRACT

A preliminary survey is first presented of the factors which have been suggested to account for the generally observed decrease in sensitivity of a photographic emulsion on lowering its temperature to that of liquid nitrogen. It is concluded that the main problem to be resolved is whether, after due allowance for the decreased absorption of the halide, the observed speed loss can be completely assigned to the effective high intensity reciprocity failure of the low temperature exposure, or whether some additional mechanism of exposure wastage comes into play. Experiments are then described, the results of which show that for a range of emulsions the observed speed loss on passing from room to liquid nitrogen temperature can be quantitatively accounted for in terms of decreased absorption of the halide and the fact that low temperature exposures are essentially of very high intensity. The fluorescence of bromo-iodide emulsions whilst undergoing a low temperature latent-image exposure is apparently not connected with the speed loss, but is merely a visual manifestation of the recombination which is occurring in an unobservable manner at room temperature. Finally the results of other investigators are discussed in the light of the new findings; several pieces of evidence emerge which confirm their generality.

§1. INTRODUCTION

THE results of experiments on the influence of temperature on photographic phenomena have provided confirmation of the validity of the fundamental hypotheses of latent-image theory now generally accepted. These were first clearly enunciated by Gurney and Mott, and state that latent-image formation takes place in two steps, namely, the release and subsequent trapping of an electron from a halide ion of the photographic grain, followed by neutralization by a silver ion, the process being repeated several times in order to form a silver speck capable of promoting development (Gurney and Mott 1938).

It is not difficult to explain how a latent image can be formed as the result of an exposure at low temperatures (e.g. liquid nitrogen, 77° K), but considerable uncertainty has persisted as to the factors which come into play in order that the sensitivity of a non-dye sensitized emulsion be reduced to about a tenth of its room temperature sensitivity (Sheppard, Wightman and Quirk 1934, Webb and Evans 1938, Berg 1939). An investigation of these factors was the purpose of the work now being reported.

---

[*] Communication No. 1407–H from the Kodak Research Laboratories.

[†] Communicated by the Author.

Anticipating the conclusions to be drawn from the experimental results it has been found that for all emulsions examined the fall in sensitivity on proceeding from room to liquid nitrogen temperature can be accounted for in terms of the decrease in absorption coefficient of the silver halide, and the fact that, from the point of view of the behaviour of the emulsion, low temperature exposures are effectively of very high intensity. In order to bring out the precise aim of the experiments performed and the meaning of the results, it is first necessary to review briefly previous suggestions as to why the sensitivity of a photographic emulsion is in general observed to decrease on temperature reduction.

§2. PRELIMINARY SURVEY

The most obvious effect of temperature variation is an alteration in the absorption coefficient of the silver halide of an emulsion. Toy and Harrison have shown that the absorption coefficient of pure silver bromide for the wavelengths of 4350 A, 4047 A and 3650 A falls by a factor of three on reduction of temperature from 20° C to −180° C (Toy and Harrison 1930). From the results of direct absorption measurements on photographic emulsions by Biltz it can be deduced that the speed of a pure bromide emulsion to tungsten radiation should be reduced by about 0·5 log E units on lowering the temperature from room to liquid nitrogen (Biltz 1949). For a bromo-iodide emulsion containing about 5 mol. per cent of silver iodide the corresponding speed loss should be about 0·4 log E units (Biltz 1951).

A second suggestion, stimulated by the nature of experimental results pertaining to the phenomenon of high intensity reciprocity failure, was that low temperature exposures were essentially of very high intensity. Berg has shown that at room temperature the reciprocity failure curve of an emulsion becomes flat below a time of 4×10^{-5} seconds, i.e. below this time the emulsion demonstrates a constant high intensity failure speed loss (Berg 1940). On lowering the temperature of the emulsion this flat portion of the reciprocity failure curve commences at longer exposure time. At liquid nitrogen temperature emulsions do not show any reciprocity failure (Berg 1939), and it is reasonable to suppose that the observed flat reciprocity failure 'curve' is merely the flat high intensity portion observable at room temperatures shifted to cover the whole range of normal exposure times. If this view is correct the speed loss observed on passing from room to liquid nitrogen temperature, if measured from the optimum of the room temperature reciprocity failure curve, will contain a component representing the speed loss which ensues on passing from the optimum to the exposure level at which the reciprocity failure curve flattens out, and which should in theory be capable of measurement at room temperature.

The general opinion to be derived from the literature on the subject of low temperature sensitivity is that decrease of absorption coefficient and effective high intensity reciprocity failure are insufficient to account for the observed loss of speed on temperature reduction (Berg 1948). It has always been assumed that some other mechanism of exposure wastage comes into play. The observation by Meidinger that bromo-iodide emulsions fluoresced strongly at liquid nitrogen temperature appeared to provide an explanation of the extra speed loss (Meidinger 1939). It was supposed that the number of electrons lost by recombination at low temperatures was greater than the number lost at room temperature, this loss being manifested by the fluorescence of the halide. Alternatively it could be said that no electrons were lost in a grain at room temperature, while some were lost at low temperatures. It has been observed by Farnell and Burton (1951) that a bromo-iodide emulsion fluoresces with the characteristic green colour of silver bromo-iodide (Meidinger 1939, Farnell, Burton and Hallama 1950) during a latent-image exposure to ultra-violet radiation. On the other hand it was not proved that this observed recombination was either merely a visual manifestation of that occurring at ordinary temperatures, or that it represented additional recombination over that occurring at room temperature.

Fig. 1

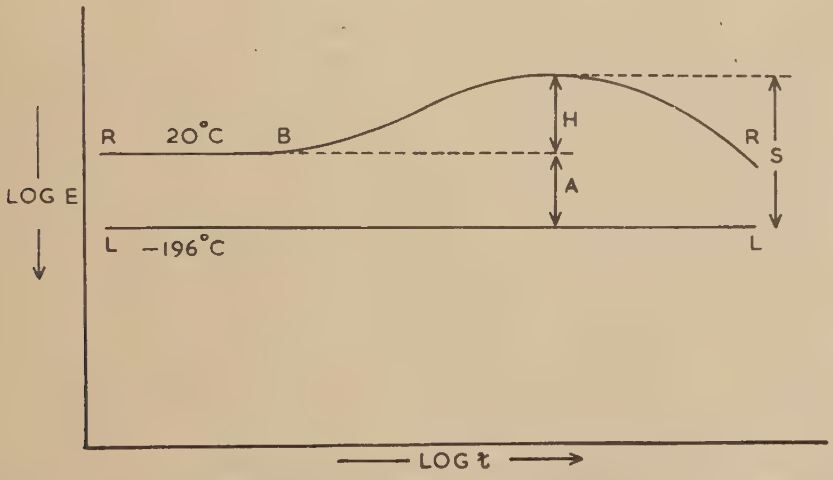

Illustration of the interrelation between room- and low-temperature sensitivity in terms of a reciprocity-failure diagram. *RBR* is the room temperature reciprocity-failure curve. The total speed loss, *S*, is equal to the total high-intensity failure, *H*, plus the quantity, *A*, which may represent reduced absorption alone, or may include a factor covering increased recombination.

The general situation regarding the loss of speed observed on temperature reduction as outlined in this survey may be conveniently summarized in diagrammatic form as illustrated in fig. 1. *RBR* is the reciprocity failure curve of an emulsion at ordinary temperatures, the point B representing the 'bend over' point first observed by Berg. LL is the 'reciprocity failure curve' of the emulsion at low temperatures, which may be regarded as a portion of RB shifted downwards by decrease in absorption, and possibly by increased recombination, and to longer times. The total log speed loss (S) from the room temperature optimum, is thus composed of the high intensity failure portion (H), plus a portion A which may be due to a fall in absorption alone, or may in addition contain a factor representing increased recombination at the low temperature.

§3. PRINCIPLE OF THE EXPERIMENTS

It will be appreciated from the previous discussion that the problem to be resolved in the field of low temperature sensitivity is whether, after allowance has been made for decreased absorption, the effective high intensity reciprocity failure of a low temperature exposure is sufficient to account for the observed speed loss, or whether other forms of exposure wastage come into play, for instance, increased recombination. The obvious experimental approach is to determine the total speed loss from the room-temperature optimum to a low-temperature exposure, and compare it with the sum of the total speed loss due to high-intensity failure (from the optimum to the bend-over point) and the speed loss due to fall in absorption. If the total loss exceeds the sum of the latter effects then it is reasonable to suppose that some additional mechanism of exposure wastage is coming into play. It is to be noted that this approach is determined by experimental facts, and the results will be valid whatever the explanation of high-intensity reciprocity failure and the bend-over point.

In practice several deviations from the above scheme were made in order to overcome experimental difficulties. For instance, it is impossible in the present state of our knowledge to calculate precisely the speed variation due to change in absorption of an emulsion for a band of wavelengths in the visible region, as is employed in exposures to tungsten radiation. This difficulty was largely resolved by making exposures to mercury 3650 A radiation, which was absorbed to the extent of about 99% at ordinary temperature and 95% at low temperatures, with the result that observed speed losses on temperature reduction were essentially due to causes other than change of absorption. Some quantitative data on this topic will be presented later. The smaller dependence of sensitivity on temperature at short wavelengths has been demonstrated by Webb (Webb 1935).

A second difficulty was that the shortest exposure time possible with the available reciprocity sensitometer was only $1{\cdot}58\times10^{-4}$ sec, which is more than ten times longer than the bend-over time at ordinary temperatures. But since the high-intensity portion of the reciprocity failure curve is shifted approximately $0{\cdot}6 \log t$ units towards longer times for a decrease in temperature of 10°, it was a simple matter to record exposures at and beyond the bend-over point when the emulsion was at the temperature of solid carbon dioxide (−78·5° c). Details of the experimental technique and emulsions employed will now be presented.

§4. Experimental Details and Techniques

4.1. *Apparatus and Exposure Technique*

A reciprocity sensitometer, with the normally fitted plateholder removed, was employed to give step wedge exposures to 6 in. × 1 in. strips of film clipped on the inside wall of a Pyrex Dewar flask. Comparative exposures of a particular emulsion were made with the flask empty and full of liquid nitrogen, the exposure at room temperature being made at the optimum of the previously determined reciprocity failure curve. It was sometimes impossible to do this with the fairly low intensity of ultra-violet radiation available, and so the results were adjusted to the optimum from the reciprocity-failure curve. The strips of film were backed by a stout strip of plastic to prevent them buckling at the low temperature.

Extraneous radiation was prevented from reaching a strip undergoing exposure by sheathing the Dewar flask in black paper, except for an exposure slot of dimensions slightly larger than the step wedge.

Reciprocity failure curves at the temperature of solid carbon dioxide (−78·5° c) were obtained by exposing strips in a similar manner to that used at liquid nitrogen temperature. Cooling was achieved by immersing strips in the Dewar flask full of ethyl or methyl alcohol with the lower half occupied by lumps of solid carbon dioxide. It was proved by several control experiments that immersion in alcohol had no influence whatsoever on the sensitivity of the emulsions employed.

At least two strips, and quite often four, were exposed in order to obtain any particular characteristic curve ; in all cases good reproducibility was obtained. The ordinary lamps of the sensitometer were employed for tungsten radiation exposures. A mercury 125 w high-pressure arc with a Wratten 18A filter was employed to give ultra-violet exposures predominantly of wavelength 3650 a.

4.2. *Emulsions*

In order that emulsions could be examined at different stages of sensitivity, as determined by their preparation, and free from impurities normally present in commercial emulsions, work was confined to simple experimental emulsions. The basic halide compositions were pure silver bromide and silver bromide + 5 mol. per cent silver iodide, ripening being carried out in excess halide solution. Details of emulsion preparation, together with the reference letters employed in this paper, are given in table 1. None of the emulsions were colour sensitized.

4.3. *Development*

Since the aim of this work was to achieve some form of general result no particular attention was paid to the type of development employed. Bromo-iodide emulsion strips were developed for 16 min in Kodak D19b developer (and occasionally for shorter times), and pure bromide strips for 5 min or 6 min. All the emulsions, with the exception of I (sulphur sensitized) formed predominantly internal image. Because of this fact no complications due to solarization appear to have been encountered.

§5. RESULTS, DISCUSSION AND CONCLUSIONS

5.1. *Absorption Change on Temperature Reduction*

The aim in this section is to show that from the recordings of room- and low-temperature characteristic curves to tungsten and ultra-violet radiation a reasonable value for the speed loss to tungsten radiation due to absorption change may be detected. Some typical results for a bromide and a bromo-iodide emulsion are illustrated in figs. 2 and 3 respectively. Section (*a*) of each figure compares the room- and low-temperature characteristic curves to tungsten radiation, while section (*b*) effects the same comparison for ultra-violet radiation. It will be noted immediately that the speed losses for ultra-violet radiation are considerably less than those for tungsten radiation, this being attributed to the fact that the fraction of incident tungsten radiation absorbed falls considerably on temperature reduction, whereas there is little change in the fraction of ultra-violet radiation absorbed. In fig. 4 a further comparison for the bromo-iodide emulsion is made ; in this case a short development

Table 1. Treatment of Experimental Emulsions

AgBr	AgBr+5 mol. per cent AgI
A. Ripened 15 min at 40° c ; undigested.	D. Ripened 5 min at 40° c ; undigested.
B. Ripened 45 min at 40° c ; undigested.	E. Ripened 15 min at 40° c ; undigested.
C. Ripened 45 min at 40° c ; digested 55 min at 55° c.	F. Ripened 45 min at 40° c ; undigested.
	G. Ripened 15 min at 40° c ; digested 35 min at 55° c.
	H. Ripened 45 min at 40° c ; digested 35 min at 55° c.
	I. Ripened 15 min at 40° c ; digested 35 min at 55° c, in presence of a sulphur sensitizer.

Fig. 2

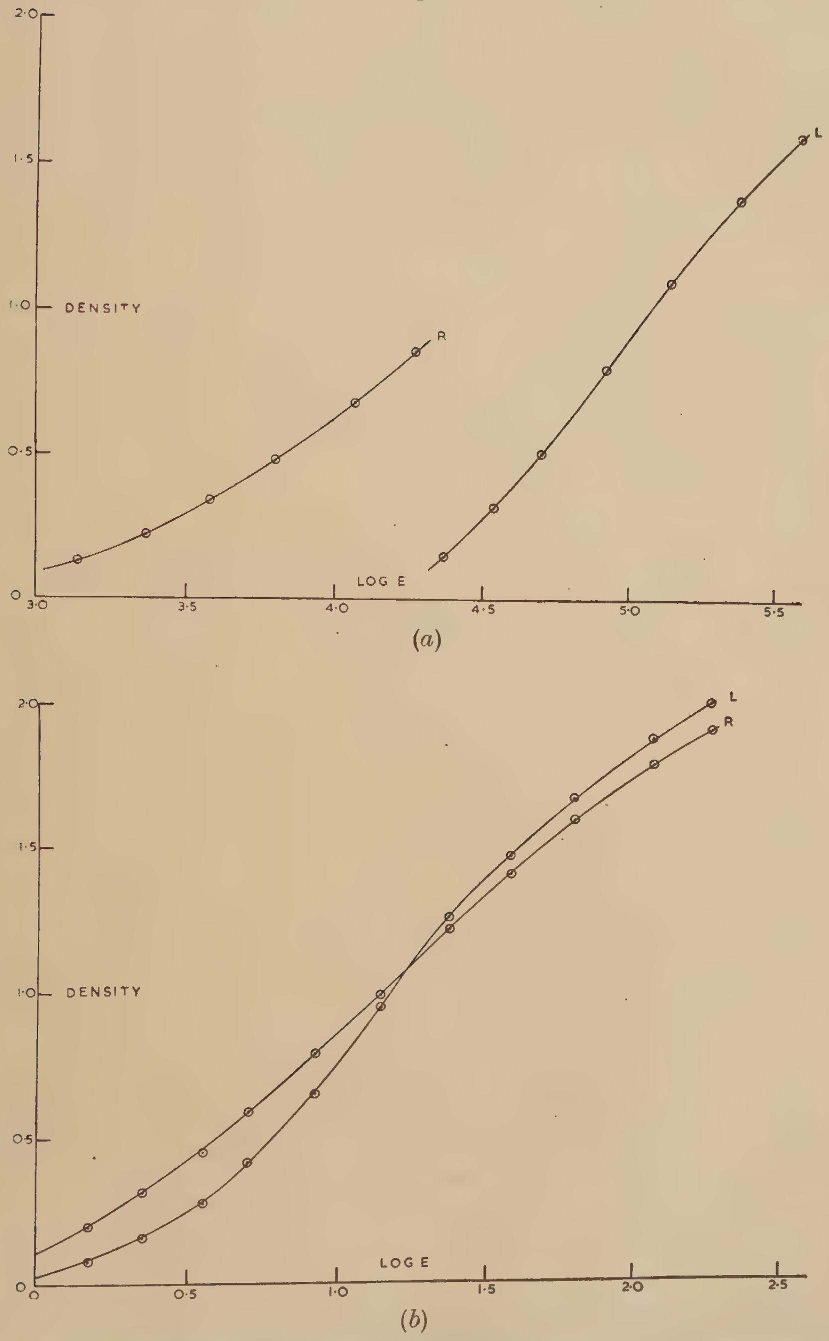

Room- and low-temperature characteristic curves (marked *R* and *L* respectively) for a pure bromide emulsion (C). (*a*) to tungsten radiation, (*b*) to ultra-violet radiation. The pure bromide emulsion was developed for 6 min in D19b. The densities have been corrected for fog.

Fig. 3

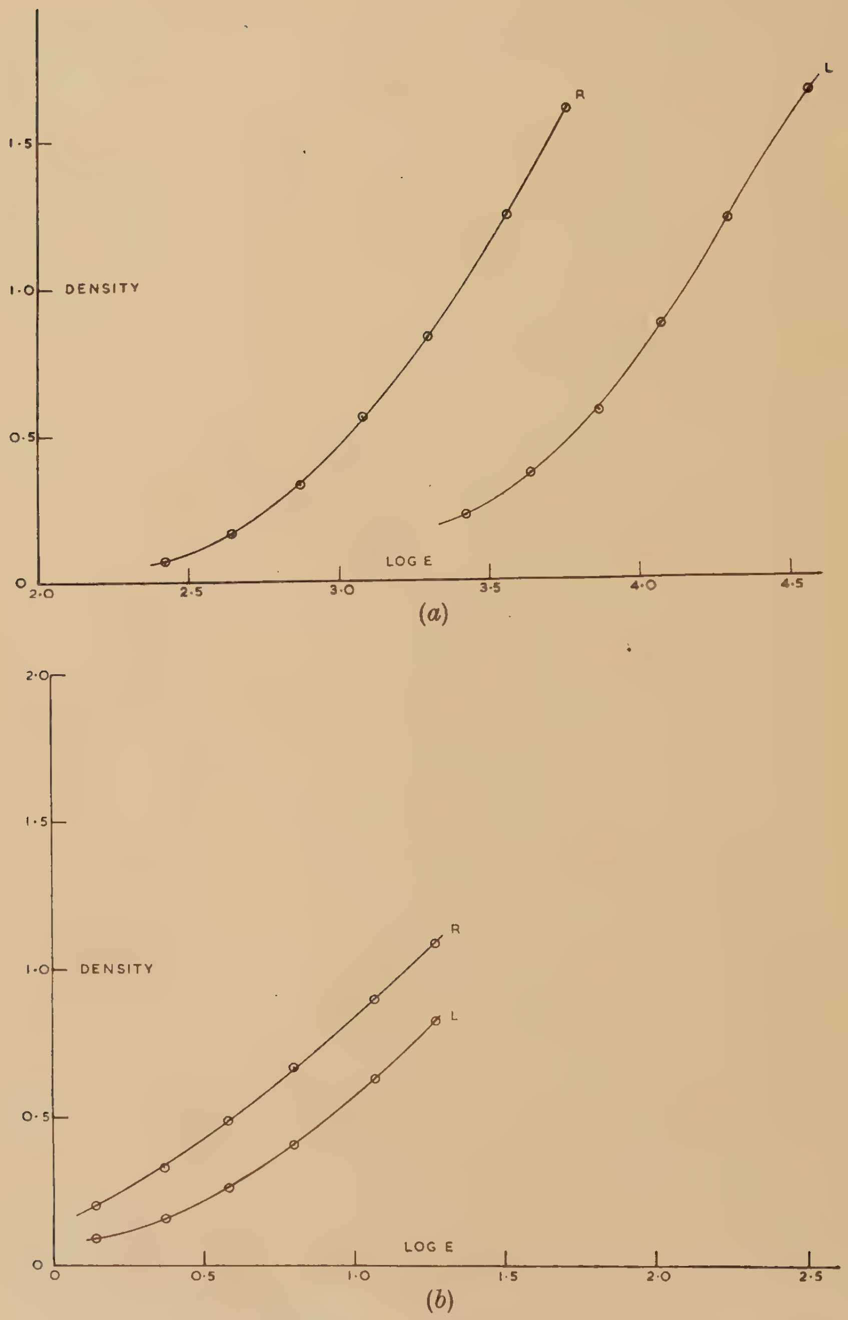

Room- and low-temperature characteristic curves (marked *R* and *L* respectively) for a bromo-iodide emulsion (I). (*a*) to tungsten radiation, (*b*) to ultra-violet radiation. The bromo-iodide emulsion was developed for 16 min in D19b. The densities have been corrected for fog.

Fig. 4

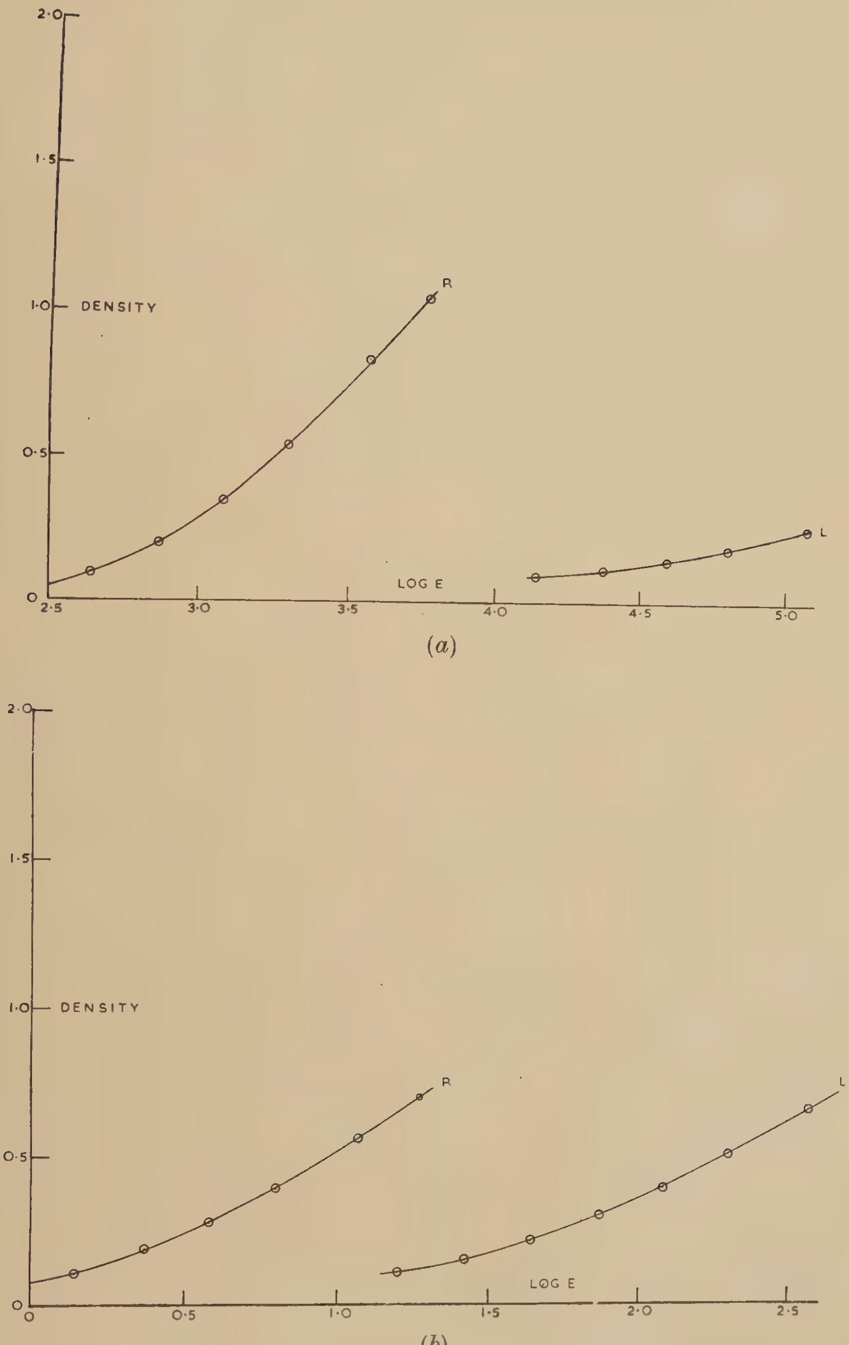

Room- and low-temperature characteristic curves for the same bromo-iodide emulsion (I) on short development (4 min D19b), (*a*) to tungsten radiation, (*b*) to ultra-violet radiation.

was employed. The actual speed losses are much larger than for the long development, but the tungsten speed loss is still greater than the ultra-violet speed loss. This result demonstrates that speed loss on temperature reduction involves a process of the high-intensity failure type, since prolongation of development is a recognized means of reducing high-intensity failure.

If it is assumed that absorption changes have little influence on the speed of an emulsion to ultra-violet radiation, then it will be clear that the difference of the speed losses to tungsten and ultra-violet radiation respectively should be equal to the speed loss due to reduced absorption of tungsten radiation at the low temperature. Since the speed losses are measured from the optimum of the room-temperature reciprocity failure curve, high-intensity failure or other forms of speed loss will be the same for both tungsten and ultra-violet exposures. A constant difference between tungsten and ultra-violet speed losses is to be expected if the emulsion coating weights are constant. This latter point was checked by silver determinations and by measuring the optical densities of unexposed strips; the maximum variations in coating weight were found to be about 20%. In table 2 the speed losses to tungsten and ultra-violet radiation are quoted for densities of 0·2 and 0·7 above fog.

Table 2. Speed Losses on Temperature Reduction from 20° C to −196° C, for Reference Densities of 0·2 and 0·7 above Fog

Values quoted in log E units

Emulsion and time of development in D19b	D=0·2 above fog			D=0·7 above fog		
	Tungsten speed loss	U.V. speed loss	Difference	Tungsten speed loss	U.V. speed loss	Difference
Bromide A. 5 min	0·78	0·20	0·58	0·85	0·14	0·71
Bromide B. 6 min	0·89	0·12	0·77	0·91	0·07	0·84
Bromide C. 6 min	1·07	0·34	0·73	0·75	0·18	0·57
Bromo-iodide D. 5 min	1·95	1·42	0·53	—	—	—
Bromo-iodide D. 16 min	1·23	0·90	0·37	1·33	0·83	0·50
Bromo-iodide E. 16 min	1·10	0·68	0·42	0·94	0·51	0·43
Bromo-iodide F. 16 min	1·23	0·79	0·44	0·99	0·64	0·35
Bromo-iodide G. 16 min	1·34	0·86	0·48	1·41	0·74	0·67
Bromo-iodide H. 16 min	1·07	0·76	0·31	0·89	0·53	0·36
Bromo-iodide I. 4 min	1·53	1·23	0·30	1·78	1·34	0·44
Bromo-iodide I. 16 min	0·71	0·40	0·31	0·79	0·34	0·45

It will be noted immediately that the difference factors for pure bromide emulsions are larger than those for bromo-iodide emulsions. This is consistent with the results of Biltz mentioned earlier, namely, that the decrease in absorption of a bromo-iodide emulsion (∼5 mol. per cent AgI) on temperature reduction is somewhat less than that of pure bromide.

The difference values for the two different types of emulsion are as constant as can reasonably be expected in view of the variations in coating weight, and the experimental errors which accrue in the derivation of the speed loss difference.

In the case of the bromo-iodide emulsions, for which more extensive results are available, the speed loss difference appears less, on the average, at the lower reference density.

This variation with reference density can be understood by referring to an expression for the relative log speed of an emulsion derived by Burton (unpublished work), and confirmed by checking against experimental data (unpublished work by Farnell). The expression is :

$$\log_{10} S=\log_{10} \Delta-x\Delta+\text{const.}, \quad . \quad . \quad . \quad . \quad . \quad . \qquad (1)$$

where S=speed in reciprocal quantic units, Δ=density of unexposed emulsion to the wavelength of the exposing radiation, and x=ratio of reference density to maximum density. From expression (1) a relation for the change in log speed on change of emulsion density can be derived, and is quoted below,

$$\delta \log_{10} S=\log_{10} (\Delta_1/\Delta_2)-x(\Delta_1-\Delta_2). \quad . \quad . \quad . \quad . \quad . \quad . \qquad (2)$$

If the change in emulsion density which occurs on lowering the temperature is such that at a low reference density the first term on the right hand side exceeds the second, raising the reference density (x) will diminish the speed change which occurs on lowering the temperature. Thus it appears that the smaller speed loss difference (tungsten—ultra-violet) at the lower reference density can be assigned to a small absorption speed loss with the ultra-violet exposures, which effectively reduces the difference between the tungsten and ultra-violet speed losses.

This deduction was checked by measuring the density of unexposed emulsions to 3650 A radiation at room- and low-temperatures and inserting the values in expression (2). The densities were determined by exposing two strips one behind the other, developing them together, and measuring the separation of the characteristic curves along the log exposure axis. In this way it was found that the densities of the bromo-iodide emulsions at room temperature were on the average 2·3 and fell to 1·5 at liquid nitrogen temperature. The average maximum density was about 3·0. Insertion of these values in expression (2) shows that for 3650 A radiation, an absorption speed loss of 0·16 log E units occurs at a reference density of 0·2 above fog, but that no absorption speed loss occurs at a reference density of 0·7 above fog. The quantitative agreement of this result with the discrepancy pointed out above was taken as confirmation of the explanation, and also as a confirmation of the original assumption that speed losses due to change in absorption of ultra-violet radiation are small.

To sum up this section, it may be said that comparisons of the speed loss to tungsten and ultra-violet radiation under equivalent conditions appear to provide a satisfactory method of determining the absorption speed loss with the former type of radiation. For an average bromo-iodide emulsion this quantity is about 0·4 log E units, and about 0·6 log E units for a pure bromide emulsion.

5.2. *High Intensity Reciprocity Failure*

It has now been shown that comparisons of room- and low-temperature sensitivity to ultra-violet radiation are sensibly free of any complication due to absorption change at a density of 0·7 above fog; a reasonable estimate can be given of the absorption speed loss at 0·2 above fog. In order to complete the correlation between room- and low-temperature sensitivity it remains to be determined whether the observed ultra-violet speed losses can be completely assigned to high intensity reciprocity failure of the low-temperature exposure, or whether there is some additional mechanism of exposure wastage coming into play.

Typical reciprocity failure curves for a bromide and bromo-iodide emulsion at room temperature (20° C) and solid carbon dioxide temperature (−78·5° C) are shown in figs. 5 and 6 respectively. The emulsions are actually those for which the characteristic curves have been presented (silver bromide and silver bromo-iodide). As described earlier the −78·5° C reciprocity failure curve is the very high intensity portion of the room temperature curve shifted to longer times; the ‘ bend-over ’ points are well defined. Owing to the rather low sensitivity of the experimental emulsions employed in this work, and the large drop in sensitivity which occurred on reduction of the emulsion temperature to −78·5° C, it was only possible to obtain satisfactory reciprocity failure curves at this temperature for densities of 0·2 above fog and with long developments. An exception, however, was the more sensitive sulphur sensitized emulsion for which satisfactory reciprocity failure curves were obtained at 0·7 above fog.

In table 3 comparisons are made of the ultra-violet speed losses on passing from 20° C to −196° C, with the high-intensity failure speed loss reckoned from the room temperature optimum to the horizontal portion of the −78·5° C curve. The latter curves were shifted up 0·12 log E units to counteract the small reflection loss which occurred at the exposure slot in making the exposures; the room temperature curves were obtained with the step wedge in direct contact with the sheet of film undergoing exposure.

A good correlation between the values in the second and third columns can be observed. The ultra-violet speed losses are invariably slightly less than the high-intensity failure speed losses. The reason for this becomes apparent when it is realized that the former values are over-estimated, for the purposes of this comparison, by an amount corresponding to the speed loss due to the fall in absorption of ultra-violet radiation on temperature reduction from 20° C to −196° C. The latter values are over-estimated by a larger amount corresponding to the speed loss due to the fall in absorption of tungsten radiation on proceeding from 20° c to $-78{\cdot}5°$ c. The bracketed values in the second column are the ultra-violet speed losses at 0·2 above fog, corrected for absorption change by measuring emulsion densities to 3650 Å radiation at room- and low-temperatures and applying expression (2). From a consideration of the results detailed in table 2 and of the temperature ranges involved, the high-intensity failure speed losses noted in the third column of

Figs. 5 and 6

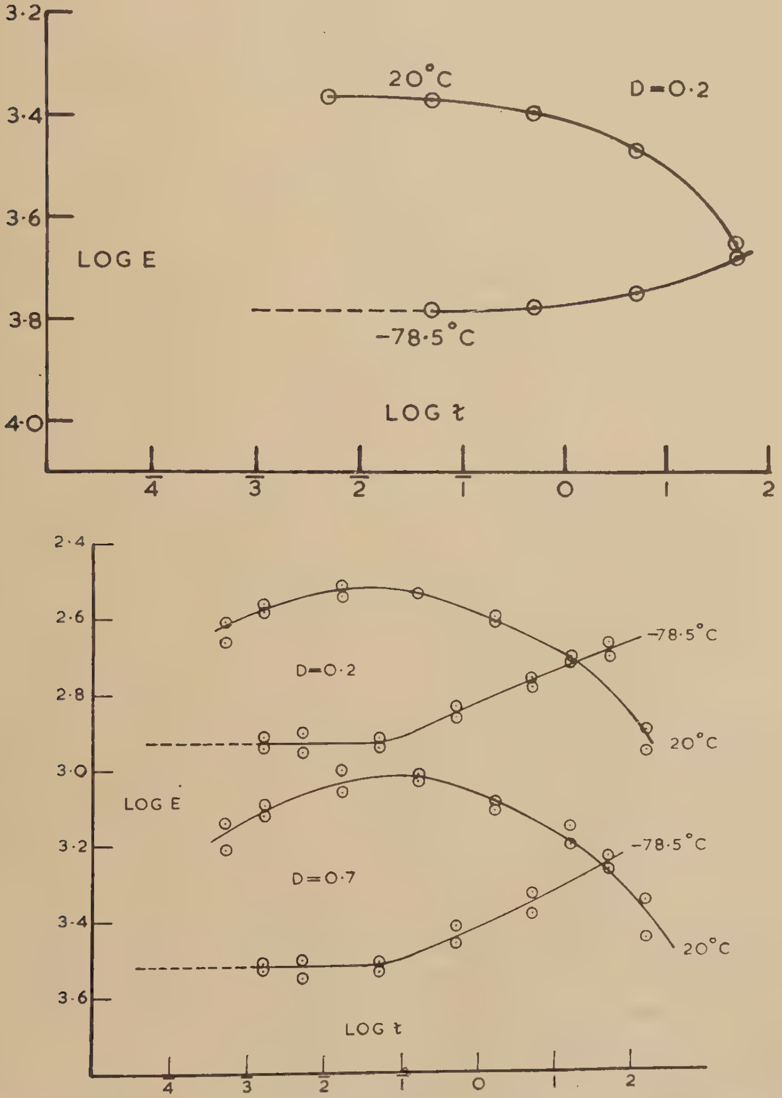

Reciprocity-failure curves of the bromide emulsion (C) and the bromo-iodide emulsion (I) at 20° c and $-78{\cdot}5°$ c (5 and 6 respectively). The reference density of the bromide emulsion curves is 0·2 above fog; for the bromo-iodide emulsion, curves are given for both 0·2 and 0·7 above fog.

table 3 should exceed the corrected ultra-violet speed losses by about 0·2 log E units for bromo-iodide and 0·3 log E units for pure bromide emulsions. These values are the estimated absorption corrections for tungsten radiation in passing from 20° C to −78·5° C, the reasonable assumption being made that the speed loss is approximately linearly related to the absorption change. The above condition will be seen to have been fulfilled within the limits of experimental error.

Table 3. Comparisons of Ultra-violet and High Intensity Reciprocity Failure Speed Losses

Reference density 0·2 above fog. All values in log E units

Emulsion and development	Ultra-violet speed loss	High intensity failure speed loss
Bromide B. 6 min D19b	0·12 (−0·09)	0·21
Bromide C. 6 min D19b	0·34 (+0·17)	0·42
Bromo-iodide E. 16 min D19b	0·68 (0·54)	0·76
Bromo-iodide F. 16 min D19b	0·79 (0·67)	0·87
Bromo-iodide G. 16 min D19b	0·86 (0·74)	0·90
Bromo-iodide H. 16 min D19b	0·76 (0·58)	0·79
Bromo-iodide I. 16 min D19b	0·40 (0·28)	0·41
	0·34 (0·7 above fog)	0·50 (0·7 above fog)

It appears, therefore, that the observed ultra-violet speed losses can be completely accounted for in terms of the high-intensity reciprocity failure of the low-temperature exposures. The generality of the result is confirmed by the fact that the pure bromide emulsions suffered little speed loss on temperature reduction, and show little high-intensity failure, while the sensitivity of the bromo-iodide emulsions fell considerably and was paralleled by strong high-intensity failure. Some check experiments confirmed the fact that emulsions D and I showed very strong high-intensity failure on short development. Although the bend-over point could not be reached at −78·5° C, the total high-intensity failure visible was almost sufficient to account for the much larger speed losses to ultra-violet radiation on short development.

5.3. *The Fluorescence of Photographic Emulsions*

The method of exposing strips at low temperatures enabled them to be observed during the actual latent-image exposure. When exposed to ultra-violet radiation pure bromide emulsions fluoresced a faint blue colour due to their gelatin content, but bromo-iodide emulsions invariably fluoresced with the characteristic green colour of bromo-iodide mixed crystals.

The interesting point about this fluorescence during exposure is its strong indication that the quantum efficiency of formation of latent-image silver is less than unity. The argument is as follows. It has been shown that the speed loss of a photographic emulsion on temperature reduction is due to reduction in absorption and high-intensity reciprocity failure ;

no additional mechanism appears to come into play. Now it is generally considered that inefficiency at high intensities is merely due to a greater dispersion of the latent-image silver, and does not involve increased recombination of electrons and positive holes. Confirmation of this point is provided by the fact that reciprocity failure disappears at very high intensities. Thus the recombination which is observed to take place at low temperatures must also occur at room temperature, and, as such, represents a quantum efficiency of silver formation of less than unity. Actual measurements of quantum efficiency which involve the production of much larger quantities of silver, for instance the recent experiments of Meidinger, have provided results which lead to a similar conclusion (Meidinger 1949).

5.4. *Results of Other Investigators and Conclusions*

Since the results described appear to provide a general explanation of the normally observed loss of sensitivity on temperature reduction, it is of interest and importance to determine whether the findings of other workers are consistent with the present viewpoint. First it will be observed that the normally reported speed loss of $\sim 1{\cdot}0 \log E$ units between the room-temperature optimum and the low-temperature exposure can be easily provided by the sum of the absorption and high-intensity reciprocity failure effects. Meidinger has shown that no obvious correlation exists between loss in sensitivity on temperature reduction and the fluorescence of the halide at the low temperature (Meidinger 1940). The results described in this paper confirm and extend his observations by showing that though low-temperature exposures are partially wasted by recombination, there is no necessity to invoke this effect in order to account for the observed loss in sensitivity. In fact it appears that recombination takes place to equal extents at both room- and low-temperatures.

The loss in sensitivity observed on proceeding from liquid-air to liquid-hydrogen temperature (90° K to 20° K) is very much smaller than the corresponding quantity observed on passing from room- to liquid-air temperature (Berg and Mendelssohn 1938). Since reciprocity failure is absent at the two low temperatures the loss in sensitivity can only be assigned to reduced absorption. From the data already presented it can be deduced that for an emulsion of normal thickness the speed loss on reducing the temperature from that of liquid air to that of liquid hydrogen should be approximately $0{\cdot}2 \log E$ units. Characteristic curves of Process film recorded by Berg and Mendelssohn at the two above-mentioned temperatures show that there is indeed a loss in sensitivity of about $0{\cdot}2 \log E$ units, at least for low and medium densities. Thus it appears that even at liquid-hydrogen temperature no other factors leading to lower efficiency are encountered other than reduced absorption and high-intensity reciprocity failure.

The large drop in sensitivity of the surface image of chemically sensitized emulsions on reduction of temperature, as reported by Biltz (Biltz 1949) is readily explained as being due to the well-known strong high-intensity failure of the surface image in such emulsions. It has already been described in § 5.2, how large speed losses observed on short, predominantly surface, development are very much reduced when development is prolonged. Biltz explained his results by saying that chemical sensitization becomes ineffective at low temperatures. This form of words may be accepted if it is added that the same breakdown occurs at room temperature and short exposure times, but the phrase is unfortunate since the speed of the chemically sensitized emulsion at low temperature did not fall simply to the speed level of the corresponding unsensitized emulsion, but considerably below it.

A similar viewpoint is applicable to the experimental results of Webb and Evans that the gamma of a low-temperature characteristic curve approaches that of an ordinary temperature curve as the number of low-temperature exposure intervals followed by warming up in the dark was increased, the total exposure in each case being kept constant (Webb and Evans 1938). A residual loss of speed was observed, however, which is to be assigned to reduced absorption. The practice of warming up after a section of the low-temperature exposure, and thus allowing some silver to be formed on which electrons can be trapped in the next section of the exposure, is just that required to eliminate high-intensity reciprocity failure ; the latent-image silver is not deposited in a disperse manner as after a single low-temperature exposure, but is allowed to build up as a few large specks. Arguing on the basis of the results described in this paper it seems certain that a result identical with that of Webb and Evans could have been obtained by giving strips single low-temperature exposures, and processing them for increasing lengths of time in a commercial developer. The mechanism coming into play in this case would be different to that involved in the experiment of Webb and Evans, but the final result, viz., the reduction of high-intensity reciprocity failure, would be the same. In order to avoid possible confusion it should be pointed out here that high-intensity failure invariably contains a component representing loss of gamma, and in some cases represents this effect alone.

A further observation now readily explained is that the sensitivity of an emulsion to X-rays is little temperature-dependent (Eggert and Kleinschrod 1941). The transit time of the photoelectron through a grain is so short that its influence corresponds to that of an extremely brief light exposure. Thus in so far as an emulsion exposed in the above manner is demonstrating maximum high-intensity failure at room temperatures, reduction of temperature can have only small effects related to the slightly increased energy required to free bound electrons in the silver halide.

Finally it is worth describing some experimental results of Berg, Marriage and Stevens which provide excellent confirmation of the deductions made from results described in this paper (Berg, Marriage and Stevens 1941). They gave spark exposures to strips of a medium-speed blue-sensitive emulsion at both room and low temperatures and processed strips in surface and internal developers (the latter after bleaching of the surface image). The surface image was considerably less sensitive than the internal but the speed loss on temperature reduction was approximately the same for the two types of image. This is significant because the spark exposure is of such short duration that it corresponds to an exposure beyond the bend-over point, and thus a decrease of temperature should only decrease the sensitivity by an amount corresponding to the decreased absorption. In turn the latter quantity should be independent of the method of development employed, which is indeed experimentally observed.

Thus in conclusion it can be said that as regards the straightforward question of the interrelation of room- and low-temperature sensitivity of non-colour-sensitized emulsions, all the available evidence is consistent with the view that the normally observed fall in sensitivity is due to the high-intensity failure of the low-temperature exposure and the decreased absorption of the emulsion halide. Experimental methods of reducing the observed speed loss are just those to be expected on the basis of the above statement. The wastage of an exposure by recombination appears to take place to an equal extent at both room and low temperatures. Finally it is to be noted that the explanation given does not depend on the theory of high-intensity reciprocity failure ; in remains true whatever the explanation of the various features of a reciprocity failure curve.

ACKNOWLEDGMENTS

The author wishes to express his thanks to Mr. P. C. Burton for much helpful discussion, and to Mr. H. Young for assistance in the execution of the experiments.

REFERENCES

BERG, W. F., 1939, *Trans. Faraday Soc.*, **35,** 445 ; 1940, *Proc. Roy. Soc.* A, **174,** 559 ; 1948, *Rep. Prog. Phys.*, **11,** 248.
BERG, W. F., MARRIAGE, A., and STEVENS, G. W. W., 1941, *Phot. J.* B, **81,** 413.
BERG, W. F., and MENDELSSOHN, K., 1938, *Proc. Roy. Soc.* A, **168,** 168.
BILTZ, M., 1949, *J. Opt. Soc. Amer.*, **39,** 994 ; 1951, *Zeits. f. Naturforschung*, **6,** 366.
EGGERT, J., and KLEINSCHROD, F. J., 1941, *Z. phys. Chem.* A, **189,** 1.
FARNELL, G. C., and BURTON, P. C., 1951, *Fundamentals of Photographic Sensitivity* (Butterworth's Scientific Publications 1951), p. 61.
FARNELL, G. C., BURTON, P. C., and HALLAMA, R., 1950, *Phil. Mag.*, **41,** 157, 545.
GURNEY, R. W., and MOTT, N. F., 1938, *Proc. Roy. Soc.* A, **164,** 151.
MEIDINGER, W., 1939, *Phys. Z.*, **40,** 517 ; 1940, *Ibid.*, **41,** 277 ; 1949, *Z. wiss. Phot.*, **44,** 1.
SHEPPARD, S. E., WIGHTMAN, F. P., and QUIRK, R. F., 1934, *J. Phys. Chem.*, **38,** 817.
TOY, F. C., and HARRISON, G. B., 1930, *Proc. Roy. Soc.* A, **127,** 613.
WEBB, J. H., 1935, *J. Opt. Soc. Amer.*, **25,** 4.
WEBB, J. H., and EVANS, C. H., 1938, *J. Opt. Soc. Amer.*, **28,** 249.

XXIV. *Note on the Angular Distribution of Radiation from Fairly Thin Targets Bombarded by High Energy Electrons*

By J. D. Lawson
Atomic Energy Research Establishment, Harwell, Berks.*

[Received December 19, 1951]

At least four papers have appeared in recent years in which a calculation is made of the angular distribution of bremsstrahlung from targets sufficiently thin that ionization loss and straggling are negligible but sufficiently thick that multiple scattering of the electrons is important (Schiff 1946, Lawson 1950, Kulenkampff, Scheer and Schittenhelm 1951, Lanzl and Hanson 1951). In no two of these is the expression obtained for the angular distribution the same, nor have the method of derivation and the approximations used in the calculations always been clearly stated. This note is intended to clarify the position, by showing that there are two essentially different ways of carrying out the analysis, which lead to slightly different results.

In the analysis which follows the small angle approximation will be used, and a gaussian law for multiple scattering will be assumed. The use of the small angle approximation means that the upper limit in integrations over all angles cannot be defined, for analytical convenience it will be taken as infinity. The following symbols will be used :

E =kinetic energy of electron.

μ =rest energy of electron.

t =thickness of target.

$f(\theta)$ =angular distribution of the radiation from a target so thin that multiple scattering is negligible (this function has an angular width of order μ/E ; its analytical form will be given later). The function is normalized so that

$$\int_0^\infty f(\theta)\, 2\pi\theta d\theta = 1.$$

$F(t, \theta)$ =normalized angular distribution of scattered electrons after passing through a thickness t of the target$=(1/\pi ct)\exp(-\theta^2/ct)$ where c is a parameter depending on the electron energy and target material. At high energies $c \propto 1/E^2$.

$\sigma\delta t$ =fraction of electron energy lost by radiation in a distance δt.

γ =Euler's constant$=1{\cdot}78$.

We shall now calculate the forward intensity and angular distribution by two methods. The first is that employed by Schiff. The fraction of energy radiated per unit solid angle in the *forward* direction from a target of thickness t is clearly given by

---

* Communicated by the Author.

$$R_0=\sigma\int_0^t\int_0^\infty F(t,\theta)\,f(\theta)\,2\pi\theta d\theta dt, \qquad (1)$$

substituting for $F(t,\theta)$ and integrating with respect to t

$$R_0=(\sigma/\pi c)\int_0^\infty -Ei(-\theta^2/ct)\,f(\theta)\,2\pi\theta d\theta, \qquad (2)$$

this may be simplified further if t is not very small. Now $f(\theta)$ is small when $\theta\gg\mu/E$, so that if μ^2/E^2ct is small then θ^2/ct will be small for values of θ for which $f(\theta)$ is not small. The expression $Ei(-\theta^2/ct)$ may then be replaced by the small angle approximation $-\ln(\gamma\theta^2/ct)$, and eqn. (2) becomes

$$R_0\doteq\frac{\sigma}{\pi c}\int_0^\infty \ln\left(\frac{E^2ct}{\mu^2}\cdot\frac{\mu^2}{\gamma E^2\theta^2}\right)f(\theta)\,2\pi\theta d\theta \qquad (3)$$

$$=(\sigma/\pi c)\,(\ln E^2ct/\mu^2-\ln\lambda) \qquad (4\,a)$$

where

$$\ln\lambda=\int_0^\infty 2\pi\theta\,f(\theta)\ln(\gamma E^2\theta^2/\mu^2)\,d\theta. \qquad (4\,b)$$

Substituting the approximate expression (Schiff 1951)

$$f(\theta)=E^2\mu^2/\pi(\mu^2+E^2\theta^2)^2 \qquad (5)$$

in eqn. (4 *b*) yields the remarkably simple result $\lambda=\gamma$, whence from eqn. (4 *a*)

$$R_0=(\sigma/\pi c)\ln(E^2ct/\gamma\mu^2). \qquad (6)$$

The assumption above that μ^2/E^2ct is small clearly breaks down when t is very small, nevertheless there is a useful range of t over which eqn. (6) is a good approximation.

So far we have found only the forward radiation intensity. It is not possible to find a simple expression for the radiation at small angles, but at large angles, where θ is large compared with the angular width of $f(\theta)$, (i.e. μ/E) the angular distribution of radiation is simply given by the total distribution of electrons throughout the thickness t of the target

$$R_{\theta\gg\mu/E}=(-\sigma/\pi c)\,Ei\,(-\theta^2/ct). \qquad (7)$$

The value of R for small θ may be found by judicious use of a French curve.

The second method of calculating the angular distribution was first used in a crude form by Lawson and then refined by Lanzl and Hanson. The refined calculation will be given here.

In this method we express $f(\theta)$ as a sum of gaussian functions of different width, (in practice two components are probably all that can be justified), thus

$$f(\theta)=\Sigma\,(a_r/\pi)\exp(-b_rE^2\theta^2/\mu^2). \qquad (8)$$

Now the angular distribution of radiation from a layer of thickness δt at a depth t in the target is given by the *convolution* of $f(\theta)$ and $F(t,\theta)$. Since both these expressions consist of gaussian functions, which convolve simply by addition of their mean squared angles we get

$$\delta R_\theta = \Sigma \frac{a_r \sigma \delta t}{\pi(ct+b_r\mu^2/E^2)} \exp\left(-\frac{\theta^2}{ct+b_r\mu^2/E^2}\right) \quad . \quad . \quad . \quad . \quad (9)$$

whence by proceeding to the limit and integrating from 0 to t

$$R_\theta = \frac{\sigma}{\pi c} \Sigma\, a_r \left[-Ei\left(-\frac{\theta^2}{ct+b_r\mu^2/E^2}\right) + Ei\left(-\frac{\theta^2}{b_r\mu^2/E^2}\right)\right]. \quad . \quad . \quad . \quad (10)$$

This expression is valid for all values of θ, and does not diverge for $\theta=0$, and t small. For t and θ large it simplifies to eqn. (7). When $\theta=0$ it simplifies to

$$R_0 = (\sigma/\pi c)\, \Sigma\, a_r \ln\,(1+ctE^2/b_r\mu^2). \quad . \quad . \quad . \quad . \quad (10\,a)$$

In Lawson's paper only one gaussian function was taken for $f(\theta)$, and b_r was taken as 2.

It is interesting to note that if a single gaussian function is taken for $f(\theta)$ and substituted in eqn. (4 *b*) we get $\lambda=b$, the expressions (4 *a*) and (10 *a*) are then identical when $ctE^2/\mu^2 \gg 1$.

Note added in proof.—Since this letter was written a paper by E. G. Muirhead, B. M. Spicer and H. Lichtblau has appeared (*Proc. Phys. Soc.* A, **65**, 59, 1952), in which yet another formula for R_θ has been suggested.

REFERENCES

KULENKAMPFF, H., SCHEER, M. and SCHITTENHELM, R., 1951, *Zeits. für Phys.*, **129,** 202.

LANZL, L. H. and HANSON, A. O., 1951, *Phys. Rev.*, **83,** 959.

LAWSON, J. D., 1950, *Proc. Phys. Soc.* A, **63,**, 653.

SCHIFF, L. I., 1946, *Phys. Rev.*, **70,** 87 ; 1951, *Ibid.*, **83,** 252.

XXV. *The Specific Heats of Germanium and Grey Tin at Low Temperatures*

By R. W. HILL and D. H. PARKINSON*
Clarendon Laboratory, Oxford†

[Received November 16, 1951]

ABSTRACT

The specific heats of germanium and grey tin have been measured from liquid helium temperatures up to 170° and 110° K respectively. A comparison of the results with existing data shows that previous measurements on germanium do not represent the behaviour of the pure material, whereas those for grey tin are satisfactory. It is also shown that the temperature variations of the Debye characteristic temperatures of these elements are very large, and qualitatively similar to those of diamond and silicon. This behaviour is thought to be characteristic of lattices of diamond structure, but the possibility of the existence of anomalous contributions to the specific heat is also discussed.

Values of the enthalpy, entropy and free energy of both substances have been calculated as a function of temperature and are presented in tabular form.

§1. INTRODUCTION

FOR many years the Debye formula was regarded as giving a very satisfactory representation of the specific heats of regularly crystallizing solid bodies, although of course its theoretical shortcomings had been realized from the beginning. It is true that there were few substances where it fitted the data completely and it had therefore become the practice to plot the Debye θ, as calculated from the individual measured points, as a function of temperature. Variations of the order of about 10% were fairly common.

However, the substances with diamond structure, particularly silicon and grey tin, showed very much bigger deviations and this was later shown to be the case for germanium also. It had therefore been proposed by Simon (1926) that one had to consider additional contributions to the specific heat in a way which will be discussed later in this paper.

When it was later found by Blackman (1937) that the real frequency spectrum of a solid could differ very appreciably from Debye's approximation the question occurred whether the great deviations in the diamond type lattices could not have been explained simply in this way. The present work on germanium and grey tin was undertaken in order to extend the existing data down to lower temperatures. Also, in the case of germanium, which in the early experiments had been available only as a small and impure specimen, new measurements over a wide range of temperatures were thought desirable.

---

* Now at T.R.E. Malvern.

† Communicated by Professor F. E. Simon, F.R.S.

§2. EXPERIMENTAL

Two samples of germanium were used : the first was 35 g of Dupont ‘ Hyperpure ’ germanium in the form of granules of 2 to 3 mm diameter. This material is ‘ spectroscopically ’ pure, but may contain some nitrogen which does not show up in spectroscopic analysis. The second sample was a single ‘ button ’ weighing about 10 g, which was kindly supplied to us by Professor K. Lark-Horovitz of Purdue University. At the time of its arrival (September 1947) it was regarded as being of very high purity, having a specific resistance of 1·2 ohm cm compared with the theoretical value of 60 ohm cm for the ideally pure material.

For the work on grey tin two samples were also available. The first was 25 g of rather coarse powder believed to have a total impurity content of about 0·05%. The second sample was kindly supplied by the Tin Research Institute, who believed it to be of the purest tin available. It is their opinion that existing methods of estimating impurities in tin are unsatisfactory, and that no significant analysis can be given. The sample used was 100 g, and was similar in form to the first sample.

The measurements on both samples of germanium and the first sample of grey tin were made in an apparatus which has been described elsewhere (Parkinson, Simon and Spedding 1951). In this apparatus, the lowest temperatures were attained by pumping away liquid helium which had been condensed into the calorimeter. This procedure was found to be unsatisfactory for grey tin, since the helium was quite strongly adsorbed on the powder sample, giving errors of up to 20% due to the progressive desorption of helium as the sample warmed up. A somewhat different calorimeter was therefore used for the low temperature measurements on grey tin, differing from the other in that a separate chamber was provided for the liquid helium. It was found necessary to admit about 10^{-5} moles of helium exchange gas into the calorimeter in order to establish thermal equilibrium between the sample and the thermometer. A comparison with the amounts adsorbed in the other calorimeter, together with the approximate error introduced by it shows the error due to adsorption in the second calorimeter to be less than 1% above 7° K.

The temperature ranges covered in this work were as follows : germanium (both samples) 4 to 175° K ; grey tin (first sample) 12 to 110° K ; grey tin (second sample) 2 to 20° K.

Above about 10° K, the results obtained are believed to be accurate to about 1%. At lower temperatures, the accuracy of measurement decreases, due to the fact that the heat capacity of the specimens becomes very small and comparable with that of the empty calorimeter. Under these circumstances, the unfavourable ratio of surface area to volume of the sample, which is inherent in work with granular or powder specimens, adversely affects the thermal insulation which can be achieved, and with it the accuracy of the result.

In the case of grey tin, a further limiting factor is the adsorption of exchange gas by the specimen at helium temperatures. The effect of this is difficult to estimate, but would appear to be rather less important than the effect of poor thermal insulation, yet the final accuracy may be as low as 20% below about 4° K. Thus these measurements do no more than establish the absence of marked anomalous behaviour between 2 and 4° K.

Fig. 1

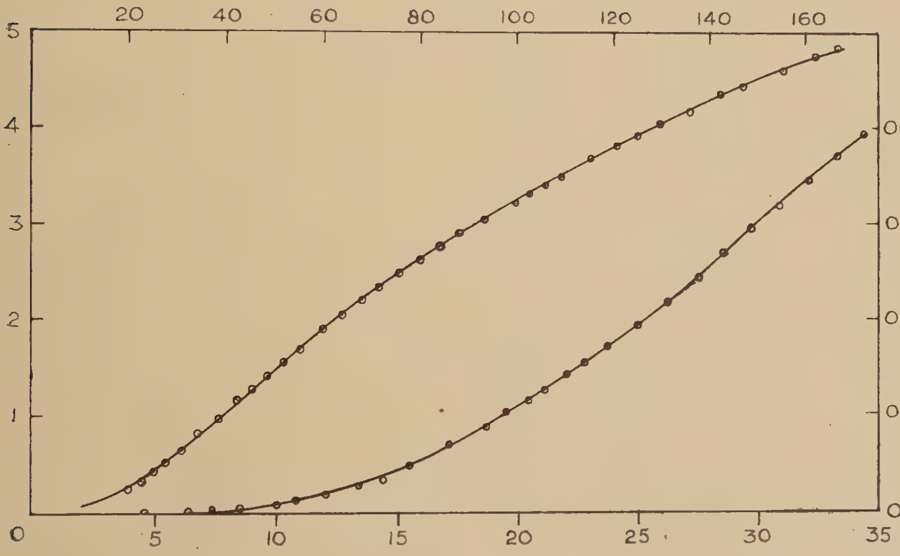

The specific heat of germanium. The upper curve shows the results at higher temperatures.

Abscissa : temperature ° K. Ordinate : C_p cal/deg. g atom.

§3. Results

(i) *Germanium*

The results obtained with both samples of germanium are shown in fig. 1, and it may be seen that both sets of results lie on the same smooth curve. These results are very different from those obtained by Cristescu and Simon (1934); no peak is found in the curve and the specific heat values are everywhere smaller. Over a wide range of temperature this difference is as large as 50%.

Smoothed values of the present results are given in table 1 together with values of the specific heat at constant volume and the Debye θ deduced from them. Also included in this table are values for the entropy S, the enthalpy H and the Gibb's free energy G. The correction from

C_p to C_v could only be made approximately since the expansion coefficient and compressibility are not known. Use was therefore made of the formula due to Nernst and Lindemann

$$C_p - C_v = 0{\cdot}0214\, C_p^2 T/T_s,$$

where T_s is the melting point of the substance. This formula is, of course, only approximate, but the corrections applied nowhere exceed 1·5% and are negligible below 70° K.

Table 1. The Specific Heats and Thermodynamic Functions of Germanium

T	C_p	C_v	θ	S	$H-H_0$	$-(G-G_0)$
5	0·0007					
7	0·0035		357	0·001	0·005	
10	0·018		297	0·005	0·035	0·01
15	0·082		268	0·024	0·28	0·08
20	0·222		256	0·068	1·04	0·31
25	0·391		264	0·135	2·56	0·82
30	0·613		269	0·226	5·06	1·72
40	1·02		293	0·457	13·2	5·08
50	1·45		313	0·731	25·6	11·0
60	1·88		329	1·03	42·2	19·8
70	2·24		346	1·35	62·8	31·8
80	2·59	2·58	358	1·67	87·0	46·8
90	2·92	2·91	369	2·00	115·0	65·3
100	3·22	3·20	375	2·32	146·0	86·5
120	3·77	3·74	385	2·95	216·0	138·0
140	4·26	4·22	381	3·56	296·0	203·0
160	4·68	4·62	371	4·15	385·0	279·0

(The thermal unit is the calorie per g atom throughout.)

(ii) *Grey Tin*

The data of Lange (1924) extends down to a little below 20° K; measurements were therefore made in the temperature range 2 to 30° K. Results obtained with both specimens agree very well with Lange's values in the region where these overlap. Further determinations in the temperature range 60 to 100° K confirm this agreement. The present results are shown in fig. 2 together with those of Lange; both sets of results have been used in compiling table 2 which contains smoothed values of C_p, C_v, θ, S, H and G. Corrections from C_p to C_v were made in the manner described above, the difference being 2% at 100° K and negligible below 40° K.

§4. DISCUSSION OF RESULTS

The results described above show that the values of θ for germanium and grey tin vary with temperature in the same way as those for diamond and silicon. In all cases, θ tends to a constant value θ_∞ at the higher temperatures, passing through a minimum at lower temperatures. If θ/θ_∞ is plotted against T/θ_∞ as in fig. 3, this essential similarity is clearly displayed. It is seen that the minimum becomes deeper and occurs at

Fig. 2

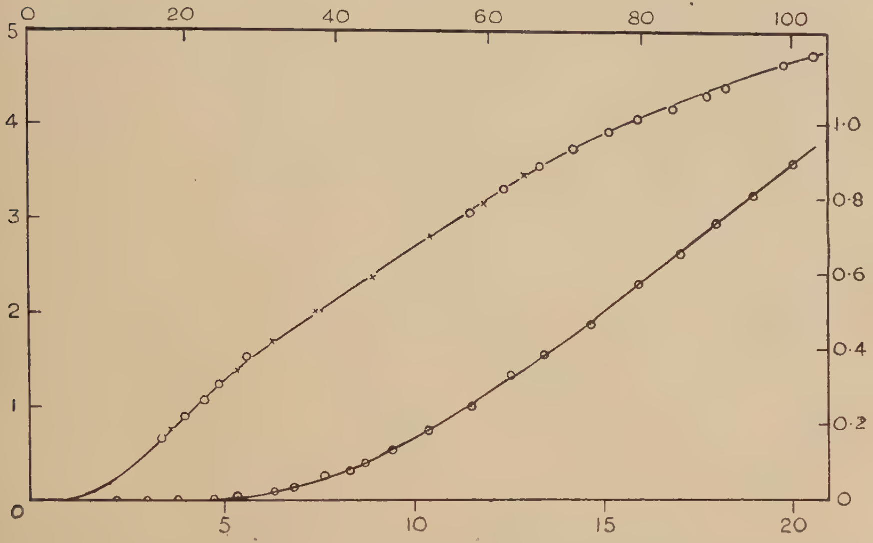

The specific heat of grey tin. The upper curve shows the results at higher temperatures.
× =Lange, ⊙ =this research.
Abscissa : temperature ° K. Ordinate : C_p cal/deg. g atom.

Table 2. The Specific Heats and Thermodynamic Functions of Grey Tin

T	C_p	C_v	θ	S	$H-H_0$	$-(G-G_0)$
7	0·043		155			
8	0·072		149			
9	0·111		145			
10	0·161		142	0·044	0·37	0·07
12	0·281		142			
15	0·498		145	0·169	1·96	0·57
20	0·893		155	0·366	5·39	2·14
25	1·27		167			
30	1·60		179	0·867	18·1	7·90
40	2·13	2·12	204	1·40	36·6	19·4
50	2·67	2·65	220	1·94	60·3	36·7
60	3·20	3·17	229	2·47	89·7	58·3
70	3·71	3·67	230	3·00	124·0	86·0
80	4·04	3·99	237	3·52	163·0	119·0
90	4·35	4·28	240	4·01	205·0	156·0
100	4·65	4·56	238	4·48	250·0	198·0

(The thermal unit is the calorie per g atom throughout.)

lower temperatures as the atomic weight increases. The data for silicon used in this diagram is that of Keesom and Pearlman (1951 a); this data, together with some for germanium, has recently been summarized (Keesom and Pearlman 1951 b). It would appear that this data for germanium is in good agreement with that presented here.

In the case of diamond, the minimum has been explained purely in terms of lattice theory by Smith (1948) and a recent note by Hsieh (1951) reports that a similar calculation for germanium yields values which are in reasonable agreement with the present results. It thus appears probable that a similar treatment would account for the behaviour of silicon and grey tin also.

Fig. 3

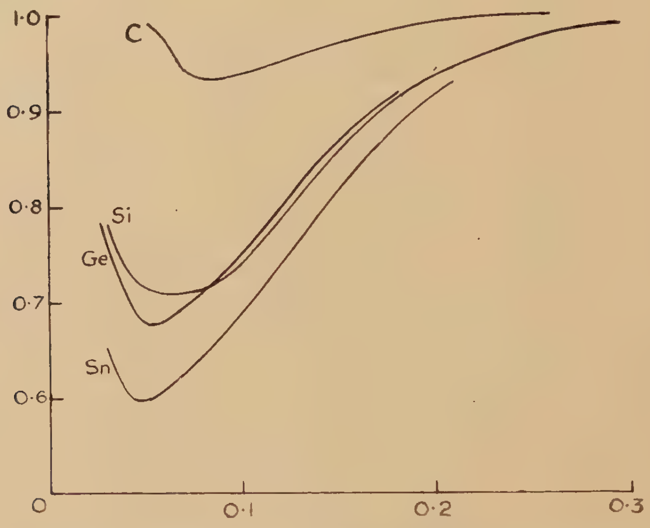

The reduced Debye temperature as a function of reduced temperature for the diamond structure elements.
Abscissa: T/θ_∞. Ordinate: θ/θ_∞.

An alternative approach to the problem is that proposed by Simon (1926), in which it is postulated that the deviations from the Debye theory are due to an additional contribution to the specific heat arising from some excitation process. Such a process could contribute a term to the specific heat which would be represented by a Schottky function. This view gains support from the fact that the experimental curve can be fitted quite accurately by the sum of a Debye and a Schottky function, using the characteristic temperatures given in table 3. Perhaps too much importance should not be attached to this fact, since the effective vibrational frequency spectrum may be rather similar in both cases, and the specific heat is insensitive to the form of this spectrum except at the lowest temperatures (Katz 1951). It must also be remembered that there is no known origin for a suitable excitation process in the pure materials at these temperatures ; indeed there is no need to invoke such a process at all for diamond. On the other hand, the existence of a negative expansion coefficient for silicon (Simon and Bergmann 1930, Erfling 1942) would seem to indicate that the behaviour of these substances is not perfectly understood. The expansion coefficients of silicon and germanium are to be measured shortly in this laboratory, and the effects of impurities investigated.

A further matter requiring explanation is the very large discrepancy between the present results on germanium and those of Cristescu and Simon. The specimen used by the older authors was small, but the difference between the two sets of results seems far too large to be explained in terms of experimental error. Aigrain and Dugas (1950) have shown that the heat content of the Cristescu anomaly can be explained in terms of a concentration of impurities of the order of 10^{19} impurity atoms/cm^3. If the remaining difference between the two sets of results is attributed to impurities in the specimen of the older authors, the specimen must have been very impure indeed. While this may have been the case, the entropy difference at 200° K is of the order of $R \ln 2$; it would therefore appear that about one extra degree of freedom per atom is required in order to explain the discrepancy, and it is difficult to see how this could be attributed to impurities. A final decision on this point must await experiments carried out with controlled amounts of impurity ; such experiments would be of very great interest in the study of all the diamond structure elements.

Table 3. The Debye and Schottky Characteristic Temperatures for the Diamond Structure Elements

Element	θ_D	θ_S
Diamond	2340	1070
Silicon	790	246
Germanium	400	127
Grey tin	260	69

ACKNOWLEDGMENTS

In conclusion, the authors wish to thank Professor F. E. Simon for valuable advice and encouragement, and for the great interest he has shown in this work. They are also indebted to Messrs. U. Bergenlid and P. L. Smith for assistance with the experiments. This work was supported by Industrial Distributors, Ltd.

REFERENCES

AIGRAIN, P., and DUGAS, C., 1950, *C.R. Acad. Sci., Paris*, **230,** 1277.

BLACKMAN, M., 1937, *Proc. Roy. Soc.* A, **159,** 416.

CRISTESCU, S., and SIMON, F. E., 1934, *Z. phys. Chem.* B, **25,** 273.

ERFLING, v. H-D., 1942, *Ann. Phys., Lpz.*, **41,** 467.

HSIEH, YÜ-CHANG, 1951, *Bull. Amer. Phys. Soc.*, **26,** 6, 34.

KATZ, E., 1951, *J. Chem. Phys.*, **19,** 488.

KEESOM, P. H., and PEARLMAN, N., 1951 a, *Purdue University Semiconductor Research* 11*th Quarterly Report* ; 1951 b, *Bull. Amer. Phys. Soc.*, **26,**, 6, 34.

LANGE, F., 1924, *Z. phys. Chem.*, **110,** 343.

PARKINSON, D. H., SIMON, F. E., and SPEDDING, F. H., 1951, *Proc. Roy. Soc.* A, **207,** 137.

SIMON, F. E., 1926, *S.B. preuss. Akad. Wiss.*, 477.

SIMON, F. E., and BERGMANN, R., 1930, *Z. phys. Chem.* B, **8,** 255.

SMITH, H. J., 1948, *Phil. Trans.* A, **241,** 105.

XXVI. *The Relation between Thermo-Optic and Piezo-Optic Phenomena in Crystals*

By G. N. Ramachandran and T. Radhakrishnan
Department of Physics, Indian Institute of Science, Bangalore*

[Received October 12, revised November 23, 1951]

Summary

It is pointed out that the change in refractive index with temperature of a crystal is different from what is calculated from the accompanying change in volume and the piezo-optic coefficients. The difference, which is a pure temperature effect, is explained as being due to the change in polarizability of the atoms produced by a change in the amplitude of vibration. The polarizability (α) can be expanded as a Taylor series in the changes of the distance (r) between the atoms and it is found that while the piezo-optic coefficient depends only on $\partial\alpha/\partial r$, the pure temperature effect is a function of $\partial^2\alpha/\partial r^2$. Making use of the experimental data, the values of α and its first two derivatives can be determined. These values are found to be of the same order as those deduced from the intensities of Rayleigh and Raman scattering of light. The theory predicts that dn/dT should vary as the coefficient of cubical expansion at different temperatures and this is verified to be true. Finally, calculations are made of the thermo- and piezo-optic coefficients, considering the electrostatic interaction between the atoms. These do not adequately explain the observed facts, since no provision is made for the distortion of electron atmospheres around the atoms and the consequent changes in polarizability.

§1. Introduction

When a transparent solid is subjected to a change of temperature or pressure, its refractive index, n is found to change. The two quantities dn/dT † and dn/dp may be referred to respectively as the thermo-optic and piezo-optic coefficients. Measurements of the former exist for a number of crystals over a range of wave-lengths and temperatures (e.g. Micheli 1902, Reed 1898, Ramachandran 1947, Radhakrishnan 1950, 1951). The piezo-optic coefficient has not been measured directly for any crystal, but it can be calculated from the piezo-optic constants q_{ij}, or the elasto-optic constants p_{ij} of the crystal. These latter have been measured for many crystals (e.g. Pockels 1902, Ramachandran 1950, Burstein and Smith 1948, 1949). The present paper is a study of the

---

* Communicated by Professor R. S. Krishnan.

† As against t for temperature, used by the authors in earlier publications, T is used here in accord with thermodynamic symbolism.

relation between dn/dT and dn/dp. Both on the application of a compressive stress and on reducing the temperature, the specific volume of a substance diminishes. If the changes in volume are made the same in both the cases, are the changes in refractive index also the same? Calculations show that they are not; in fact, in some crystals, even the signs of the refractive index change are opposite in the two cases. It is therefore clear that a factor affecting the refractive index is operative, purely caused by a change in temperature, in addition to that due to thermal dilatation. The existence of this factor has been discovered long ago (Pockels 1902); but no explanation appears to have been given for it. An explanation is attempted in this paper, in terms of the polarizabilities of atoms and the influence of thermal vibrations on polarizability.

§2. Comparison of dn/dT and dn/dp

The dispersion formula for a crystal can be written in the form

$$f(n)=4\pi\sum_{r} N_r\alpha_r, \qquad \text{. . . . . (1)}$$

where N_r is the number per unit-volume of the r type of oscillator which has a polarizability α_r. The form of the function $f(n)$ depends on the so-called ' internal field ' in the crystal. Two forms are commonly used, viz., the Sellmeier form $f(n)=n^2-1$ and the Lorentz–Lorenz form $f(n)=(n^2-1)/(n^2+2)$. In a paper appearing elsewhere, the authors have shown from the experimental refraction and absorption data that the first form is more applicable to crystals, which is therefore adopted in this paper. Replacing the summations on the right-hand side of eqn. (1) by a term $N\alpha$, where N is the total number of oscillators per cm^3 and α the average polarizability of each, we have

$$n^2-1=4\pi N\alpha. \qquad \text{. . . . . (2)}$$

For an analysis of thermo-optic and piezo-optic data in the visible region, where the absorption frequencies are far away, we can justifiably use this simplified ' one-term dispersion formula '.

When p or T is changed, both N and α will alter. The change in N is completely determined by the change in the density, i.e.,

$$\frac{dN}{dp}=\frac{dN}{d\rho}\cdot\frac{d\rho}{dp}\,; \qquad \frac{dN}{dT}=\frac{dN}{d\rho}\cdot\frac{d\rho}{dT}, \qquad \text{. . . . . . (3)}$$

and since N is proportional to ρ, $dn/d\rho=N/\rho$. The polarizability α is, in general, a function of both the density and the temperature i.e.,

$$\frac{d\alpha}{dp}=\frac{\partial\alpha}{\partial\rho}\cdot\frac{d\rho}{dp}\,; \qquad \frac{d\alpha}{dT}=\frac{\partial\alpha}{\partial\rho}\cdot\frac{d\rho}{dT}+\left(\frac{\partial\alpha}{\partial T}\right)_{\rho}. \qquad \text{. . . . . (4)}$$

Now

$$\frac{d\rho}{dp}=\beta\rho \quad\text{and}\quad \frac{d\rho}{dT}=-\gamma\rho, \qquad \text{. . . . . . . (5)}$$

where β and γ are respectively the compressibility and the coefficient of cubical expansion.

Differentiating eqn. (2) and substituting from eqns. (3), (4) and (5) we have

$$\frac{dn}{dp}=\beta\frac{n^2-1}{2n}\left[1+\frac{\rho}{\alpha}\left(\frac{\partial\alpha}{\partial\rho}\right)_T\right], \quad \ldots\ldots \quad (6)$$

and

$$\frac{dn}{dT}=-\gamma\frac{n^2-1}{2n}\left[1+\frac{\rho}{\alpha}\left(\frac{\partial\alpha}{\partial\rho}\right)_T+\frac{1}{\alpha}\left(\frac{\partial\alpha}{\partial T}\right)_\varrho\right]. \quad \ldots \quad (7)$$

It is thus possible to separate dn/dT into three parts, due to (*a*) the change in number of oscillators per cm³, (*b*) the change in polarizability caused by thermal expansion, (*c*) a pure temperature effect on polarizability. These parts are respectively denoted by P, Q, R in conformity with the earlier notation of one of the authors (Ramachandran 1947). We have from eqns. (6) and (7)

$$\left.\begin{aligned}
P&=\left(\frac{\partial n}{\partial N}\right)_\alpha\cdot\frac{dN}{dT}=-\gamma\frac{n^2-1}{2n},\\
Q&=\left(\frac{\partial n}{\partial\alpha}\right)_N\cdot\frac{\partial\alpha}{\partial\rho}\cdot\frac{d\rho}{dT}=-\gamma\left[\frac{1}{\beta}\frac{dn}{dp}-\frac{n^2-1}{2n}\right],\\
R&=\left(\frac{\partial n}{\partial\alpha}\right)_N\left(\frac{d\alpha}{\partial T}\right)_\varrho=\frac{dn}{dT}+\frac{\gamma}{\beta}\frac{dn}{dp}.
\end{aligned}\right\} \quad \ldots \quad (8)$$

These equations enable us to calculate P, Q, R in terms of the macroscopically measurable quantities dn/dp, dn/dT, γ and β. It is also evident that

$$\frac{dn}{dT}=P+Q+R; \qquad \frac{dn}{dp}=-\frac{\beta}{\gamma}(P+Q). \quad \ldots\ldots \quad (9)$$

Using the data for γ and β available in the standard tables, values of P, Q, R have been computed for a number of crystals and are shown in table 1.

Table 1. Values of P, Q, R in Crystals at 5893 Å

Crystal		n	$10^5\,dn/dT$	$10^5\gamma$	$\rho\left(\frac{\partial n}{\partial\rho}\right)_T$	$P.10^5$	$Q.10^5$	$R.10^5$	$\lvert Q/R\rvert$
NaCl		1·544	−3·8	12·0	0·24	−5·4	2·5	−0·9	2·8
KCl		1·490	−3·6	11·4	0·23	−4·7	2·1	−1·0	2·1
KBr		1·559	−3·6	12·0	0·35	−5·6	1·4	+0·6	2·4
KI		1·667	−5·0	13·5	0·43	−7·2	1·4	+0·8	1·8
LiF		1·392	−1·3	10·2	0·1	−3·4	2·4	−0·3	8·0
CaF_2		1·434	−1·2	5·7	0·25	−2·1	0·7	+0·2	3·5
MgO		1·736	+1·6	3·9	−0·4	−2·2	3·6	+0·2	1·8
Diamond		2·417	+1·0	1·3	−0·28	−1·3	1·66	+0·64	2·7
Quartz	ω	1·544	−0·65	3·5	0·32	−1·6	0·3	+0·6	0·5
	ϵ	1·553	−0·75	3·5	0·40	−1·6	0·2	+0·7	0·3
Topaz	α	1·596	+0·81	1·52	0·03	−0·6	0·55	+0·9	0·6
	β	1·610	+0·90	1·52	0·04	−0·7	0·6	+0·9	0·7
	γ	1·6778	+0·80	1·52	0·04	−0·7	0·6	+0·9	0·7
Calcite	ω	1·658	+0·07	1·58	0·75	−0·8	−0·06	+1·3	0·05
	ϵ	1·486	+1·06	1·58	−0·13	−0·6	0·45	+0·9	0·5

The table shows that, irrespective of the sign of dn/dT, Q is always positive and R is generally positive. Thus the polarizability increases with expansion and usually increases with temperature. The universal negative value of P is clearly due to the decrease in density on heating.

The table has been so arranged that the first half consists of crystals which are usually classed as ionic and the second half consists of crystals having covalent linkages. Calcite is considered covalent since its optical properties are determined by the CO_3 ion, which in itself is covalent in character. It is seen that in ionic crystals the magnitude of the pure temperature coefficient R is smaller relatively to Q, than in covalent crystals. This is only a general trend, diamond being a notable exception. Further our derivation of P, Q, R pertains, strictly speaking, only to isotropic crystals, so that the values for calcite should not be regarded as accurate. Finally, it should be mentioned that the experimental determination of elasto-optic constants are not very accurate. Since the magnitudes of P, Q and R are very much affected by the value of dn/dp used, the whole of table 1 should be regarded only as semiquantitative in character.

§3. EXPLANATION OF THE PURE TEMPERATURE EFFECT

Consider the simple example of a diatomic molecule, and let r_0 be the equilibrium inter-atomic distance at the temperature T. As the temperature is raised, r_0 increases and further the instantaneous separation distance r executes vibrations of increased amplitude about the mean value r_0. If ν_r be the frequency of vibration and A its amplitude, then the displacement of an atom at any instant from its equilibrium position with respect to the other atom may be written

$$\Delta r = A \cos 2\pi\nu_r t. \qquad (10)$$

Now the optical polarizability α may be expanded in a Taylor series in Δr as

$$\alpha(r_0+\Delta r)=\alpha(r_0)+\left(\frac{\partial\alpha}{\partial r}\right)_0 \Delta r+\frac{1}{2}\left(\frac{\partial^2\alpha}{\partial r^2}\right)_0 (\Delta r)^2+\ldots \qquad (11)$$

We shall hereafter neglect higher terms than the second since $\Delta r \ll r$. We have assumed that the molecule vibrates harmonically about an equilibrium position, since the presence of non-linear restoring forces would only result in the mean distance being different from r_0 and in the presence of higher harmonics of ν_r. These will not affect our discussion.

Substituting value of Δr from eqn. (10) in eqn. (11) and integrating over a cycle of ν_r, one finds the mean polarizability to be

$$\alpha=\alpha(r_0)+\frac{A^2}{4}\left(\frac{\partial^2\alpha}{\partial r^2}\right)_0 . \qquad (12)$$

This picture is valid for a diatomic molecule. But as a simplified extrapolation, we suppose it to be valid for a crystal also. In doing this we neglect many finer details. For instance a crystal will have not one, but many thermal lattice vibration frequencies. We shall provide in a rough way for this by taking A to be the root mean square amplitude of the thermal vibrations. From eqn. (12) we have

$$\left(\frac{\partial\alpha}{\partial\rho}\right)_T=\left(\frac{\partial\alpha}{\partial r}\right)_0\frac{dr_0}{d\rho}+\left(\frac{\partial^2\alpha}{\partial r^2}\right)_0\left(\frac{\partial A^2/4}{\partial\rho}\right)_T. \quad . \quad . \quad . \quad (13)$$

When the crystal is compressed isothermally, all linear distances are altered, and since $r_0\propto\rho^{-1/3}$,

$$dr_0/d\rho=-r_0/3\rho. \quad . \quad . \quad . \quad . \quad . \quad . \quad . \quad . \quad . \quad (14)$$

Further, the vibration amplitude A is, at least to a first order, only a function of the temperature of the crystal, so that we may write

$$(\partial A^2/\partial\rho)_T=0. \quad . \quad . \quad . \quad . \quad . \quad . \quad . \quad . \quad . \quad (15)$$

Hence we obtain

$$\left(\frac{\partial\alpha}{\partial\rho}\right)_T=-\frac{r_0}{3\rho}\left(\frac{\partial\alpha}{\partial r}\right)_0. \quad . \quad . \quad . \quad . \quad . \quad . \quad . \quad (16)$$

Likewise

$$\left(\frac{\partial\alpha}{\partial T}\right)_\rho=\frac{1}{4}\frac{dA^2}{dT}\left(\frac{\partial^2\alpha}{\partial r^2}\right)_0. \quad . \quad . \quad . \quad . \quad . \quad . \quad . \quad (17)$$

Thus we see that the pure temperature effect arises from the presence of the additional factor dA^2/dT governing thermo-optic phenomena. Since this factor is always positive, the sign of R depends on $(\partial^2\alpha/\partial r^2)$, i.e., the coefficient of the quadratic term in the Taylor expansion.

From the above equations it is possible to find the relative orders of magnitude of α, $(\partial\alpha/\partial r)_0$ and $(\partial^2\alpha/\partial r^2)_0$. We have

$$\alpha\bigg/\left(\frac{\partial\alpha}{\partial r}\right)_0=-\frac{r_0}{3}\frac{P}{Q}, \quad . \quad . \quad . \quad . \quad . \quad . \quad . \quad . \quad (18)$$

and

$$\left(\frac{\partial\alpha}{\partial r}\right)_0\bigg/\left(\frac{\partial^2\alpha}{\partial r^2}\right)_0=\frac{3}{4}\frac{dA^2/dT}{\gamma r_0}\frac{Q}{R}. \quad . \quad . \quad . \quad . \quad . \quad (19)$$

From table 1, it will be seen that P/Q and Q/R are of the order of unity. Now the following values may be taken as representative of the various quantities involved : $r=2\times10^{-8}$ cm, $\gamma=10^{-4}$, $A=0{\cdot}2$ Å (Lonsdale 1948) at room temperature. Neglecting zero-point energy, we may estimate dA^2/dT simply as A^2/T, T being 300° K. From these values one obtains

$$\alpha\sim10^{-8}(\partial\alpha/\partial r)\sim10^{-16}(\partial^2\alpha/\partial r^2). \quad . \quad . \quad . \quad . \quad . \quad . \quad (20)$$

Thus, if the distance r is measured in Ångströms, α and its derivatives are all of the same order of magnitude. Substituting this result in the Taylor expansion (11), and remembering that Δr is of the order of 0·2 Å, we see that terms in the Taylor expansion beyond the second may be safely neglected.

§4. COMPARISON WITH LIGHT SCATTERING DATA

It is well known that the intensities of Rayleigh and Raman scattering by a transparent medium are also governed by the quantities α, $\partial\alpha/\partial r$ and $\partial^2\alpha/\partial r^2$. A rigorous theoretical treatment which enables one to predict the scattered intensities in any particular crystal is a very complicated problem, and is in any case beyond the scope of this paper. But as a very rough approximation one may take the well-known expressions for the intensity scattered by molecules (cf. Bhagavantham's 'Scattering of Light and the Raman Effect', Ch. V) and modify these to suit the case of crystals. Using the Sellmeier dispersion formula, one obtains the following expressions for the ratios between Rayleigh scattering intensity I_R, first order Raman scattering I_1 and second order Raman scattering I_2:

$$\frac{I_R}{I_1}=4\left(\frac{P+Q}{P}\right)^2\frac{NkT\beta}{\sigma^2}\left(\frac{\alpha}{\partial\alpha/\partial r}\right)^2, \quad . \; . \; . \; . \quad (21)$$

and

$$\frac{I_1}{I_2}=\frac{4}{\sigma^2}\left(\frac{\partial\alpha/\partial r}{\partial^2\alpha/\partial r^2}\right)^2, \quad . \; . \; . \; . \; . \; . \; . \quad (22)$$

where N is the number of oscillators per cm³, and σ is the amplitude of oscillation, given by

$$2\pi^2\mu\sigma^2\nu_r^2=h\nu_r, \quad . \; . \; . \; . \; . \; . \; . \; . \; . \quad (23)$$

μ being the reduced mass of the oscillator.

These expressions are not rigorous formulae for scattered intensities, but demonstrate how the ratio of α to its derivatives influences the intensity in the three types of scattering. Experimental data on scattered intensities are very scanty. But from values in diamond (Krishnan and Narayanan 1950) and quartz (Krishnan and Chandrasekharan 1950) and from the experience of workers in this laboratory (Chandrasekharan, personal communication) one concludes that, in crystals, first order Stokes–Raman lines have an intensity lying between 0·1 to 10 times the intensity of unmodified scattering, while the second order lines have a few hundredths of the intensity of the first order. Taking β as 3×10^{-12} and N as 10^{23}, which are representative values for many crystals, and $(P+Q)/P$ as 2, we can evaluate the ratio of α to its derivatives from eqns. (21) and (22). We then get the results

$$\alpha/(\partial\alpha/\partial r)\sim10^8 \quad\text{and}\quad (\partial\alpha/\partial r)/(\partial^2\alpha/\partial r^2)\sim10^8, \quad . \; . \quad (24)$$

which are in accord with the orders of magnitude obtained from thermo-optic and piezo-optic data.

§5. THE VARIATION OF *dn/dT* WITH TEMPERATURE

Substituting eqns. (16) and (17) in eqn. (7) we have

$$Q=\gamma\frac{n^2-1}{2n}\frac{r_0}{3\alpha}\left(\frac{\partial\alpha}{\partial r}\right)_0; \qquad R=\frac{n^2-1}{2n}\frac{dA^2}{dT}\frac{1}{4\alpha}\left(\frac{\partial^2\alpha}{\partial r^2}\right)_0. \quad . \; . \; . \quad (25)$$

Since dA^2/dT is proportional to the rate of change of thermal energy with temperature, i.e., C_v, we may write

$$\frac{dn}{dT}=P+Q+R=a\gamma+bC_v, \qquad (26)$$

where a and b are practically constants. Now for solids, $C_v \approx C_p$ and further, C_p is approximately proportional to γ (Gruneisen's law). Hence we get the approximate relation

$$\frac{dn}{dT} \propto C_p \text{ or } \propto \gamma. \qquad (27)$$

This in fact is found to be the case in crystals, dn/dT being very small at low temperatures and increasing with temperature in a manner similar to γ. Of course the proportionality cannot be expected to be strictly valid at all temperatures, since we have no reason to assume that $\partial\alpha/\partial r$ or $\partial^2\alpha/\partial r^2$ is unaffected by temperature changes. But in diamond and quartz it holds to a fair degree of accuracy as shown in table 2.

Table 2. Relation between dn/dT and γ in Diamond and Quartz

Temp. (deg. c)	Diamond			Quartz		
	(1) $+10^5\,dn/dT$	(2) $10^5\gamma$	$(dn/dT)/\gamma$	(3) $-10^5\,dn/dT$	(4) $10^5\gamma$	$(dn/dT)/\gamma$
−150	0·01	—	—	4·4	1·9	2·3
−100	0·19	0·09	2·1	4·8	2·52	1·9
−50	0·50	0·17	2·9	5·2	2·98	1·8
0	0·84	0·29	2·9	5·65	3·36	1·7
50	1·19	0·43	2·8	6·15	3·68	1·7
100	1·54	0·55	2·8	6·75	4·00	1·7
150	1·91	0·65	2·9	7·40	4·33	1·7
200	2·41	0·77	3·1	8·20	4·66	1·8
250	2·67	0·85	3·1	9·20	5·04	1·8
300	2·98	0·92	3·2	10·5	5·49	1·9
350	3·32	0·98	3·4	13·0	—	—
400	3·62	1·03	3·5	14·6	6·74	2·2

(1) Ramachandran, 1947 ; (2) Krishnan, 1946 ; (3) Radhakrishnan, 1947 ; (4) Sosman, 1927.

For a crystal having a dispersion formula of the form

$$n^2-1=b/(\nu_0^2-\nu^2), \qquad (28)$$

the variation of dn/dT with wavelength can be expressed by the formula (Ramachandran 1947)

$$\frac{dn}{dT}+\frac{n^2-1}{2n}\gamma=\frac{b\nu_0^4}{n(\nu_0^2-\nu^2)^2}\cdot\chi_T, \qquad (29)$$

where χ_T is defined by the relation

$$\chi_T=-\frac{1}{\nu_0}\frac{d\nu_0}{dT}=\frac{1}{\lambda_0}\frac{d\lambda_0}{dT}. \qquad (30)$$

It is found that χ_T is in general positive, is very small at low temperatures, and increases with temperature. Since both the terms on the left hand side are proportional to γ, one should also expect that

$$\chi_T \propto \gamma. \qquad (31)$$

This enables one to understand the trend of the observed variation of χ_T with temperature.

§ 6. CALCULATION OF dn/dT AND dn/dp FOR A CUBIC LATTICE

In crystals like the alkali halides, the polarizability and hence the refractive index is mostly due to one type of ion. Let α_g be its polarizability in isolation (e.g. in the gaseous state) and α_c its polarizability in the crystal, which has only one component for a cubic crystal. Then α_c is given by (Bragg 1924)

$$\alpha_c = \alpha_g + \sum_j \frac{3\cos^2\theta_j - 1}{r_j^3}\alpha_g^2, \qquad (32)$$

where r_j is the length of the vector $\mathbf{r}_j$ joining an atom j (coordinates x_j, y_j, z_j) to a chosen origin and θ_j is the angle between $\mathbf{r}_j$ and the direction of the incident electric vector. But the last term in eqn. (32) is identically equal to zero for a cubic arrangement of ions about a central ion* (Mott and Gurney 1940). Thus

$$\alpha_c = \alpha_g, \qquad (33)$$

so that

$$\rho\left(\frac{\partial\alpha}{\partial\rho}\right)_T = 0, \qquad (34)$$

and from eqn. (6),

$$\frac{dn}{dp} = \beta\frac{n^2-1}{2n}. \qquad (35)$$

The right hand side is proportional to P and the theory leads to the result that $Q=0$. This is not in agreement with experiment, since Q is finite and positive for most crystals. This is not surprising since the theory takes into account only the purely electrostatic interactions between neighbouring ions. It is conceivable that the polarizability would alter owing to deformation of the electron atmosphere of the ions when the crystal is compressed and the effect of this has been neglected. Actually, even the result (33) is contrary to facts for the values of α_g and α_c, derived by Burstein and Smith (1948) from the experimental data, are not equal to each other. The difference arises because one cannot assume *a priori* that the ion has exactly the same structure in the gaseous and the crystalline states. Owing to the packing in the crystal, the electron atmosphere of the ion would suffer a certain amount of distortion, leading to a change in its inherent polarizability.

---

* We are grateful to the referee for certain suggestions on this point.

On the basis of the same considerations, one can also work out the value of the pure temperature effect, R. As a simplification, we may picture the random thermal motion of the atoms in a cubic crystal to be as follows: A particular atom is considered to be executing simple harmonic vibrations with all possible orientations, the other atoms being considered to be at rest. If Δr is the amplitude of vibration for a particular orientation, with components Δx, Δy, Δz, then its time-averaged contribution to the polarizability is, to a second order, given by the generalization of eqn. (11) as

$$\Delta\alpha = \frac{1}{4}\Bigg[\left(\frac{d^2\alpha}{\partial x^2}\right)_0 (\Delta x)^2 + \left(\frac{\partial^2\alpha}{\partial y^2}\right)_0 (\Delta y)^2 + \left(\frac{\partial^2\alpha}{\partial z^2}\right)_0 (\Delta z)^2$$

$$+2\left(\frac{\partial^2\alpha}{\partial x\partial y}\right)_0 \Delta x\Delta y + 2\left(\frac{\partial^2\alpha}{\partial y\partial z}\right)_0 \Delta y\Delta z + 2\left(\frac{\partial^2\alpha}{\partial z\partial x}\right)_0 \Delta z\Delta x\Bigg]. \quad . \quad . \quad (36)$$

Writing

$$\Delta x = \Delta r \sin\phi\cos\theta, \quad \Delta y = \Delta r \sin\phi\sin\theta, \quad \Delta z = \Delta r\cos\phi, \qquad (37)$$

and integrating over all possible values of θ and ϕ, one obtains the mean value of $(\Delta x)^2$ over all orientations as

$$\frac{1}{4\pi}\int_0^{2\pi}\int_0^{\pi/2} (\Delta x)^2\, 2\pi \sin\phi\, d\phi\, d\theta = \frac{(\Delta r)^2}{3} \quad . \quad . \quad . \quad . \quad (38)$$

and the same values for $(\Delta y)^2$ and $(\Delta z)^2$. The mean values of the cross-products $\Delta x \Delta y$ etc., vanish. Thus

$$\Delta\alpha = \frac{(\Delta r)^2}{12}\left(\frac{\partial^2\alpha}{\partial x^2} + \frac{\partial^2\alpha}{\partial y^2} + \frac{\partial^2 y}{\partial z^2}\right)_0 = \frac{(\Delta r)^2}{12}\nabla^2\alpha. \quad . \quad . \quad . \quad (39)$$

Now,

$$\nabla^2\{(3\cos^2\theta_j - 1)/r_j^3\} \equiv 0, \quad . \quad . \quad . \quad . \quad . \quad . \quad (40)$$

for every atom j. Thus, even if the summation in the last term in eqn. (32) does not lead to zero, $\Delta\alpha_c = 0$, provided the vibrations of the individual atoms are isotropic. In any case, we obtain the result that $(\partial\alpha/\partial T)_\varrho = 0$. On the other hand, the fact that the coefficient R is finite in cubic crystals shows that actually $(\partial\alpha/\partial T)_\varrho$ is not equal to zero. As in the case of the piezo-optic coefficient, this discrepancy between theory and experiment is to be attributed to the fact that we have neglected the distortion of the electron atmospheres caused by thermal vibration. Such effects appear to be quite sensible, judged from the magnitude of the discrepancy both for Q and R. It follows therefore that one cannot expect to furnish a reasonable theory of photo-elasticity in crystals, based only on considerations of electrostatic interaction between neighbours.

We are grateful to Prof. R. S. Krishnan for his interest in this work.

REFERENCES

BHAGAVANTAM, S., 1942, *Scattering of Light and the Raman Effect* (Waltair : Andhra University), Ch. V.

BRAGG, W. L., 1924, *Proc. Roy. Soc.* A, **105,** 370.

BURSTEIN, E., and SMITH, P., 1948 a, *Proc. Ind. Acad. Sci.* A, **28,** 377 ; 1948 b, *Phys. Rev.*, **74,** 229 ; 1949, *Ibid.*, **76,** 175.

KRISHNAN, R. S., 1946, *Proc. Ind. Acad. Sci.* A, **24,** 33.

KRISHNAN, R. S., and CHANDRASEKHARAN, V., 1950, *Proc. Ind. Acad. Sci.* A, **31,** 427.

KRISHNAN, R. S., and NARAYANAN, P. S., 1950, *Proc. Ind. Acad. Sci.* A, **32,** 352.

LONSDALE, K., 1948, *Acta Cristallogr.*, **1,** 142.

MICHELI, F., 1902, *Ann. d. Phys.*, **7,** 772.

MOTT, N. F., and GURNEY, R. W., 1946, *Electronic Processes in Ionic Crystals* (Oxford : Clarendon Press), Ch. I.

POCKELS, F., 1902, *Ann. d. Phys.*, **7,** 745.

RADHAKRISHNAN, T., 1947, *Proc. Ind. Acad. Sci.* A, **27,** 44 ; 1950, *Ibid.*, **32,** 224, 229 ; 1951, *Ibid.*, **33,** 22.

RAMACHANDRAN, G. N., 1947, *Proc. Ind. Acad. Sci.* A, **25,** 266 ; 1950, *Ibid.*, **32,** 171.

REED, J. O., 1898, *Ann. Phys. Chem.*, **65,** 734.

SOSMAN, R. B., 1927, *Properties of Silica*, A. C. S. Monographs.

XXVII. *A Calculation of the Cohesive Energies and Pressure/Volume Relations of the Divalent Metals*

By S. Raimes
Department of Mathematics, Imperial College, London*

[Received November 7, 1951]

Summary

A method is described for calculating the energy of the lowest state ψ_0 of a divalent metal. This approximates to the well-known cellular method, but assumptions made regarding ψ_0, together with the use of a single empirical ionization potential, render unnecessary the explicit calculation of an ion-core field. An expression for the total energy of the valence electrons is obtained, the free-electron approximation being used tentatively in evaluating all terms except the energy of the lowest state, and this is then applied to the calculation of the atomic radii, compressibilities, and cohesive energies of the divalent metals. The change of volume for a range of pressures up to 100 000 kg/cm^2 is also calculated and found to be in good agreement with the experimental data of Bridgman.

§1. Introduction

The difficulties encountered when an ion-core field of the Hartree type is used in calculating the cohesive energy of a polyvalent metal have been demonstrated in a recent application of the cellular method to magnesium (Raimes 1950). In particular, it is necessary to know the correlation energy of the valence electrons in a free atom, which, at present, can only be estimated in a heuristic manner. This difficulty might be overcome by the use of a semi-empirical ion-core field, like that of Prokofjew (1929) for sodium, but so far no such field has been constructed for a polyvalent metal. The present work attempts to circumvent both the drawbacks of the Hartree field and the labour of constructing a semi-empirical field by extending to polyvalent metals an approximate method first applied by Fröhlich (1937) to the alkali metals. Only the divalent metals are considered here, because it is believed that the various approximations involved apply best to these metals, but the treatment can easily be made quite general.

Although the method was originally designed for the purpose stated above, its greatest advantage has been found in calculating changes of volume with pressure. The total energy of a metal is here obtained as an analytical function of the atomic radius, so that the pressure corresponding to a given volume can be computed directly with an accuracy

---

* Communicated by Professor H. Jones.

greater than in the ordinary cellular method, where the total energy is obtained as a tabulated function. It will be seen in § 4 that the theoretical curves giving compression as a function of pressure, in the calculation of which no empirical data for the solids have been used, are in good agreement with the experimental results of Bridgman (1941, 1948), for a range of pressures up to 100 000 kg/cm^2.

The possibility of employing the present method depends upon a result of the work on magnesium mentioned previously. The field there used in computing ψ_0, the wave function for the state of lowest energy, consisted of two parts—the field of the ion-core and the field of the valence electrons. Two alternatives were considered for the latter part, namely, the field due to all the valence electrons and that due to electrons with one type of spin only, and it was found that the calculated total energy of the metal was not significantly different in the two cases. This suggests that ψ_0 could, with slight loss in accuracy, be calculated using the ion-core field only, as for the monovalent metals, provided that the Coulomb interaction of the valence electrons is accounted for by an additional term in the expression for the total energy. The Coulomb term, per atom of the metal, is just the self-potential energy of the valence-electron charge distribution within an atomic sphere.

§ 2. THE STATE OF LOWEST ENERGY

According to the argument presented above, a good approximation to the wave function $\psi_0(r)$ of the lowest state may be obtained by solving the Schrödinger equation

$$\frac{d^2\psi_0}{dr^2}+\frac{2}{r}\frac{d\psi_0}{dr}+[\epsilon_0(r_s)-V(r)]\psi_0=0, \quad . \quad . \quad . \quad . \quad . \quad . \quad (1)$$

subject to the boundary condition

$$\left(\frac{d\psi_0}{dr}\right)_{r=r_s}=0, \quad . \quad . \quad . \quad . \quad . \quad . \quad . \quad . \quad . \quad (2)$$

where $V(r)$ is the potential energy of an electron in the field of the ion-core, and r_s is the atomic radius.*

We wish to evaluate $\epsilon_0(r_s)$ for atomic radii in the neighbourhood of r_0, where r_0 is the value of r_s for which ϵ_0 reaches its minimum. It will be assumed that, in this range of r_s, $\psi_0(r)$ is nearly constant over most of the atomic volume. Furthermore, we shall confine ourselves to the region lying outside the ion-core, so that it is sufficiently accurate to put $V(r)=-4/r$, for a divalent metal; it is, of course, necessary that r_0 lie in this region, and it will be seen later (table 1) that this is so for all the divalent metals except mercury. The calculation may follow almost exactly that of Fröhlich (1937) for the alkali metals, but the following modification has the advantage of showing more clearly what approximations are essential to each stage of the work.

---

* In this paper, unless otherwise stated, energies are in Rydberg units and lengths in Bohr units.

Writing $R = r\psi_0$, eqn. (1) becomes

$$\frac{d^2R}{dr^2} + [\epsilon_0(r_s) - V(r)]R = 0, \qquad (3)$$

and the boundary condition (2) becomes

$$\frac{dR}{dr} = \frac{R}{r} \quad \text{at} \quad r = r_s. \qquad (4)$$

It is to be noted that, through eqn. (4), R is a function of r_s as well as of r. Hence, denoting differentiation with respect to r_s by a dash, we have

$$\frac{d^2R'}{dr^2} + [\epsilon_0 - V(r)]R' + \epsilon_0'R = 0, \qquad (5)$$

or, using eqn. (3),

$$\frac{d^2R'}{dr^2} - \frac{R'}{R}\frac{d^2R}{dr^2} + \epsilon_0'R = 0. \qquad (6)$$

Therefore,

$$\epsilon_0' \int_0^{r_s} R^2\,dr = \int_0^{r_s} \left[R'\frac{d^2R}{dr^2} - R\frac{d^2R'}{dr^2} \right] dr = \left[R'\frac{dR}{dr} - R\frac{dR'}{dr} \right]_{r=r_s} \qquad (7)$$

We now differentiate boundary condition (4) with respect to r_s, and obtain

$$\left[\frac{d^2R}{dr^2} + \frac{dR'}{dr} \right]_{r=r_s} = \left[\frac{R'}{r} \right]_{r=r_s}, \qquad (8)$$

so that eqn. (7) reduces to

$$\epsilon_0' \int_0^{r_s} R^2\,dr = \left[R\frac{d^2R}{dr^2} \right]_{r=r_s} = [V(r_s) - \epsilon_0][R(r_s)]^2. \qquad (9)$$

So far the treatment (cf. Bardeen 1938) has been exact, but now, consistent with our assumption that ψ_0 is nearly constant, we make the approximation that

$$\frac{4\pi}{3} r_s^3[\psi_0(r_s)]^2 = \frac{4\pi}{3} r_s[R(r_s)]^2 = 1,$$

when ψ_0 is normalized to unity in the atomic sphere; in other words, we assume that the charge density at the surface of the atomic sphere is equal to the mean charge density taken over the volume of the sphere. Eqn. (9) now becomes

$$\frac{d\epsilon_0}{dr_s} = \frac{3}{r_s}[V(r_s) - \epsilon_0]. \qquad (10)$$

Using the further approximation that $V(r_s) = -4/r_s$ in the required range of r_s, eqn. (10) may be integrated to give

$$\epsilon_0(r_s) = \frac{A}{r_s^3} - \frac{6}{r_s}, \qquad (11)$$

where A is a constant.

Since r_0 is the atomic radius corresponding to the minimum eigenvalue, it follows that $A=2r_0^2$ and

$$\epsilon_0(r_s)=2\left(\frac{r_0^2}{r_s^3}-\frac{3}{r_s}\right). \quad . \quad . \quad . \quad . \quad . \quad . \quad . \quad . \quad (12)$$

This differs from the expression obtained for the alkali metals only in the factor 2. It remains to determine r_0.

Let $\psi_{0,0}$ be the wave function for atomic radius r_0, so that

$$\frac{d^2\psi_{0,0}}{dr^2}+\frac{2}{r}\frac{d\psi_{0,0}}{dr}+[\epsilon_0(r_0)-V(r)]\psi_{0,0}=0, \quad . \quad . \quad . \quad . \quad (13)$$

and

$$\left(\frac{d\psi_{0,0}}{dr}\right)_{r=r_0}=0. \quad . \quad . \quad . \quad . \quad . \quad . \quad . \quad . \quad (14)$$

Also, let us write ψ_0 and its corresponding eigenvalue $\epsilon_0(r_s)$ as

$$\psi_0=\psi_{0,0}f(r), \quad . \quad . \quad . \quad . \quad . \quad . \quad . \quad . \quad . \quad (15)$$

and

$$\epsilon_0(r_s)=\epsilon_0(r_0)+\eta(r_s). \quad . \quad . \quad . \quad . \quad . \quad . \quad . \quad . \quad (16)$$

Substituting (15) and (16) in eqn. (1), and using eqn. (13), we find

$$\frac{d^2f}{dr^2}+\frac{2}{\psi_{0,0}}\frac{d\psi_{0,0}}{dr}\frac{df}{dr}+\frac{2}{r}\frac{df}{dr}+\eta f=0. \quad . \quad . \quad . \quad . \quad . \quad (17)$$

We shall only be interested in the values of $d\psi_0/dr$ and ψ_0 at $r=r_0$, where $d\psi_{0,0}/dr$ is zero, so that, for our purposes, eqn. (17) reduces almost exactly to

$$\frac{d^2f}{dr^2}+\frac{2}{r}\frac{df}{dr}+\eta f=0. \quad . \quad . \quad . \quad . \quad . \quad . \quad . \quad . \quad (18)$$

Hence

$$f(r)=B\frac{\cos\beta r}{r}+C\frac{\sin\beta r}{r},$$

where $\beta=\sqrt{\eta}$, and B and C are functions of r_s. Now, when $\beta\rightarrow 0$, $f(r)$ must tend to the constant value unity, so that, provided β is small, it is reasonable to neglect the cosine term and write, near $r=r_0$,

$$f(r)=\frac{\sin\beta r}{\beta r}. \quad . \quad . \quad . \quad . \quad . \quad . \quad . \quad . \quad . \quad (19)$$

From eqns. (14), (15), and (19) we obtain

$$\left(\frac{1}{\psi_0}\frac{d\psi_0}{dr}\right)_{r=r_0}=\frac{1}{r_0}(\beta r_0\cot\beta r_0-1), \quad . \quad . \quad . \quad . \quad (20)$$

which will be required in the evaluation of r_0. It may be observed that in deriving this expression it has not been necessary to determine $\psi_{0,0}$ explicitly, as in Fröhlich's treatment, nor has any assumption been made regarding $V(r)$; in fact, the only real approximation has been the neglect of the cosine term in $f(r)$.

When r_s tends to infinity, eqn. (1) becomes that of the single remaining valence electron in a free atom when one valence electron has been removed, and $-\epsilon_0(r_s)$ is then just the second ionization potential of the neutral atom, which we shall denote by I_2. In the case of the alkali metals, of course, the first ionization potential is used, but the rest of the procedure follows closely that of Fröhlich. In the region where $V(r)$ is hydrogenic the Schrödinger equation for the state ψ of the valence electron in the free, singly-charged, ion is

$$\frac{d^2\psi}{dr^2}+\frac{2}{r}\frac{d\psi}{dr}+\left(\frac{4}{r}-I_2\right)\psi=0. \qquad . \quad . \quad . \quad . \quad . \quad . \quad (21)$$

This equation may be solved to give an asymptotic series for ψ, of which only the first two terms need be retained; thus,

$$\psi=e^{-\omega r}r^{m-1}\left[1-\frac{m(m-1)}{2\omega r}\right], \qquad . \quad . \quad . \quad . \quad . \quad . \quad (22)$$

where $\omega^2=I_2$, and $m=2/\omega$.

Now ψ is simply that particular function ψ_0 which corresponds to the value of β given by

$$\beta_\infty{}^2=-\epsilon_0(r_0)-I_2=\frac{4}{r_0}-\omega^2. \qquad . \quad . \quad . \quad . \quad . \quad . \quad . \quad (23)$$

Hence, from eqn. (20), we may write

$$\left(\frac{1}{\psi}\frac{d\psi}{dr}\right)_{r=r_0}=\frac{1}{r_0}(\beta_\infty r_0 \cot \beta_\infty r_0-1),$$

and, using eqns. (22) and (23), the resulting equation for r_0 is

$$r_0{}^2-\frac{2+\omega}{\omega^3}r_0+\frac{(2-\omega)^2}{\omega^5}+\left[\frac{r_0}{\omega}-\frac{2-\omega}{\omega^4}\right]\xi \cot \xi=0, \qquad . \quad . \quad (24)$$

where $\xi=\sqrt{(4r_0-\omega^2r_0{}^2)}$.

The experimental values of the ionization potentials, taken from the compilation of Bacher and Goudsmit (1932), together with the calculated values of r_0, are shown in table 1. The values of the ionic radius r_i, as calculated by Pauling (1927), are also given, and it is seen that r_0 is less than r_i only in the case of mercury; the present method is therefore inapplicable to this metal, and it will be omitted from further consideration.

Table 1

	Be	Mg	Ca	Sr	Ba	Zn	Cd	Hg
I_2	1·332	1·100	0·869	0·807	0·732	1·315	1·238	1·373
r_0	1·96	2·56	3·49	3·83	4·33	1·99	2·17	1·87
r_i	0·59	1·23	1·87	2·14	2·55	1·40	1·83	2·08

I_2 (Rydberg units) is the second ionization potential of a free atom, from Bacher and Goudsmit (1932); r_0 (Bohr units) is the calculated atomic radius corresponding to the minimum value of $\epsilon_0(r_s)$; r_i (Bohr units) is the ionic radius, from Pauling (1927).

§3. THE TOTAL ENERGY OF THE METAL

The eigenvalue $\epsilon_0(r_s)$ is only one of several terms comprising the total energy of the metal, and the remaining terms will be evaluated tentatively as for free electrons. This is, of course, a more doubtful approximation for the divalent metals than for the alkali metals, but previous work on magnesium indicates that it may not be unreasonable ; in any case comparison of the results with experiment might give some information about the true magnitudes of the energy terms, particularly the Fermi energy, in relation to the free-electron values.

Using the same method as for magnesium (Raimes 1950, pp. 575–6) the total energy per electron of the metal is found to be

$$E(r_s)=2\left(\frac{r_0^2}{r_s^3}-\frac{3}{r_s}\right)+\frac{2\cdot4}{r_s}+\frac{3\cdot51}{r_s^2}-\frac{1\cdot154}{r_s}-\frac{0\cdot726}{r_s+6\cdot43}, \qquad (25)$$

the terms having been kept separate for identification. The first term is $\epsilon_0(r_s)$, and the last three terms, in order, are the Fermi, exchange, and correlation energies, all calculated according to the free-electron approximation. As far as these terms are concerned the expression is the same, apart from the actual value of ϵ_0, as that obtained for magnesium (eqn. (17) in the above-mentioned paper). However, owing to the use of the ion-core field only in eqn. (1), which results in a different value for ϵ_0, an additional term is required here, and this turns out to be one half the self-potential energy of the valence-electron charge distribution within an atomic sphere. Assuming a uniform charge distribution, as for free-electrons, and remembering that there are two valence electrons to each atomic sphere, so that the electron density is $\sigma=6/4\pi r_s^3$, this additional energy becomes, in our present units,

$$\frac{16\pi^2\sigma^2}{3}\int_0^{r_s} r^4\,dr=\frac{2\cdot4}{r_s},$$

which is the second term in eqn. (25).

The atomic radius ρ corresponding to the minimum of $E(r_s)$, and the compressibility κ, can be obtained directly from (25). The cohesive energy S is given by the difference between $E(\rho)$ and the *experimental* value of the mean energy per valence electron in a free atom, the latter being minus one half the sum of the first two ionization potentials.

Table 2 shows the calculated and observed values of ρ, κ, S and $E(\rho)$ for the divalent metals. The set of results marked (*a*) for beryllium were calculated as above, while those marked (*b*) were obtained using the Fermi energy calculated by Herring and Hill (1940) for this metal instead of the free-electron formula ; this will be discussed in § 5.

§4. THE RELATION BETWEEN PRESSURE AND VOLUME

Since there are two valence electrons to each atomic cell the total energy per atomic volume is $2E(r_s)$. The pressure p at the absolute zero of temperature is therefore given by

$$p=-2\frac{dE}{dv}=-\frac{1}{2\pi r_s^2}\frac{dE}{dr_s}, \qquad (26)$$

and this can be found directly from eqn. (25).

The *compression* is defined as

$$-\frac{\Delta v}{v_0}=\frac{v_0-v}{v_0}=1-\left(\frac{r_s}{\rho}\right)^3, \quad . \quad . \quad . \quad . \quad . \quad . \quad (27)$$

where v_0 is the volume corresponding to zero pressure. Bridgman (1941, 1948 a) has found experimentally the compressions of the divalent metals for a range of pressures up to 100 000 kg/cm², and his results are compared with those of the present theory in figs. 1 and 2, the full lines being the theoretical curves and the broken lines the experimental curves. Beryllium is omitted owing to the unreliability of both the theoretical and experimental results for this metal.

Table 2

	ρ (Å)		$10^{12}\kappa$ (cm²/dyne)		S (kcal/mole)		$-E(\rho)$ (kcal/mole)	
	Calc.	Obs.	Calc.	Obs.	Calc.	Obs.	Calc.	Obs.
Mg	1·94	1·77	2·8	3·0	8	36	528	556
Ca	2·47	2·16	7·0	5·7	16	48	429	461
Sr	2·66	2·36	9·3	8·2	17	47	401	431
Ba	2·93	2·47	13·2	10·3	17	49	366	398
Zn	1·62	1·53	1·5	1·7	−14	27	614	655
Cd	1·72	1·73	1·8	2·2	−11	27	584	622
(*a*)	1·60		1·4		−13		619	
Be		1·25		0·8		75		707
(*b*)	1·48		0·4		76		708	

ρ is the atomic radius corresponding to the minimum of $E(r_s)$; κ is the compressibility ; S is the cohesive energy ; and $E(\rho)$ is the total energy of the valence electrons in the metal. The observed values are at room temperature.

Bridgman (1948 a) has given values for magnesium up to 100.000 kg/cm², but only the first half of the resulting curve is shown in fig. 2, on a larger scale than the others, together with the theoretical curve. The discrepancy between the two curves is greater than one would expect for this metal, which, of the divalent metals, is probably best suited to the present theory. However, in a later paper Bridgman (1948 b) gives the results of more refined measurements on magnesium, up to 30 000 kg/cm², and these, shown by crosses in fig. 2, agree almost exactly with the theoretical results. It seems likely, therefore, that at higher pressures the experimental curve should follow the theoretical curve more closely than does the one shown.

It should be noted that the experimental results are at room-temperature while the calculated ones are at absolute zero. An accurate correction to absolute zero over such a large pressure range would hardly be feasible with the experimental data available, but a rough calculation on the lines of that given by Bardeen (1938) shows that the correction would decrease

Fig. 1

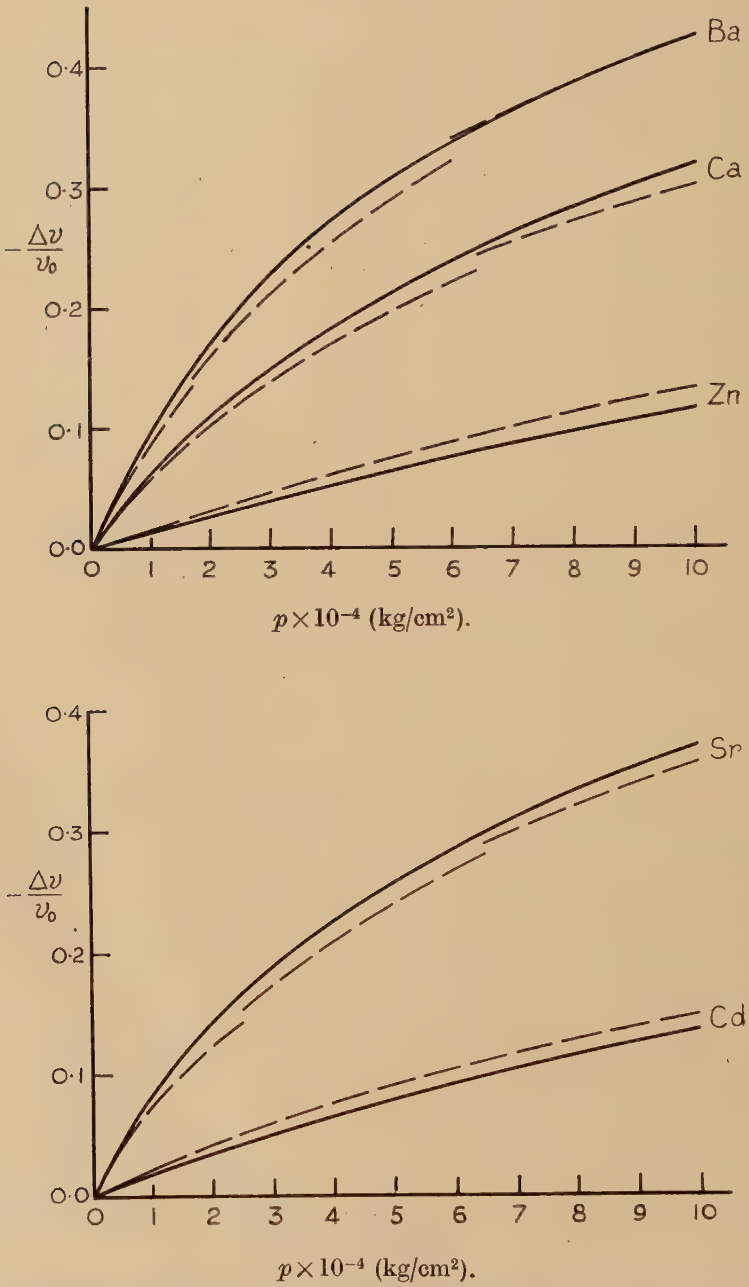

Curves showing compression as a function of pressure. The full curves are theoretical, and the broken curves are from the experimental results of Bridgman (1948 a). The separation of the curves into two groups has no significance, but is merely intended to avoid confusion.

the ordinates of the experimental curves by less than 3%. Such a correction would alter very little the correspondence between the observed and the calculated curves; that for the alkaline earth metals would be slightly worsened, and that for Zn and Cd slightly improved.

The volume v_0 used in obtaining the *calculated* curves was that corresponding to the *calculated* atomic radius ρ, so that these curves are entirely theoretical—a fact which should be borne in mind when comparing the present results with those of Bardeen for the alkali metals. The discontinuities in the experimental curves for Ba and Sr at about 20 000 kg/cm² are almost certainly caused by polymorphic transitions to close-packed structures; Bridgman (1941) states that a similar transition for Ca has been smoothed over in his results. The discontinuities at higher pressures are presumably due to transitions of the type discussed by Sternheimer (1950) for Cs.

Fig. 2

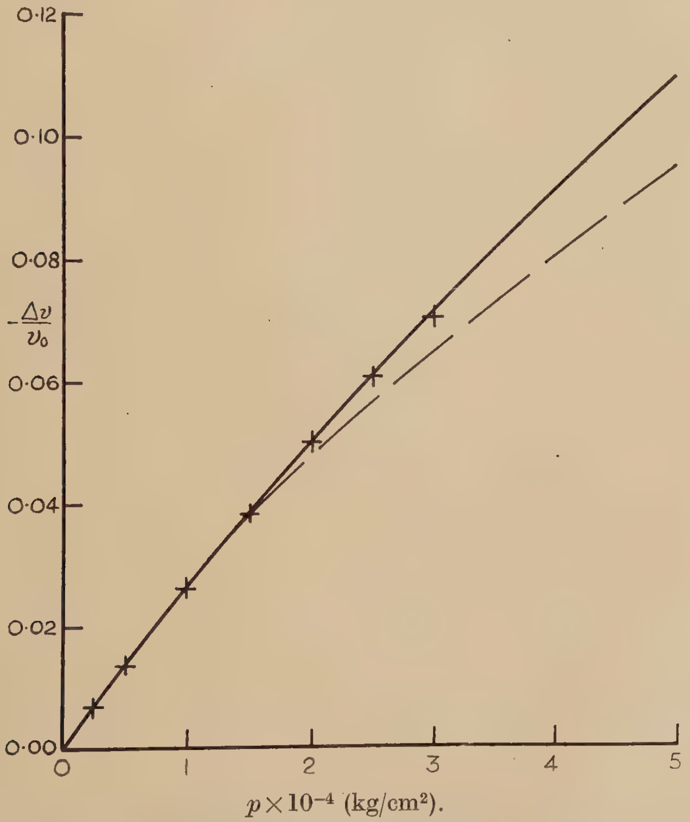

Curves showing compression as a function of pressure for magnesium. The full curve is theoretical, and the broken curve is from the experimental results of Bridgman (1948 a). The crosses are more accurate experimental points from a later paper of Bridgman (1948 b); these do not go beyond 30 000 kg/cm².

§ 5. FURTHER DISCUSSION OF RESULTS

Table 2 shows that the calculated values of ρ and κ are in fairly good agreement with the observed values. The agreement is poor in the case of S, but this is understandable since the calculated cohesive energy is the small difference between two large energies, one calculated and one empirical. It is for this reason that the values of $E(\rho)$ have also been tabulated, and the correspondence between theory and experiment is here seen to be quite good—it is clear that this is not a necessary consequence of the use of the empirical ionization potential I_2, since $E(r_s)$ contains four terms of similar size, only one of which depends, indirectly, upon I_2.

The principal concern of the work has been to calculate the eigenvalue ϵ_0 belonging to ψ_0, and the assumptions made in doing this were essentially those made by Fröhlich (1937) in dealing with the alkali metals, plus the additional one that ψ_0 can, for polyvalent as well as for monovalent metals, be calculated using the ion-core field only. The work on magnesium (Raimes 1950) indicates that these assumptions are reasonable, and it is believed that the values of ϵ_0 so obtained are not greatly in error. Owing to the further approximations involved in calculating E, however, the final results do not give a true idea of the accuracy of ϵ_0 ; rather, assuming that ϵ_0 is fairly accurate, the results show the effect of using the free-electron approximation to evaluate the remaining terms in E, and it is evident from table 2 and figs. 1 and 2 that this is by no means so bad as might have been expected. The most serious error probably occurs in the Fermi energy, and here it might be noted that the calculated energies would all be improved if the Fermi energy were slightly less than the free-electron value.

The results for Be have some bearing on the foregoing remarks. The use of the free-electron Fermi energy, in eqn. (25), gives very poor results for this metal, but when the Fermi energy calculated by Herring and Hill (1940, p. 150, table VIII) is used, the other terms being unchanged, a great improvement occurs, the cohesive energy almost exactly equalling the observed value. The calculated value of ρ is improved, and that of κ altered in the right direction, but a little too far ; this over-correction of the compressibility is probably a consequence of our interpolating quadratically from the values of the Fermi energy for three atomic radii given by Herring and Hill.

The same assumption regarding the use of the ion-core field only in calculating ψ_0 would permit the application of the recent method of Kuhn and Van Vleck (1950) to polyvalent metals. This method, which the authors apply to the alkali metals, is in principle very similar to that of Fröhlich, except that assumptions regarding ψ_0 are obviated to some extent by the use of several empirical atomic term values. Apart from the disadvantages involved in the latter, however, the computational labour would be much heavier, and it is doubtful whether the significance of the results would be greatly enhanced.

It was remarked in § 1 that the present method can easily be extended to metals of higher valency, and it has, in fact, already been applied to several of these. It is found that the calculated compressibilities do not compare so well with experiment as in the case of the divalent metals, but the calculated values of ρ and $E(\rho)$ remain quite good. Perhaps it should be mentioned that the method can only be applied directly to metals for which ψ_0 and the state of the single remaining valence electron in a free ion, from which all other valence electrons have been removed, are both s states.

My thanks are due to Professor H. Jones for his kind advice and encouragement at all times.

REFERENCES

BACHER, R. F., and GOUDSMIT, S., 1932, *Atomic Energy States* (New York: MacGraw Hill).

BARDEEN, J., 1938, *J. Chem. Phys.*, **6,** 372.

BRIDGMAN, P. W., 1941, *Phys. Rev.*, **60,** 351; 1948 a, *Proc. Am. Acad. Sci.*, **76** (3), 55; 1948 b, *Ibid.*, **76** (4), 89.

FRÖHLICH, H., 1937, *Proc. Roy. Soc.* A, **158,** 97.

HERRING, C. C., and HILL, A. G., 1940, *Phys. Rev.*, **58,** 132.

KUHN, T. S., and VAN VLECK, J. H., 1950, *Phys. Rev.*, **79,** 382.

PAULING, L., 1927, *J. Am. Chem. Soc.*, **49,** 765.

PROKOFJEW, W., 1929, *Z. f. Phys.*, **58,** 255.

RAIMES, S., 1950, *Phil. Mag.*, **41,** 568.

STERNHEIMER, R., 1950, *Phys. Rev.*, **78,** 235.

XXVIII. *The Electronic Structure of Diamond*

By G. G. HALL
Department of Theoretical Chemistry, University of Cambridge*

[Received November 30, 1951]

SUMMARY

In this paper the theory of equivalent orbitals is used to consider the electronic structure of diamond. The description in terms of equivalent orbitals is closely related to the usual chemical description since each orbital is localized and corresponds to one of the CC bonds. The Bloch orbitals can be expressed exactly as transforms of these equivalent orbitals. This leads to a new and more accurate method of determining the Bloch orbitals and their energies. For diamond, it is found that the energies can be expressed as an explicit function of the coordinates in reciprocal space. The results are compared with those obtained by Kimball, using the cell method, and the agreement is good. This method has the advantage of relating the valence description of diamond directly with the zone description.

§1. INTRODUCTION

THE electronic structure of diamond has been considered, using the Wigner-Seitz-Slater method of calculating the wavefunctions, by Kimball (1935). He has calculated the energies of the Bloch functions in terms of their wave vectors **k** and discussed the significance of his results in determining the properties of diamond. The object of this paper is to show how similar results may be obtained, with less labour and in a more general form, by using an equivalent orbital method proposed by Hall (1951). This method also enables the relation between the tetrahedrally-directed CC bonds and the zone structure to be clarified.

§2. EQUIVALENT AND MOLECULAR ORBITALS

The modern orbital theory of valency is an attempt to study the electronic structure of molecules, in their ground states, by using an approximate wavefunction in the form of a single determinant. The elements of this determinant are functions of the coordinates of one electron only, known as orbitals, each multiplied by a suitable spin factor. In order that a wavefunction of this form should be the best approximation to the true wavefunction, it has been shown that the orbitals must satisfy certain

---

* Communicated by the Author.

integro-differential equations. These equations do not, however, determine the orbitals uniquely for both the form and magnitude of a determinant are unaltered if the elements are subjected to an arbitrary unitary transformation among themselves. Thus we may distinguish orbitals of several different types which, nevertheless, lead to the same total energy, the same total electron density etc. Two particular kinds of orbitals, equivalent orbitals and molecular orbitals, have been found to have special significance. Equivalent orbitals are relatively well localized in a part of the molecule and correspond to the description of the molecule in terms of inner shells, lone pairs and bonds. Molecular orbitals, on the other hand, are spread throughout the molecule and are the appropriate orbitals to use in describing ionization or excitation. A fuller account of these orbitals and their properties has been given by Hall and Lennard-Jones (1951).

This theory can be applied with very few modifications to valence crystals such as diamond or silicon. The molecular orbitals are the Bloch orbitals but the equivalent orbitals do not seem to have been introduced previously in the theory of solids. These equivalent orbitals certainly exist for valence crystals since these crystals can be described in terms of the usual directed chemical valencies of the elements concerned. For metallic crystals this is not so and, while there may be equivalent orbitals of the delocalized type such as there are in conjugated molecules, their existence as transforms of the occupied Bloch orbitals would have to be proved in each instance.

§3. The Structure of Diamond

In chemical terms, diamond consists of a lattice of carbon atoms each surrounded, in tetrahedral directions, by four other carbon atoms and with all the interatomic distances equal. The equivalent orbital description is also fairly simple since there are only two equivalent sets, one of inner shell orbitals around the various nuclei and the other of bond orbitals between each pair of neighbouring nuclei. The orbitals in these sets are equivalent in the sense that an inner shell orbital localized around one nucleus is transformed into an inner shell orbital localized around any other nucleus by some symmetry operation of the space group and similarly for the CC bond orbitals. The equivalent orbital description serves, therefore, as a translation of the chemical description into quantum mechanical terms.

Crystallographically, the atoms of diamond lie on two interpenetrating face-centred cubic lattices. The unit cell of this structure is a parallelopiped of a quarter the volume of the cube and containing only two atoms. If the three basic lattice vectors are $\mathbf{a}_1$, $\mathbf{a}_2$, $\mathbf{a}_3$ the two atoms in the (l, m, n) cell will be at the positions

$$\mathbf{a}=l\mathbf{a}_1+m\mathbf{a}_2+n\mathbf{a}_3,$$

$$\mathbf{a}'=(l+\tfrac{1}{4})\mathbf{a}_1+(m+\tfrac{1}{4})\mathbf{a}_2+(n+\tfrac{1}{4})\mathbf{a}_3.$$

§4. THE ENERGY ZONES

For certain purposes the descriptions of diamond already given are insufficient and the molecular or Bloch orbital description is required. This can be derived most easily from the equivalent orbital description. The method depends on the properties of the matrix e_{rs} which measures the interaction between the equivalent orbitals χ_r and χ_s. The matrix T_{rs} which reduces e_{rs} to diagonal form is the matrix which transforms the equivalent orbitals to molecular orbitals, and the eigenvalues E_{tt} are the energies of the corresponding molecular orbitals ψ_t. This property is used as the definition of molecular orbitals. The problem becomes, therefore, the solving of the system of homogeneous linear equations

$$\sum_s e_{rs}T_{ts} - E_{tt}T_{tr} = 0 \qquad (r=1, 2, \ldots), \tag{4.01}$$

for each value of t. The unknowns T_{ts} are partly determined by the symmetry of the crystal and this simplifies the problem enormously.

If the equivalent orbitals for the CC bonds of diamond are, in fact, localized, then the interaction e_{rs} between two non-neighbour orbitals will be zero. Although these interactions may not be exactly zero, it is reasonable to assume that, in the neighbourhood of the equilibrium internuclear distance, they are of negligible importance compared with the remaining interactions. Consequently we shall assume that

$$e_{rr} = a, \tag{4.02}$$

$$e_{rs} = b, \text{ if } \chi_r \text{ and } \chi_s \text{ are first neighbour bonds,} \tag{4.03}$$

$$= 0 \text{ otherwise.} \tag{4.04}$$

Apart from the original assumption of a single-determinant wavefunction, this is the only approximation made in this method and, if required, it could be relaxed and higher order interactions included. There is no loss of generality in putting the interaction of inner shell orbitals and bond orbitals equal to zero so we may omit any further reference to the inner shell orbitals.

In each unit cell there are four CC bonds which may be labelled $1(l, m, n)$, $2(l, m, n)$, $3(l, m, n)$ and $4(l, m, n)$. The matrix T_{rs} can then be written

$$\left.\begin{aligned} T_{\mathbf{q},s} &= A_{\mathbf{q},\mathbf{a}} \text{ if } s=1(l, m, n), \\ &= B_{\mathbf{q},\mathbf{a}} \text{ if } s=2(l, m, n), \\ &= C_{\mathbf{q},\mathbf{a}} \text{ if } s=3(l, m, n), \\ &= D_{\mathbf{q},\mathbf{a}} \text{ if } s=4(l, m, n). \end{aligned}\right\} \tag{4.05}$$

The translational symmetry suggests the substitutions

$$\left.\begin{aligned} A_{\mathbf{q},\mathbf{a}} &= A_{\mathbf{q}}\, e^{i\mathbf{q}\cdot\mathbf{a}}, \\ B_{\mathbf{q},\mathbf{a}} &= B_{\mathbf{q}}\, e^{i\mathbf{q}\cdot\mathbf{a}}, \\ C_{\mathbf{q},\mathbf{a}} &= C_{\mathbf{q}}\, e^{i\mathbf{q}\cdot\mathbf{a}}, \\ D_{\mathbf{q},\mathbf{a}} &= D_{\mathbf{q}}\, e^{i\mathbf{q}\cdot\mathbf{a}}, \end{aligned}\right\} \tag{4.06}$$

where $\mathbf{q}$ is a vector in the reciprocal lattice, viz.

$$\mathbf{q}=f\mathbf{b}_1+g\mathbf{b}_2+h\mathbf{b}_3, \tag{4.07}$$

and

$$\mathbf{a}_i \,.\, \mathbf{b}_j=\delta_{ij}. \tag{4.08}$$

The effect of this substitution is to reduce the infinite set of equations (4.01) to the finite set

$$\left.\begin{aligned}
&(a-E)A_{\mathbf{q}}+b(1+e^{-if})B_{\mathbf{q}}+b(1+e^{-ig})C_{\mathbf{q}}+b(1+e^{-ih})D_{\mathbf{q}}=0,\\
&b(1+e^{if})A_{\mathbf{q}}+(a-E)B_{\mathbf{q}}+b(1+e^{if-ig})C_{\mathbf{q}}+b(1+e^{if-ih})D_{\mathbf{q}}=0,\\
&b(1+e^{ig})A_{\mathbf{q}}+b(1+e^{ig-if})B_{\mathbf{q}}+(a-E)C_{\mathbf{q}}+b(1+e^{ig-ih})D_{\mathbf{q}}=0,\\
&b(1+e^{ih})A_{\mathbf{q}}+b(1+e^{ih-if})B_{\mathbf{q}}+b(1+e^{ih-ig})C_{\mathbf{q}}+(a-E)D_{\mathbf{q}}=0.
\end{aligned}\right\} \tag{4.09}$$

The eigenvalues of the original matrix e_{rs} are, therefore, the roots of the equation

$$\begin{vmatrix}
a-E & b(1+e^{-if}) & b(1+e^{-ig}) & b(1+e^{-ih})\\
b(1+e^{if}) & a-E & b(1+e^{if-ig}) & b(1+e^{if-ih})\\
b(1+e^{ig}) & b(1+e^{ig-if}) & a-E & b(1+e^{ig-ih})\\
b(1+e^{ih}) & b(1+e^{ih-if}) & b(1+e^{ih-ig}) & a-E
\end{vmatrix}=0. \tag{4.10}$$

For each value of $\mathbf{q}$, there are four roots to this equation so that the values of E fall into four zones. Since each E is a triply-periodic function of $\mathbf{q}$, it is only necessary to consider its form inside a single Brillouin zone. The first Brillouin zone for a face-centred cubic lattice has the form of a truncated octahedron. Each root E may be considered inside this zone or the root of lowest energy may be considered in it and the remaining roots in the second, third and fourth zones outside it.

The eqn. (4.10) has a double root at

$$E=a-2b, \tag{4.11}$$

so that the remaining roots can be found explicitly as

$$E=a+b[2\pm\sqrt{\{4+2\cos f+2\cos g+2\cos h+2\cos(f-g)+2\cos(g-h)} \\ +2\cos(h-f)\}]. \tag{4.12}$$

This means that two of the roots are independent of $\mathbf{q}$ and so remain constant throughout their zones. The other two roots are symmetrical with respect to

$$E=a+2b, \tag{4.13}$$

and so have contours of exactly the same shape.

§5. THE PLANE SECTION BY $h=0$

The main feature of the energy surfaces inside the zones may be found by taking cross-sections of the zones. The section by $h=0$ is one of the most useful since, by symmetry, there are five other planes giving exactly the same cross-section.

On the plane $h=0$ the energies are

$$E=a+b[2\pm\sqrt{\{6+4\cos f+4\cos g+2\cos(g-f)\}}], \tag{5.01}$$

$$E=a-2b \qquad \text{(twice).} \tag{5.02}$$

If we choose to measure the energy from an origin at a and in units of b, both of the parameters may be eliminated and the energy expressed as a pure number. This means that the shape of the energy surfaces is independent of any particular assumptions about the values of a and b. Eqns. (5.01) and (5.02) now become

$$\mathscr{E}=2\pm\sqrt{\{6+4\cos f+4\cos g+2\cos(g-f)\}}, \quad . \quad . \quad . \quad . \tag{5.03}$$

$$\mathscr{E}=-2 \qquad\qquad \text{(twice)}. \quad . \quad . \quad . \quad . \quad . \tag{5.04}$$

The contours given by these equations are shown in fig. 1. The positive root of (5.03) is the lowest and is plotted inside. The negative root is plotted outside the first zone and the constant roots (5.04) outermost.

Fig. 1

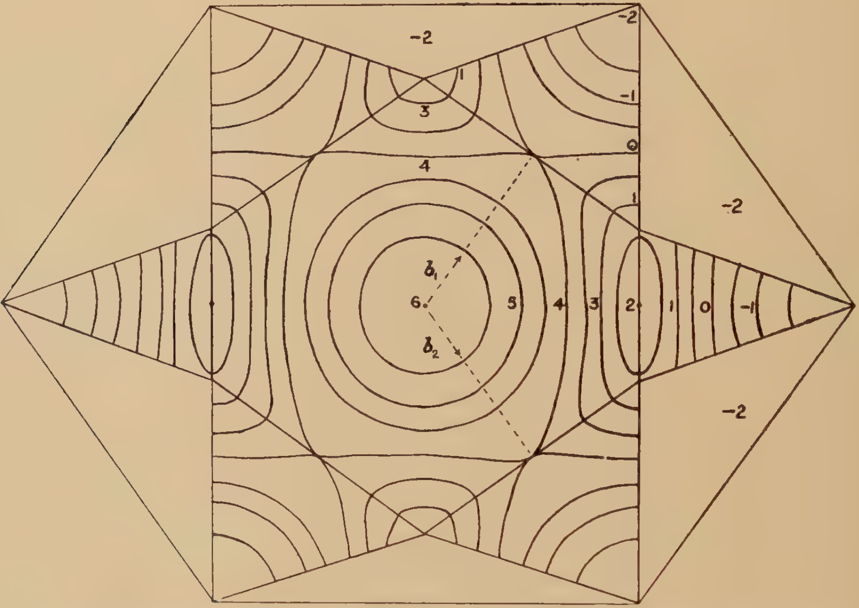

Energy of the molecular orbitals as a function of **q** over the plane $h=0$.

Because of the symmetry of the roots, the energy contours appear to be continuous across the boundaries of the first zone. The only direction in which they are continuous is $f=g$.

A comparison of fig. 1 with fig. 3 of Kimball's paper shows that there is close agreement between the two treatments as to the general shape of the energy contours, but that there are a number of differences in details. This figure is more general than Kimball's in that it applies, not only at the equilibrium internuclear distance, but also on both sides of it. It ceases to be a good approximation only when, at large or very small internuclear distances, the interaction of second-neighbour equivalent orbitals is comparable with the first-neighbour interactions. Again, since Silicon forms a valence crystal with the same structure as diamond, the equations and the figure are equally applicable to it.

§6. NUMERICAL RESULTS

To convert the results already obtained into physical units the values of a and b at the equilibrium separation are required. Empirical values of these parameters have already been deduced from the ionization potentials of paraffin molecules (Hall 1951, Lennard-Jones and Hall 1952). They are, in ev

$$a=-12{\cdot}978, \qquad b=-1{\cdot}458. \qquad \qquad (6.01)$$

The energy levels range, therefore, from $a+6b=-21{\cdot}726$ at the origin to $a-2b=-10{\cdot}062$ at the outside.

These results do not agree exactly with those of Kimball. The values

$$a=-11{\cdot}579, \qquad b=-1{\cdot}471, \qquad \qquad (6.02)$$

would give almost exact agreement with his results but he himself admits that his results are uncertain, to the extent of a small change of origin, so the a of (6.01) is to be preferred. The agreement between the two values of b is most satisfactory.

§7. CONCLUSION

It has been convenient, in this paper, to start from the equivalent orbital description of the crystal and to derive the Bloch or molecular orbital description from it by a suitable transformation. This transformation can be determined explicitly by completing the solution of the eqns. (4.09). It is then possible to find the inverse transformation and to use it to transform Bloch orbitals, obtained, for example, by the Wigner-Seitz method, into equivalent orbitals corresponding to the bonds. Thus the orbitals used by Kimball can be transformed into equivalent orbitals each localized around two neighbouring carbon atoms in accordance with chemical expectations.

The author is indebted to Sir John Lennard-Jones for suggesting this problem.

REFERENCES

HALL, G. G., 1951, *Proc. Roy. Soc.* A, **205**, 541.
HALL, G. G., and LENNARD-JONES, Sir J. E., 1951, *Proc. Roy. Soc.* A, **205**, 357.
KIMBALL, G. E., 1935, *J. Chem. Phys.*, **3**, 560.
LENNARD-JONES, Sir J. E., and HALL, G. G., 1952 (in course of publication).

XXIX. *Separation of the Boundary Layer at a Slightly Blunt Leading Edge in Supersonic Flow*

By O. Bardsley and W. A. Mair
Fluid Motion Laboratory, University of Manchester *

[Received November 30, 1951]

Summary

Schlieren photographs have been taken to show the supersonic flow past a two-dimensional wedge placed at an incidence large enough to give an expansion region on one side. The leading edge was blunt in all cases, and its thickness t was varied between 35 and 200 microns. For values of t greater than about 80 microns the photographs showed a weak shock wave on the downstream side of the expansion region. A shock wave in this position indicates that there is a separation of the boundary layer near the leading edge, followed by re-attachment. The Reynolds number was about $1{\cdot}3\times 10^5$ per cm, giving a value of about 1 000 for $t=80$ microns. It is concluded that separation of the boundary layer occurs when the Reynolds number, based on the thickness of the leading edge, is greater than about 1 000. For smaller Reynolds numbers there was no evidence of separation.

§1. Introduction

In an earlier paper by Bardsley (1951) an account was given of the supersonic flow past a wedge with a nearly sharp leading edge, the wedge being set at an incidence large enough to give an expansion region on one side. It was found that the weak shock wave that occurred immediately upstream of the expansion region was caused by the slight bluntness of the leading edge, although the thickness of the leading edge in these experiments was only about 8 microns. Because no shock wave could be seen on the *downstream* side of the expansion region, it was concluded that there was no separation of the boundary layer.

In Bardsley's experiments the leading edge was very thin and it was difficult to determine its exact shape. The enlarged shadowgraphs that were reproduced in the paper showed that the edge was irregular and not rounded ; the flow past such an edge, at large distances from the edge, would probably be similar to that past the shape shown in fig. 1.

Holder, Tomlinson and Rogers (1949) have investigated the supersonic flow past two-dimensional blunt-nosed plates, with leading-edge thicknesses of the order of 1 cm. They found that for nose sections at least as blunt as a semicircle there was a separation of the boundary layer on the downstream side of the ‘ shoulder ’. An oblique shock wave occurred where the boundary layer became re-attached after the separation. This will be called the ‘ second shock wave ’ in this paper, to distinguish it from the bow shock-wave.

---

* Communicated by the Authors.

The experiments of Holder *et al.* were made with the plates set at zero incidence, but it is likely that separation of the boundary layer would also have been observed if the plates had been set at such an incidence that an expansion occurred on one side. The experiments of Holder *et al.* were made with a leading-edge thickness about 1 000 times as great as in Bardsley's case. This suggests that the separation of the boundary layer on a blunt-nosed plate may depend on the Reynolds number based on the thickness of the leading edge. In the experiments of Holder *et al.* this Reynolds number was about 100 000 and the boundary layer separated ; in Bardsley's experiments the Reynolds number was about 100 and there was no evidence of separation. (The possibility of separation occurring in the latter case, with a second shock wave either too weak or too short to be detected by the schlieren system, is considered in the present paper.)

The experiments described below were made to investigate the effect of leading-edge thickness on the separation of the boundary layer.

§ 2. NOTATION

d	distance from surface to point at which shock wave attains maximum strength.
h	height of separation ‘ bubble ’ (see fig. 11).
k	constant in eqn. (4).
l	length of separation ‘ bubble ’ in direction of stream (see fig. 11).
M	Mach number.
p	pressure before shock wave.
Δp	rise of pressure in shock wave.
r	radius of curvature of concave part of ‘ bubble ’ profile (see fig. 12).
R_t	Reynolds number based on thickness t.
$s = \Delta p/p$	strength of shock wave.
t	thickness of leading edge (see fig. 1).
u	velocity outside boundary layer.
x	distance from leading edge.
y	distance from wedge, measured normal to undisturbed stream.
γ	ratio of specific heats.
δ	thickness of boundary layer (without separation).
δ_1	displacement thickness of boundary layer (without separation).
λ	inclination of tangent at point of inflexion to surface of wedge (see fig. 12).
μ	micron ($=0{\cdot}001$ mm).
ν	coefficient of kinematic viscosity.

§ 3. EXPERIMENTAL DETAILS

The experiments were made in the intermittent supersonic wind tunnel described by Bardsley and Mair (1951). The working section was 12·7 cm high and 10·2 cm wide, and the Mach number was 1·96. The stagnation pressure was approximately atmospheric and the Reynolds number in the working section was about $1{\cdot}3 \times 10^5$ per cm. A silica-gel drier was used at the intake to the tunnel, and the absolute humidity was always below 0·0005.

The wedge used was 1·27 cm long in the direction of the stream, had an apex angle of 10·0° and extended across the whole width of the tunnel. It was supported by two arms on the downstream side, and the angle of incidence could be changed by altering the position of these arms. If the experiments had been made at a low incidence, with a fairly strong bow shock-wave on both sides of the wedge, the second shock wave occurring after the separation might have been obscured by the bow shock-wave. The experiments were therefore made at incidences high enough to give an expansion region above the wedge, so that in cases where the boundary layer separated this expansion region lay between the bow shock-wave and the second shock wave, and the latter could be easily seen.

Fig. 1

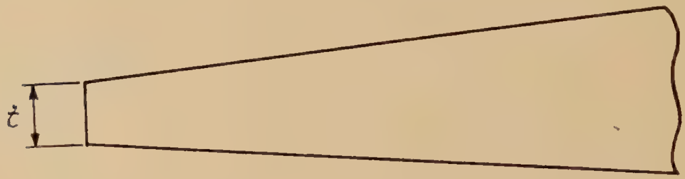

Section of front part of wedge.

The wedge was made of high-carbon steel, ground and lapped to the shape shown in fig 1. For the first experiments the leading-edge thickness t was 0·2 mm ($200\,\mu$). By lapping one face of the wedge, this thickness was then reduced in stages without changing the shape of the leading edge. Thus for all the values of t the shape was as shown in fig. 1. The dimension t was determined, in each case, by measuring the wedge thickness at several distances from the leading edge. It was found that the values of t obtained by this method were consistent within about $15\,\mu$, and it is estimated that the possible error in t is about $\pm 15\,\mu$.

The knife edges in the schlieren system were horizontal and were arranged so that increasing density in an upward direction was represented by a dark region. A flash tube having an effective duration of a few microseconds was used as a light source because it was available; there was no evidence of any serious unsteadiness in the flow.

Schlieren photographs were taken for leading-edge thicknesses of 200, 110, 60 and 35 microns, with the upper surface of the wedge inclined at 5° and at 10° to the direction of the undisturbed stream.

To ensure that the optimum conditions for detecting the weak second shock wave were realized, all the photographs were taken with two different sensitivities of the schlieren system. It was found that the smaller of the two sensitivities gave better results in all cases. The photographs taken with this sensitivity are reproduced as figs. 2 to 9 (Plates IX and X*), and details are given in table 1.

Table 1

Fig. No.	2	3	4	5	6	7	8	9
Stream deflection	5°	5°	5°	5°	10°	10°	10°	10°
t (microns)	200	110	60	35	200	110	60	35
R_t	2700	1500	800	500	2700	1500	800	500

The flow is from left to right and the position of the back of the wedge is shown by the light expansion region on the lower side ; the supporting arms continue downstream beyond the edge of the field of view. In some of the photographs the rubber sealing material between the ends of the wedge and the glass windows obstructs the field of view slightly on the lower side ; care was taken to ensure that this did not occur on the upper side of the wedge.

§4. INTERPRETATION OF THE PHOTOGRAPHS

The photographs resemble those reproduced as figs. 4, 5, 7 and 8 in the paper by Bardsley (1951), except that a second shock wave can be seen on the downstream side of the expansion region for leading-edge thicknesses of 200 and 110 μ (figs. 2, 3, 6 and 7, Plates IX and X). For thicknesses of 60 and 35 μ (figs. 4, 5, 8 and 9, Plates IX and X) no such second shock wave can be seen. The second shock wave extends for a considerable distance, even for the smaller value of t at which it is visible (110 μ). Since the shock wave cannot be seen at all when $t=60\,\mu$, this suggests that an important change occurs in the flow as t varies between 60 and 110 μ. It may also be noted that the appearance of the second shock wave, and the value of t at which it becomes visible, are the same for stream deflections of 5° and 10°.

In cases where there is a separation of the boundary layer, followed by re-attachment, the flow is probably similar to that shown in fig. 10. A second shock wave is formed near the point of re-attachment, and the existence of this shock wave is an indication of boundary-layer separation. Hence it is concluded that separation occurs for values of t greater than about 80 μ, while for smaller values of t there is no separation.

Values of R_t, the Reynolds number based on the leading-edge thickness t, are given in table 1. The variation in flow pattern with the thickness t must be interpreted as a change depending on this Reynolds number R_t. Thus the experiments show that separation of the boundary layer occurs for values of R_t greater than about 1000.

---

* For plates see end of issue.

For smaller values of R_t no second shock wave can be detected, indicating that there is probably no separation. However, it is still necessary to consider the possibility that for small values of t the second shock wave may be too weak to be detected by the schlieren system. This question is discussed below.

§5. STRENGTH OF THE SECOND SHOCK WAVE

By consideration of the sensitivity of the schlieren system, Mair (1951) has shown that it should be possible to detect a shock wave having a strength ($s = \Delta p/p$) of order 0·01. At the Mach number of these experiments the deflection of the stream at a shock wave of this strength is only about 0·2°. Thus we must consider whether it is possible for separation to occur in such a way that the deflection of the stream at the second shock wave is less than about $\frac{1}{2}°$.

For a preliminary consideration of the strength of the second shock wave, it will be assumed that there is a sharp corner at the point of re-attachment, as shown in fig. 11. Let the separation ‘ bubble ’ have a length l in the direction of the stream and a height h above the surface of the wedge.

Examination of figs. 4, 5, 8 and 9 (Plates IX and X), where no second shock wave is visible, shows that if there is a separation, l cannot be greater than about 2 mm. (This is an upper limit, given by the apparent width of the expansion region at the wedge.) If there is a separation in these cases, the height of the bubble cannot be less than the thickness δ of a normal unseparated boundary layer on a flat plate at a distance $l/2$ from the leading edge. As shown by Bardsley (1951) the displacement thickness of a laminar boundary layer on a flat plate at a Mach number of about 2 is given approximately by

$$\delta_1 \approx 4(\nu x/u)^{1/2}. \qquad \ldots \ldots \ldots \quad (1)$$

At this Mach number the total thickness δ is about twice the displacement thickness. This is shown, for example, by Cope and Hartree (1948). Hence

$$\delta \approx 8(\nu x/u)^{1/2}. \qquad \ldots \ldots \ldots \quad (2)$$

If $l = 2$ mm we may put $x = l/2 = 1$ mm. Then $\delta \approx 0{\cdot}1$ mm, and if h is not less than δ the ratio h/l for this value of l cannot be less than 1/20. For any smaller value of l the minimum possible value of h/l is greater than this, so that the inclination of the downstream end of the bubble to the surface of the wedge cannot be less than 1/20 radian (i.e. about 3°) for any possible value of l. The strength of a shock wave giving a deflection of this magnitude is about 15 times that of the weakest shock wave that can be detected with the schlieren apparatus.

These calculations suggest that any separation of the boundary layer should be accompanied by a second shock wave that can easily be detected, but they ignore the fact that the true shape of any separation bubble that may exist is probably as shown in figs. 10 and 12, with a concave transition curve on the downstream side instead of a sharp corner. This will now be taken into account.

For the present, the variation of entropy behind the bow shock-wave will be neglected. In fig. 12, the shock wave starts at the same point as the envelope formed by the Mach lines from the concave curve, and lies a little upstream of the first Mach line in the compression region, i.e. just inside the expansion region formed by the Mach lines from the convex part of the bubble. Let λ be the angle between the upper surface of the wedge and the tangent drawn at the point of inflexion on the separation bubble. By calculating the positions of the Mach lines for a typical case it was shown that, if λ was small, the shock wave penetrated such a short distance into the expansion region that the latter could only have a small effect on the strength of the shock wave. Thus the deflection at

Fig. 10

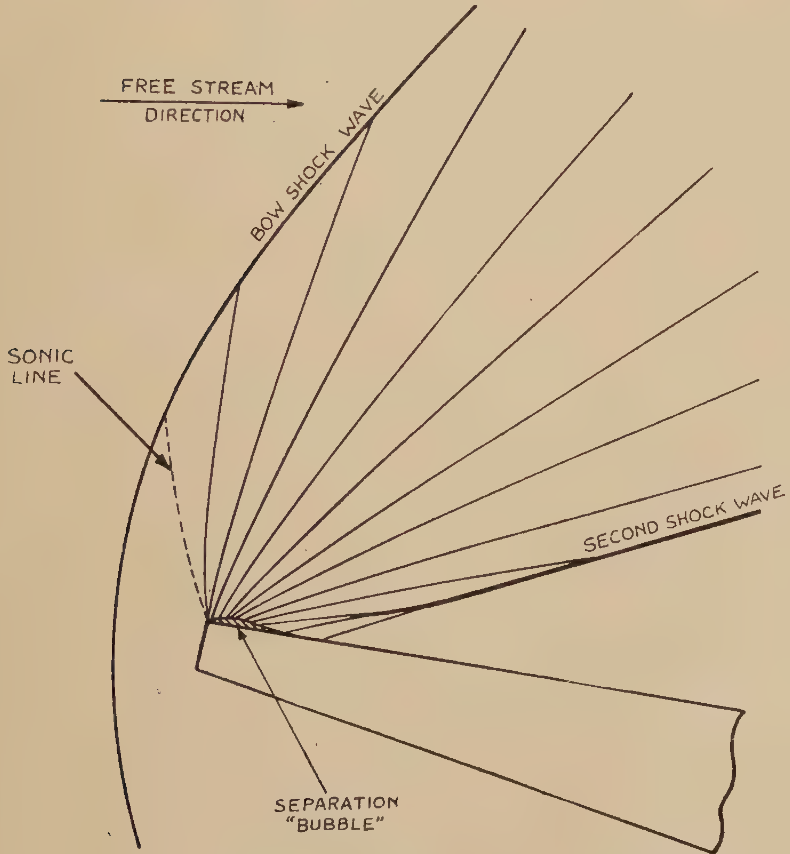

Flow past wedge with blunt leading edge.

the strongest part of the shock wave was nearly equal to λ, a result that was also obtained by using the first-order theory given by Whitham (1951). This means that the previous discussion of the simplified flow shown in fig. 11 is applicable to the more realistic case shown in fig. 12.

Fig. 11

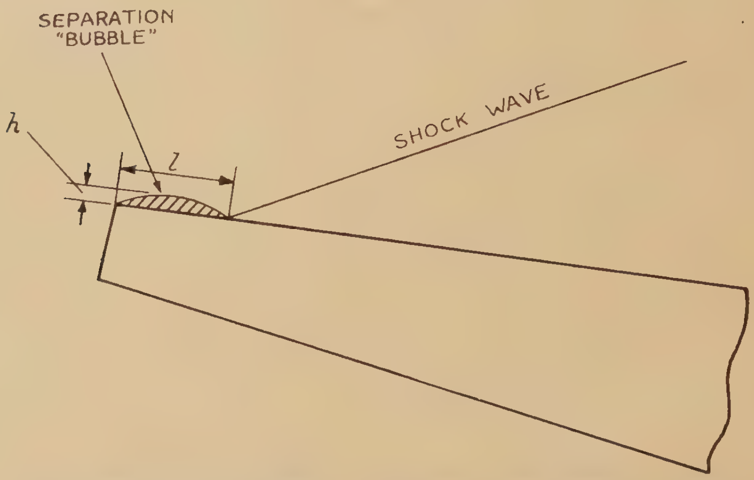

Simplified form of separation " bubble ", with sharp corner at point of re-attachment.

Fig. 12

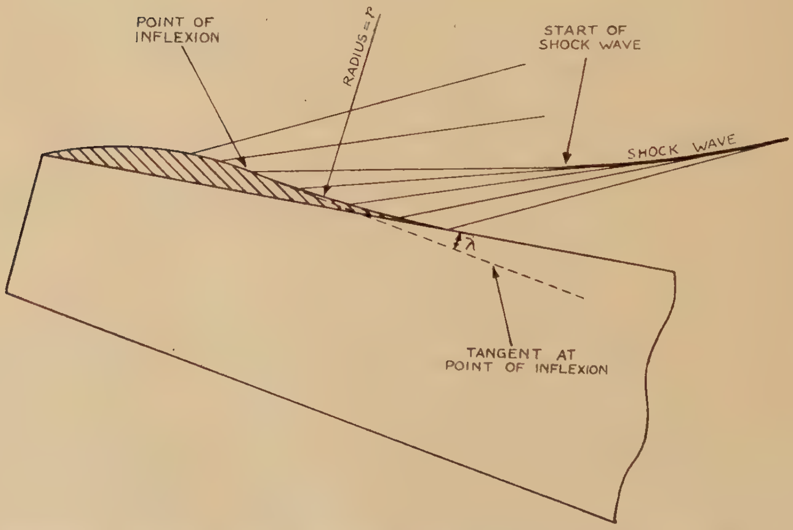

Separation " bubble " with concave transition curve on downstream side.

It is of interest to calculate the order of magnitude of the distance d from the surface of the wedge to the point at which the shock wave attains its maximum strength. By calculating the Mach-line pattern for a typical case (still neglecting the variation of entropy behind the bow shock-wave) it was shown that the distance from the point at which the shock wave *started* to the point of maximum strength was small compared with the distance d. Hence d is approximately equal to the distance from the wedge to the point at which the shock wave starts. Meyer (1948) has shown that for a circular-arc boundary of radius r this is given by

$$d=\left[\frac{2(M^2-1)}{(\gamma+1)M^4}\right]r\approx\frac{r}{7}\quad(\text{for } M\approx 2{\cdot}2). \quad . \quad . \quad . \quad . \quad (3)$$

(The presence of an expansion region on the upstream side of the compression region has no effect on this distance.)

In the limiting case when the second shock wave is only *just* detectable, the concave part of the boundary has a length of order 1 mm and subtends an angle of order 0·01 radian, so that its radius of curvature r is of order 100 mm and the distance d is of order 10 mm. This means that the maximum shock-wave strength as calculated above occurs far enough from the wedge for the shock wave to be easily seen.

The effect of variation of entropy behind the bow shock-wave will now be considered. For the present purpose we may define the ‘ entropy boundary-layer ’ as the layer adjacent to the wedge in which the increase of entropy due to the effect of the bow shock-wave is greater than 10% of the maximum increase of entropy (occurring at the normal part of the bow shock-wave). Consideration of the photographs given by Holder *et al.* (1949) shows that the thickness of this entropy boundary-layer is of the order $10\,t$. But in the important case where the second shock wave is only just detectable the distance d is at least $100\,t$. This means that the thickness of the entropy boundary-layer is small compared with the distance from the surface to the point at which the shock wave starts. Thus the Mach-line curvature caused by the variation of entropy can only have a small effect on the strength or position of the second shock wave.

It is interesting to note that if $t=0{\cdot}1$ mm the thickness of the entropy boundary-layer is about 10 times the thickness of the ordinary ‘ viscosity boundary-layer ’ at a distance of 1 mm from the leading edge (assuming no separation).

It may be concluded that, if the boundary layer separates, the second shock wave that is formed near the point of re-attachment will be strong enough to be detected by the schlieren system. Thus the absence of any visible second shock wave for $R_t<1000$ indicates that the boundary layer does not then separate.

§6. STRENGTH OF THE BOW SHOCK-WAVE

The angle between the bow shock-wave and the incident stream was measured on the photographs at various distances from the leading edge. From these angles approximate values of the shock-wave strength were calculated, but because the shock-wave angles were only slightly greater than the Mach angle the errors in these calculated strengths were rather large. Hence a small error in measuring the shock-wave angle produced a relatively large error in the calculated strength.

The theory given by Friedrichs (1948) shows that the strength of the bow shock-wave at large distances from a blunt-nosed body should be inversely proportional to the square root of the distance y from the body, measured normal to the stream, so that

$$s=k(t/y)^{1/2}, \qquad (4)$$

where k is a constant for geometrically similar bodies. Values of k were calculated for all the different cases, for various values of y. Although the results showed considerable scatter (as would be expected because of the large errors in determining s), there was no systematic difference in k between the cases with and without separation of the boundary layer. This result is to be expected if h (see fig. 11) is small compared with the distance from the leading edge to the point of maximum bubble height, even if h is *not* small compared with t. The effective thickness of the leading edge is then only slightly influenced by the separation bubble.

§7. CONCLUSION

It has been shown that the boundary layer separates if the Reynolds number R_t is greater than about 1000, while for smaller values of R_t there is no separation. This result disagrees with the usual conclusion from laminar boundary-layer theory that the position of separation should be unaffected by changes of Reynolds number. The explanation of this is that when the surface curvature is very high (as at the shoulder) the assumptions of boundary-layer theory are not valid, especially at such low Reynolds numbers, so that the occurrence of separation can depend on the Reynolds number.

ACKNOWLEDGMENTS

The authors wish to thank Dr. N. H. Johannesen and Mr. G. B. Whitham for their help in estimating the strength of the second shock wave. During the course of the research one of the authors (O. B.) was assisted by a grant from the Aeronautical Research Council.

REFERENCES

BARDSLEY, O., 1951, *Phil. Mag.*, **42,** 255–262.
BARDSLEY, O., and MAIR, W. A., 1951, *Phil. Mag.*, **42,** 29–36.
COPE, W. F., and HARTREE, D. R., 1948, *Phil. Trans. Roy. Soc.* A, **241,** 1–69.
FRIEDRICHS, K. O., 1948, *Communications on Applied Mathematics*, vol. I, pp. 211–245.
HOLDER, D. W., TOMLINSON, R. C., and ROGERS, E. W. E., 1949, *A.R.C.* 12418 (to be published).
MAIR, W. A., 1951, *Aero. Quart.*, (in press).
MEYER, R. E., 1948, *Quart. J. Mech. App. Math.*, **1,** 451–469.
WHITHAM, G. B., 1951 (to be published).

XXX. *A Note on Estimating Yield-Point Loads in a Plastic–Rigid Body*

By R. Hill
Department of Theoretical Mechanics, University of Bristol*

[Received November 27, 1951]

Summary

Bounds are obtained for the error committed when any approximate theory of plasticity is used to estimate yield-point loads. It is shown, for example, that, if the Mises yield function and potential are used to approximate the Taylor-Quinney data for copper, the error is less than 1% for a wide variety of loading programmes.

In applications of the mathematical theory of plasticity it is usually necessary to assume a yield function and plastic potential which are convenient approximations to the available experimental data. The purpose of this note is to state explicit bounds to the error committed when estimating yield-point loads with any such approximate theory.

We suppose that the arbitrary scale-factor in the plastic potential is so chosen that the corresponding surface in stress-space is inscribed in the yield surface. We use the maximum work principle (Hill 1948) for a plastic-rigid body caused to deform, in whole or part, by forces $\mathbf{F}$ per unit area prescribed over a portion S_F of the surface, and velocities $\mathbf{u}$ prescribed over the remainder S_U. The principle states that

$$\int \mathbf{F}\,.\,\mathbf{u}\,dS_U \geqslant \int \mathbf{F}^*\,.\,\mathbf{u}\,dS_U,$$

where $\mathbf{F}^*$ corresponds to any arbitrary equilibrium distribution of stress, not violating the yield-condition anywhere in the body and such that $\mathbf{F}^*=\mathbf{F}$ on S_F. This is valid if the yield function and plastic potential are identical at each point of the body. When they differ, the principle is still true provided that the arbitrary stress, represented by a vector $\boldsymbol{\sigma}^*$ in stress-space, is restricted to lie within the potential surface. For, if the actual stress-vector $\boldsymbol{\sigma}$ cuts the potential surface at the point $\lambda\boldsymbol{\sigma}(0<\lambda\leqslant 1)$, then

$$(\boldsymbol{\sigma}-\boldsymbol{\sigma}^*)\,.\,\dot{\boldsymbol{\epsilon}} \geqslant (\lambda\boldsymbol{\sigma}-\boldsymbol{\sigma}^*)\,.\,\dot{\boldsymbol{\epsilon}} \geqslant 0,$$

since the strain-rate vector $\dot{\boldsymbol{\epsilon}}$ is parallel to the outward normal at the point $\lambda\boldsymbol{\sigma}$, and the actual rate of work $\boldsymbol{\sigma}\,.\,\dot{\boldsymbol{\epsilon}}$ is positive. The result follows on integrating throughout the body.

---

* Communicated by the Author.

For the given boundary conditions let W denote the rate of work of forces over S_U in a yield-point state associated with some given theory or experimental data. W is independent of the previous loading programme if the yield function and potential are identical (Hill 1951), but may not be if they are different (so far as is known at present). For simplicity, suppose that the respective *shapes* of the yield and potential surfaces are constant throughout the body, though the degree of hardening may vary (as measured locally by the absolute size of the yield surface). For a hardness distribution similar to this given one, we can calculate the rate of work of forces over S_U in a yield-point state associated with any convenient choice of yield function and potential. Let W_H be the work-rate for any chosen harder material whose *potential* surface circumscribes the given *yield* surface, and W_S the work-rate for any chosen softer material whose *yield* surface inscribes the given *potential* surface. Then, by the maximum work principle,

$$W_S \leqslant W \leqslant W_H.$$

In particular, the closest upper bound is obtained when the chosen yield function and potential are both equal to the given yield function, and the closest lower bound when they are both equal to the given potential. For certain given variations of $\mathbf{u}$, or for prescribed load-ratios over the whole surface, the equation may be replaced by a similar one for the yield-point loads. It is to be noted that, when $\mathbf{F}=0$ on S_F, W_H/W_S is equal to the ratio of the respective hardnesses when similar yield and potential surfaces are used for both bounds (since there then exist associated yield-point states differing only by this factor of proportionality).

As an illustration, suppose that it is required to approximate the Taylor-Quinney data for copper and aluminium (nominally isotropic) by the Mises yield function and Lévy-Mises potential. The data, plotted in principal-stress space, are conveniently shown in fig. 1 of the paper by Bishop and Hill (1951). It will be observed that the Mises circular cylinder, when circumscribed to the actual yield surface, touches it along generators corresponding to pure tension or compression; the actual potential surface also touches it there, while the inscribed cylinder touches the potential surface along generators corresponding to pure shear. The ratio of the radii of the two cylinders is about 1·03 for aluminium, and not more than 1·02 for copper. If, then, when $\mathbf{F}=0$ on S_F, we use yield stresses respectively $1\frac{1}{2}\%$ and 1% less than the actual ones, the error in W is less than $1\frac{1}{2}\%$ for aluminium and less than 1% for copper. Of course, local stresses or the deformation mode may differ much more, depending on the particular application. Alternatively, if we were to take as the standard of comparison the yield function and potential calculated by Bishop and Hill for a polycrystal, the ratio of the cylinder radii would be 1·07 and the error in W $3\frac{1}{2}\%$.

Finally, suppose that the Mises yield function and potential are the standard of comparison, and that the former is approximated by the Tresca yield function. The corresponding hexagonal prisms, circumscribed and inscribed to the circular cylinder, are in ratio $2/\sqrt{3} \sim 1{\cdot}155$; by taking the mean hexagon the error in W can therefore be limited to less than 8% (when $\mathbf{F}=0$ on S_F). A similar conclusion holds if we use the hexagon with sides normal to vectors representing pure tension (Hill 1950). The limits of error are the same, too, if the Tresca yield function is also used as plastic potential; work in progress indicates that this facilitates the solution of axially-symmetric and other three-dimensional problems.

REFERENCES

BISHOP, J. F. W., and HILL, R., 1951, *Phil. Mag.*, **42**, 1298.
HILL, R., 1948, *Quart. J. Mech. App. Math.*, **1**, 18; 1950, *Phil. Mag.*, **41**, 733; 1951, *Ibid.*, **42**, 868.

XXXI. *On Photometry in Thick Nuclear Emulsions*

By M. Ceccarelli and G. T. Zorn
H. H. Wills Physical Laboratory, University of Bristol*

[Received November 1, 1951]

Abstract

Photometric methods of determining the ionization produced by a charged particle in passing through nuclear emulsions are discussed and a technique based on measuring the mean width of a track is described. The method has been tested by applying it to a study of the heavy primary component of cosmic radiation. It is concluded that the photometry of tracks produced by charged particles passing through electron sensitive emulsions may be used as a sensitive measure of the specific ionization for values of the rate of loss of energy less than 30 Mev/g/cm^2, and greater than 200 Mev/g/cm^2. Similar methods can also be applied for identifying multiply charged particles, if they are arrested in the emulsions, and if the length of their tracks exceeds 200 μ.

§1. Introduction

One of the most important technical problems in nuclear physics is to measure the ionization produced by a charged particle in passing through matter. In nuclear emulsions and for particles of small charge, this ionization can usually be expressed as a function of the number of developed grains along the trajectory of the particle. Thus, it was shown by Fowler (1950) that for tracks in Ilford G5 emulsions with a grain density less than 100 grains/100 μ, the number of grains is, to a sufficient approximation, proportional to the energy loss of the particle. For larger values of the grain density, however, the effect of ‘ saturation ’ becomes important, and the subjective difficulties of counting make the results unreliable. This difficulty can sometimes be overcome, for the larger values of the specific ionization, by grain counting in less sensitive or under-developed emulsions. With emulsions of low sensitivity, however, we may expect a non-linear variation of grain density with energy loss so that careful calibration is necessary.

In regions where grain counting becomes impossible, an alternative method of measuring the ionization is to count the number of δ-rays along the track. In electron sensitive emulsions, δ-rays of energy above $\sim$15 kev produce short tracks containing three or more grains, and their number per unit length can also be taken as a measure of the specific ionization of the particle, (Frier, Lofgren, Ney, Oppenheimer, Bradt and

---

* Communicated by Professor C. F. Powell, F.R.S.

Peters 1948). This method has been of great importance in extending the range of values of the specific ionization which can be measured, but it suffers from the fact that it is sometimes difficult to decide whether a particular electron track is associated with that of the multiply charged particle. It is also difficult to maintain a constant criterion to ensure accepting only those δ-rays with an energy above a certain lower limit. Finally, if the number of δ-rays/100 μ exceeds 20, counting becomes very difficult and the results are subject to large errors.

An alternative to these methods is to make photometric measurements of the obscuration produced by a track, and very encouraging results have been obtained with electron sensitive emulsions 200 μ thick by von Freisen and Kristianson (1950). These authors showed by such methods that it is possible to distinguish between π and μ mesons stopping in the emulsion. Other interesting results have been obtained by Blau, Rudin and Lindenbaum (1951) in studies of tracks of the heavy component of the primary cosmic radiation, using Kodak NT4 emulsions 80 μ thick.

The present experiments were undertaken to investigate the possibility of photometric methods in electron sensitive emulsions 400 μ thick. The extension of the methods to such thick emulsions is important because they provide favourable conditions for energy measurements by the scattering method.

§2. EXPERIMENTAL

Direct Measurement of Obscuration Produced by a Track

Measurements have been made on Ilford G5 Nuclear Research emulsions 400 μ thick using the procedure of von Freisen and Kristianson. An image of the track was formed in the plane of a narrow slit of which the long axis was parallel to the track, by an objective with magnification × 95. The light passing through the slit was directed on to the cathode of a photo-multiplier tube and the resulting anode-current was measured by a galvanometer. A galvanometer reading was first taken when the image of the track was contained within the area of the slit. After moving the plate approximately 50 μ in a direction perpendicular to that of the track, a second reading was taken to determine the background. If these two galvanometer readings are R_t and R_b, respectively, then the relation $R=(R_b-R_t)/R_b$ is a measure of the 'total obscuration' produced by the track. Provided that the image of the track in the slit is black, and that the number of background grains is small, R expresses the ratio between the projected area of the track contained in the slit and the area of the slit. This interpretation of R is valid if thin emulsions of high transparency are used, but owing to scattering of light, difficulties are met in experiments with thick emulsions.

Effect of Scattering of Light in Thick Emulsions

In order to examine the effect of the scattering of light, measurements of R were made, at different depths in the emulsions, on the tracks of particles which traversed it. Fig. 1, curve F, shows the values of R for a typical track, produced by an oxygen nucleus moving at a relativistic velocity, at different depths in the emulsion. It will be seen that the results suggest a marked decrease in the opacity of the track with increasing depth. It follows that the value of R can be taken as a measure of the projected area of the track only in a region very near the surface of the emulsion. Even in this region, however, measurements are not reliable because of processing irregularities. We have found that the function relating the value of $R/R_{\max}$ with the depth varies in passing across a single plate so that a correction for the apparent decrease of opacity with depth is generally impracticable.

Fig. 1

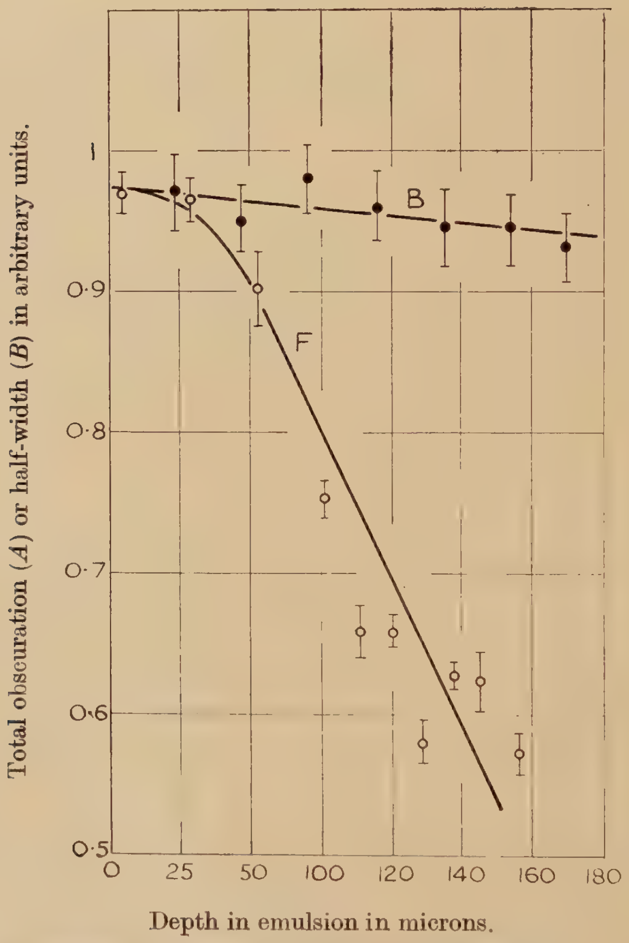

The 'total obscuration' (curve A), and the 'half-width' (curve B), as a function of depth below the surface of the processed emulsion, for the track of an oxygen nucleus which traversed an Ilford G5 emulsion, 400 μ thick.

Several attempts to overcome these difficulties were made by decreasing the effect due to the scattering of light by the emulsion above the track. These included the use of red light and of polarized light. Changes were also made in the optical equipment such as a decrease of the 'numerical aperture' of the objective, illumination by a narrow slit, and dark field illumination. They were unsuccessful and an alternative approach was therefore adopted.

Distribution of Blackening of a Track

A slit, having an apparent width in the object plane of approximately 0·25 μ, was set parallel to the image of a track formed in the plane of the slit. By means of the horizontal stage motion, the plate was then moved in a direction perpendicular to that of the track through a distance of about 100 μ. In effect, the image of the track passed across the slit, remaining always parallel with it. At regular intervals during this movement, galvanometer readings were made, and a plot of these as a function of the distance moved gives a measure of the 'blackening' of the track as a function of the distance from its axis. Examples of such observations for tracks of different specific ionization are shown in fig. 2.

Fig. 2

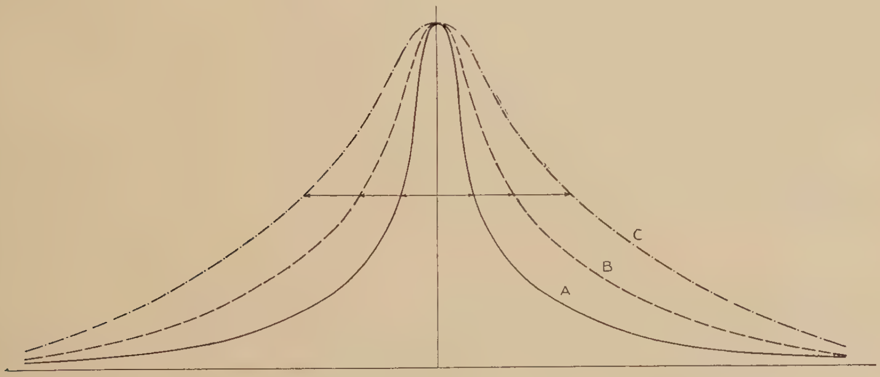

Distance from axis of track.

'Blackening distributions' for the tracks of three particles A, B and C, the ionization loss of which were 350, 820 and 1400 Mev/g/cm^2, respectively. The curves have been normalized to correspond to the same maximum amplitude.

Experiments showed that the shape of a curve obtained by the above method is independent of the width of the slit if its image in the object plane is less than the mean diameter of a silver grain. The general form of the curves is also independent of the ionization of the particle producing the track.

Further, fig. 1, curve *B*, shows the result of measurements of the widths of the curves at half amplitude (' half-width '), for the same track as that considered in curve *F*, and proves the that value of the half-width is independent of the depth of the track in the emulsion. The half-width may therefore be taken as a measure of the ionization of the particle.

Fig. 3

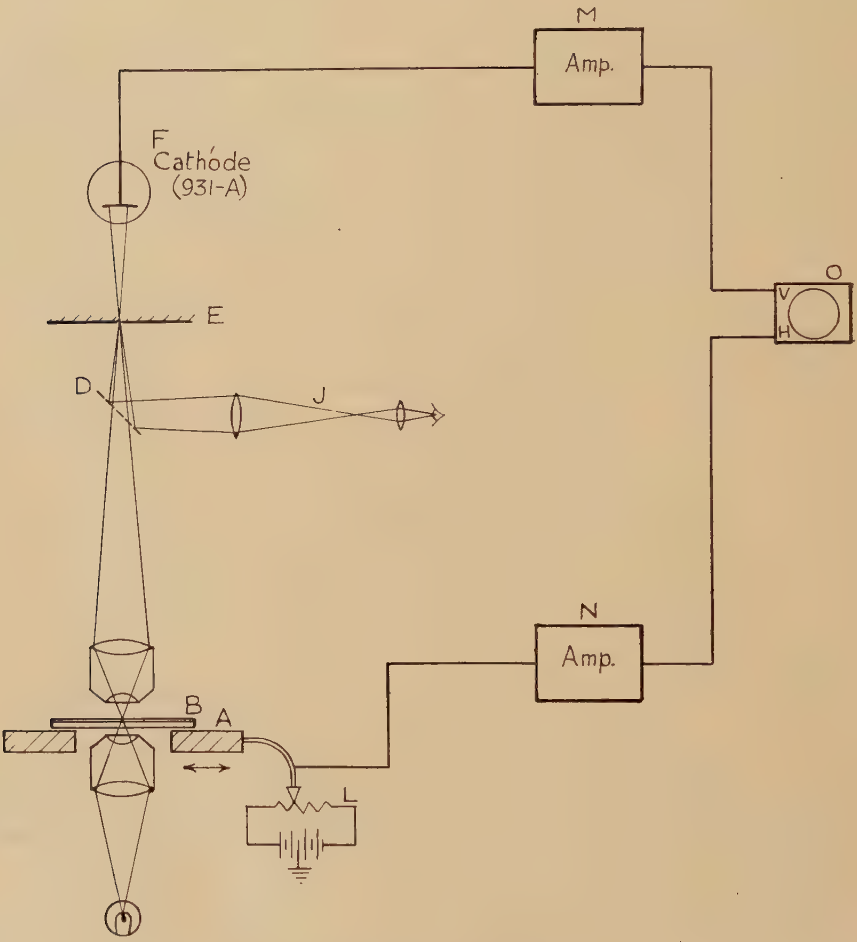

Diagram of the apparatus.

In order to decrease the time required for the measurements and to improve their accuracy and statistical weight, a semi-automatic apparatus was built which traces the blackening distribution on the screen of an oscilloscope.

§ 3. Apparatus

Fig. 3 is a schematic diagram of the apparatus used in the latter part of this investigation. The basic component is a Cooke, Troughton and Simms M4000 microscope, equipped with a nuclear research stage, *A*. An 'event' in nuclear plate B, is illuminated by a substage condenser and its image is formed on a glass mirror surface, E. This image is viewed with an auxiliary low-power microscope, J, by means of a partially silvered glass surface, D. Through the auxiliary microscope one can observe a slit 20 μ wide by 4 mm long, contained in the mirror surface. This slit permits light from the objective to fall on a photo-multiplier tube, F, and the voltage output of the photo-multiplier is proportional to the intensity of the light incident upon it. This output voltage is amplified by linear d.c. amplifier, M, which activates the vertical deflection coils, V, of the oscilloscope O.

The horizontal deflection of the electron beam is controlled by the stage movement ; when the stage is moved by the rotation of a micrometer screw, the voltage output of the potentiometer, L, varies linearly with this motion, as is shown schematically in fig. 3. This varying potential is amplified by another d.c. amplifier, N, which activates the horizontal deflection coils H of the oscilloscope.

In making measurements, the photographic plate is placed on the microscope stage in such a position that the track to be studied is aligned perpendicular to the direction of the motion of the stage indicated in fig. 3. The slit is then adjusted until it is parallel to the image of the track by observation through the auxiliary microscope. The oscilloscope pattern is now traced by moving the image of the track across the field of view.

The resultant trace represents the output of the photo-multiplier tube as a function of the stage movement and has the same form as the curves of fig. 2.

§4. Results and Discussion

Using the apparatus described in the preceding section, a preliminary experiment was made to determine the change in the shape and dimensions of the patterns traced by the oscilloscope when the image of the track in the plane of the slit was defocused or was misaligned with the slit. It was found that the errors introduced into the measurements by small subjective inaccuracies, either of focussing or alignment, were negligible. It was found also that, to a first approximation, the area of the patterns for the same section of the track was independent of the focussing position. This indicates that the obscuration produced by a silver grain in the emulsion does not depend upon the focussing and that only the apparent area of the grain is affected.

In order to determine the blackening distribution as a function of the distance from the centre of the track, measurements were made on a selection of tracks of heavy nuclei of which the charge had been determined by measurements of δ-ray density and multiple scattering. (Dainton, Fowler and Kent 1951). At regular intervals along the track the oscilloscope patterns were recorded on tracing paper and the ‘ average ’ pattern determined. Several of these curves, normalized to correspond both to a given value of the half-width and to a given maximum amplitude are shown in figs. 4 and 5. Fig. 4 shows such normalized distributions for four tracks, A, B, C and D, of which the parent particles had approximately the same velocity but values of the specific energy loss equal to 160, 680, 1100 and 3000 MeV/g/cm^2, respectively. Similar results are shown in fig. 5 for particles with specific ionization above 100 MeV/g/cm^2 but with very different velocities.

The curves shown in fig. 4 indicate that, within the experimental errors, the form of the curve showing the distribution of blackening across the track is independent of the ionization produced by the particle, provided that it has an energy loss greater than 200 MeV/g/cm^2. This confirms the view that the magnitude of the half-width gives a satisfactory measure of the ionization of the particle. It also establishes in this range of specific energy loss the fact that the half-width of the distribution and the total obscuration are proportional to one another.

Fig. 4

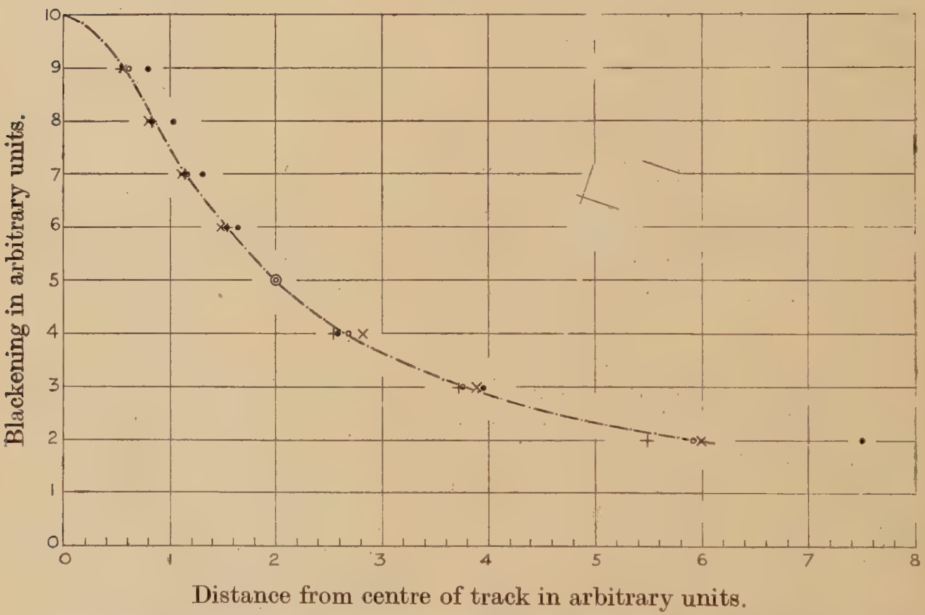

'Blackening distribution' for the tracks of four particles, *A*, *B*, *C* and *D*, each with approximately the same velocity but with specific energy-loss 160, 680, 1100 and 3000 MeV/g/cm^2, respectively. The corresponding symbols are ●, ○, × and +, respectively. The distributions have been normalized to correspond both to a given maximum amplitude and to a given value of the half-width.

Since the obscuration produced by a grain does not depend appreciably on the sharpness with which it is in focus, any of the curves in figs. 4 and 5 gives an approximate representation of the distribution of ionization in the neighbourhood of the track of the particle, except for the 'saturated' region of the core. It is not practicable to deduce the distribution in range of the δ-rays from such curves, for this involves difficult and uncertain corrections. Our results show, however, that this distribution does not change appreciably after the velocity exceeds 10^{10} cm/sec of the particle, even if it is in the extreme relativistic region.

Another investigation was made in order to compare the obscuration caused by a track with the specific ionization of the particle producing it. Measurements of total obscuration and half-width were made on the tracks in Ilford G5 emulsion of 98 particles with a specific ionization varying from that of relativistic α-particles to that of iron nuclei in the region of maximum ionization. These particles were identified by measurements of multiple scattering and δ-ray density. Alternatively, identity was established in the case of particles which were arrested in the emulsion, either by range and δ-ray measurements or by secondary effects occurring at the end of the track.

Fig. 5

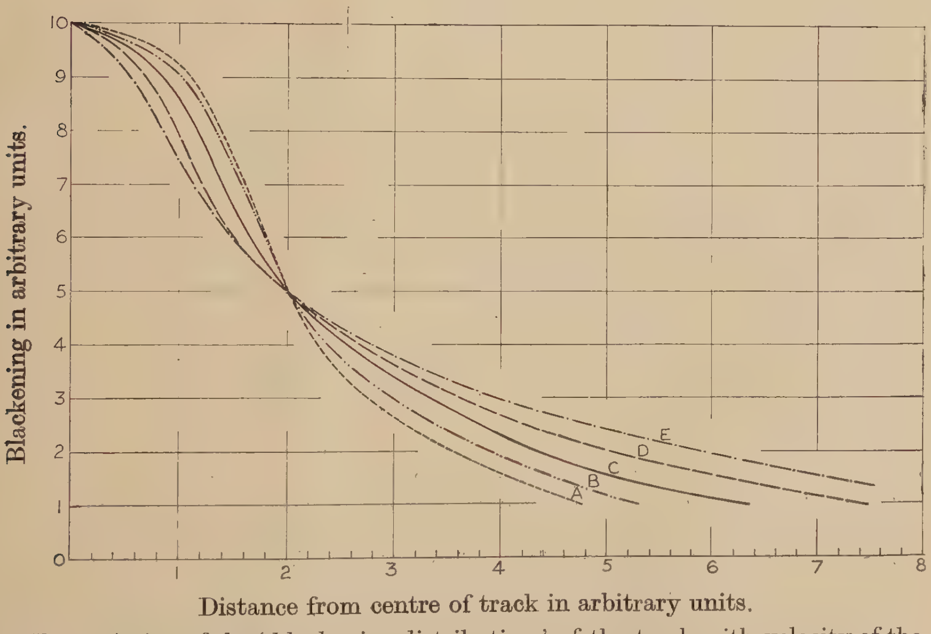

The variation of the ' blackening distribution ' of the track with velocity of the parent particle. Curves *A*, *B*, *C*, *D* and *E* were obtained from measurements on the track of a magnesium nucleus, at average residual ranges of 150, 300, 500, 900 and 1500 μ respectively. The curves have been normalized to correspond to the same value of the half-width and to a given maximum amplitude. Curve *E* coincides with the average curve of fig. 4, and corresponds to a velocity of the parent nucleus of approximately 10^{10} cm/sec.

Values of the ' total obscuration ' and ' half-width ' of these tracks are represented as a function of the specific energy loss of the particle in fig. 6, curves A_1 and A_2 respectively. In this figure we have also plotted the following quantities as a function of the specific ionization loss : B, the number of δ-ray tracks with more than 3 grains per 100 μ (Dainton, Fowler and Kent 1951); *C*, the number of grains/50 μ in under developed Kodak NTA emulsion (Bradt and Peters 1950); and *D*, the number of developed grains/50 μ in normally developed emulsions (Fowler 1950).

The lower part of Curve A_1, fig. 6, shows a linear relationship between the obscuration and energy loss. Curve A_2 is a plot of the half-width in arbitrary units as a function of the specific energy loss and shows the approximately linear relation between the two quantities, the saturation being significant for a specific energy loss less than 100 MeV/g/cm². The saturation effect is probably due to the fact that a very large percentage of the energy is expended in the projection of electrons of which the range is less than the mean diameter of a silver grain. For particles having a specific energy loss greater than 300 MeV/g/cm² however, the number of developed grains caused by δ-rays is larger than the number of grains in the saturated core of the track. This fact, together with a small correction due to the superposition of grains belonging to different planes of the emulsion, allows us to explain the proportionality between half-width and specific energy loss.

Fig. 6

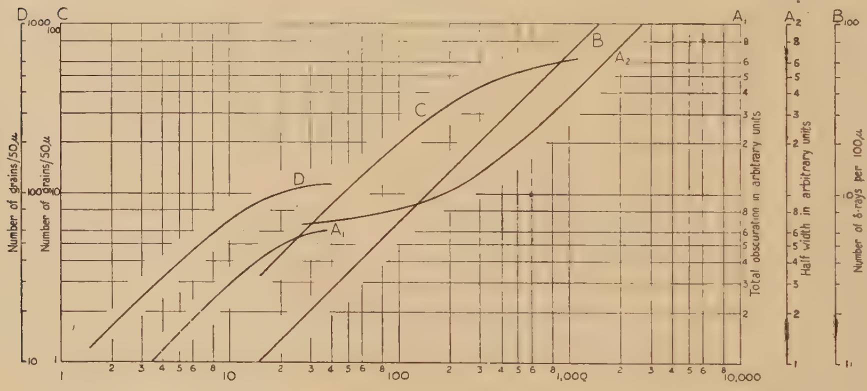

Specific energy loss in MeV/g/cm².

Comparison of methods used to determine the specific energy loss of particles in photographic emulsions :—

A_1, 'total obscuration' in arbitrary units, for Ilford G5 emulsion.
A_2, 'half-width' in arbitrary units for Ilford G5 emulsions.
B, number of δ-ray tracks with more than 3 grains per 100 μ in Ilford G5 emulsion (Dainton, Fowler and Kent 1951).
C, number of grains per 50 μ in underdeveloped Kodak NTA emulsion (Bradt and Peters 1950).
D, number of grains per 50 μ in normally developed Ilford G5 emulsions (Fowler 1950)

plotted as a function of the specific energy loss in MeV/g/cm².

For particles with an energy loss greater than 300 MeV/g/cm² and with a velocity greater than 10^{10}cm/sec, the linear relation between photometric opacity and energy loss suggests the use of photometry as the most suitable method of determining the ionization. For rates of energy loss between 30 and 100 MeV/g/cm^2 photometry is unsuitable because the method is too insensitive.

Fig. 7

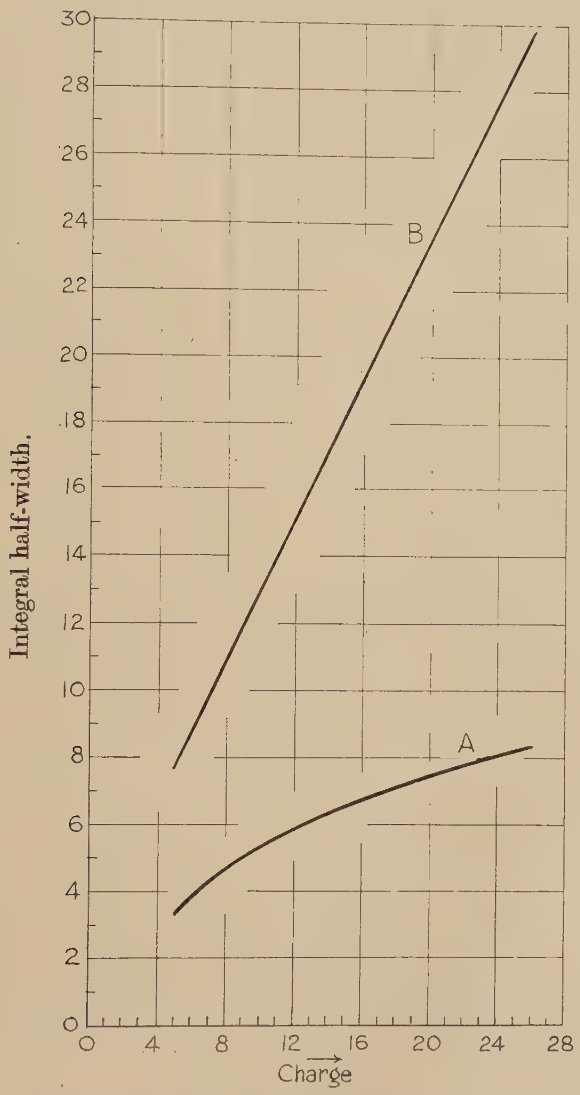

'Integral half-width' for tracks of nuclei ending in the emulsion. Curves *A* and *B* represent the integrated half-width, measured over ranges from the end of the track of 200 and 500 μ respectively, and plotted as a function of the charge of the parent particle.

Another investigation was made to determine the possibility of identifying, by similar methods, particles arrested in the emulsion. If the tracks of such particles are too short, other means of identification cannot be applied. Measurements were made of the half-width of the track at a succession of points $50\,\mu$ apart, starting from the end of the track. The sum of the values thus obtained, up to any particular range from the end of the track, was called the 'integral half-width' and curves A and B of fig. 7 show values of this quantity for nuclei of different charge. For curve A values of the integral half-width have been determined by measurements on the last $200\,\mu$ of the tracks of particles of different charge. Curve B represents the result of similar observations on $500\,\mu$ of each track. These curves, together with the results of von Freisen and Kristianson, show that photometry provides a satisfactory method of identifying charged particles which stop in the emulsion.

§5. CONCLUSION

The results of the present work on the application of photographic methods in studying tracks of charged particles in photographic emulsions can be summarized as follows :

A. It is confirmed that photometry is a very useful method for studying particles with a specific ionization so great that grain counting cannot be employed, and it can be applied in cases where the energy loss is less than 30 MeV/g/cm^2. In this region the only technique that can be used is the measurement of the total obscuration and, for such measurements, thick emulsions of low transparency are generally unsuitable.

B. For studying particles with a specific energy loss greater than 300 MeV/g/cm^2 the use of underdeveloped emulsions involves difficult calibration, and δ-ray counting is unreliable. For such particles, photometric methods, and in particular the measurement of the half-width can be successfully applied even with emulsions of low transparency.

C. Multiply charged particles which produce short tracks terminating in the emulsion (Range $\geqslant 200\,\mu$) can be identified by determining the integral half width, for this quantity varies rapidly with the charge of the particle.

ACKNOWLEDGMENTS

This work was originally undertaken in collaboration with Mr. J. Webb to whom we are particularly indebted.

We have pleasure in thanking Prof. C. F. Powell, F.R.S., for his continued interest and encouragement ; Messrs. A. D. Dainton, D. W. Kent and P. H. Fowler, for supplying the identified tracks for this investigation, and for helpful discussion and advice ; and Mr. M. A. Roberts and Mr. G. Coombs for considerable technical assistance.

REFERENCES

BLAU, RUDIN, and LINDENBAUM, 1950, *Rev. Sci. Instrum.*, **21,** 978.
BRADT and PETERS, 1950, *Phys. Rev.*, **80,** 943.
DAINTON, FOWLER, and KENT, 1951, *Phil. Mag.*, **42,** 317.
FOWLER, 1950, *Phil. Mag.*, **41,** 169.
FREIER, LOFGREN, NEY, OPPENHEIMER, BRADT, and PETERS, 1948, *Phys. Rev.*, **74,** 213.
VON FREISEN and KRISTIANSON, 1950, *Nature, Lond.*, **166,** 686.

XXXII. *The Low Energy Beta-Ray Spectrum of* ^{170}Tm

By R. Richmond and H. Rose
Cavendish Laboratory, Cambridge*

[Received January 3, 1952]

Abstract

A thin magnetic lens beta-ray spectrometer in conjunction with a coincidence circuit employing a pair of photo-multipliers has been used to examine the low energy beta-ray spectrum of ^{170}Tm, which was expected to exhibit a forbidden shape. The spectrum was, however, found to have an allowed shape. The results may best be interpreted on the assumption that the transition is first forbidden with axial vector or tensor interaction, the latter interaction being slightly favoured.

§ 1. Introduction

The low energy beta-ray spectrum of ^{170}Tm (see fig. 1) might be expected to have a forbidden shape, because of its high $\log_{10} ft$ value of 9·71 (Feingold 1951) and because of the beta–gamma angular correlation reported by Novey (1950). An investigation to determine the degree of forbiddenness and to distinguish the type of interaction is described in this paper.

Fig. 1

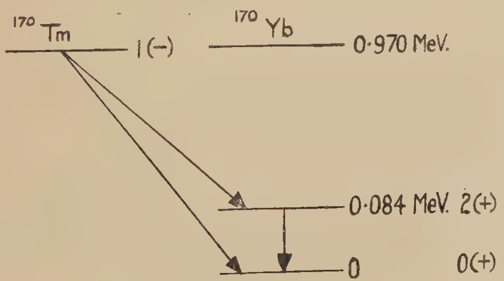

Decay Scheme of ^{170}Tm.

§ 2. Experimental Details

The spectrum was examined by means of a thin magnetic lens beta-ray spectrometer and coincidences were recorded between the low energy beta group and the 84 kev gamma-ray. This method gives a more accurate spectrum than the conventional one of subtracting the 80–90% high energy component from the Kurie plot of the complex spectrum. A photo-multiplier (E.M.I. type 6262) and an anthracene crystal were used to count the beta particles and by examination of spectra with known shapes the combination was shown to have an efficiency which was independent of electron energies in the region 0·15 MEV to 2·5 MEV. The gamma-rays were counted by a similar photo-multiplier used with a liquid phosphor (terphenyl dissolved in toluene) which was contained in a glass flask placed outside the spectrometer vacuum chamber. A polythene window in the wall of the spectrometer transmitted the gamma-rays from the source but completely absorbed the beta-particles. Experiments using brass absorbers showed that 60% of the gamma-ray counting rate was due to the 84 kev gamma-radiation and the remaining 40% to the K x-rays of ^{170}Yb. The flask containing the liquid phosphor subtended a solid angle of about 3½ steradians at the source. This angle was sufficiently large to ensure that no distortion of the spectrum was caused by an energy-dependent beta–gamma angular correlation. No angular correlation is expected between the beta-particles and the K x-radiation (Novey 1950).

---

* Communicated by Mr. E. S. Shire.

Both multipliers were magnetically shielded and the resolving time of the coincidence circuit used with them was 10^{-8} sec. In order to obtain maximum transmission the spectrometer was used with a momentum resolution of 12% and corrections for this resolution were made near the end point of the spectrum. Since for an adequate coincidence counting rate it was necessary to use a thick source (35 mg cm^{-2}) several isotopes giving known spectral shapes were examined using sources of this thickness in order to determine the effects of scattering and absorption in the source and of possible back-scattering from the polythene window. In no case was distortion of the spectrum observed for electron energies greater than 0·4 MEV. The coincidence spectra of ^{24}Na and ^{198}Au gave allowed shapes with end points of 1·36 ± 0·02 MEV and 0·973 ± 0·012 MEV respectively. As an additional check the spectra of ^{24}Na and ^{90}Y were examined with the beta counter alone. An allowed shape was again obtained for ^{24}Na with an end point of 1·37 ± 0·02 MEV. The Kurie plot of the ^{90}Y spectrum was transformed by the a $(=p^2+q^2)$ correction factor (Konopinski 1943) into a straight line with an end point of 2·27 ± 0·02 MEV. All these results are in close agreement with accepted values.

§3. EXPERIMENTAL RESULTS

An uncorrected Kurie plot of the low energy spectrum of ^{170}Tm obtained in our experiments for energies greater than 0·4 MEV is shown in fig. 2, together with Kurie plots to which the first forbidden correction factors a, A_+' and A_-' (using the notation of Konopinski 1943) have been applied. The best straight line is given by the uncorrected plot or the A_+' correction, while the A_-' correction gives a rather worse line. The a correction and also a general second forbidden correction factor

$(W_0-W)^2$ are definitely ruled out. (The $A_{\pm}'$ correction differs only slightly from the $A_{\pm}$ and $A_{\pm}''$ corrections and from the allowed shape owing to the predominance of the energy-independent term $(\alpha Z/2R)^2$.)

The high energy spectrum of ^{170}Tm was found to have an end point of 0·970±0·010 MeV, in agreement with the results of Fraser (1949). The end point of the low energy spectrum should be the difference between the high energy end point and the energy of the gamma-ray, i.e. 0·886±0·010 MeV. Table 1 gives the end points obtained by the method of least squares for the curves of fig. 2.

Fig. 2

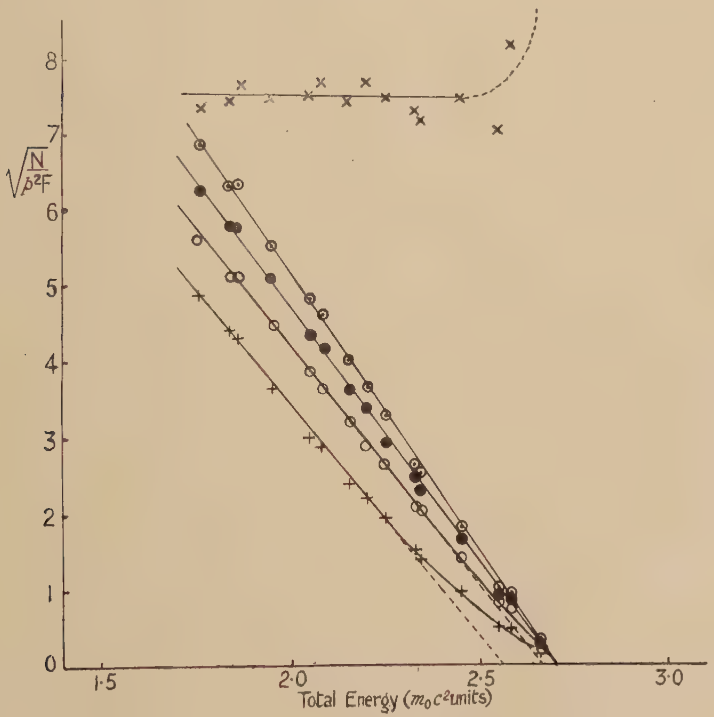

Kurie plots for low energy spectrum of ^{170}Tm.

⊙ Uncorrected, ● A_+' correction, ○ A_-' correction, + a correction, × general second forbidden correction factor. (A further × occurs at $2{\cdot}66m_0c^2$, $\sqrt{(N/p^2F)}=10$.)

Table 1

Correction	Uncorrected	A_+'	A_-'	$a=p^2+q^2$
End point (MeV)	0·874±0·010	0·876±0·013	0·870±0·015	0·800±0·040

Again the a correction may be excluded, while the A_-' correction gives a result slightly further from the expected value than the A_+' correction or the uncorrected shape.

§4. Discussion

^{170}Yb is an even–even nucleus and its ground state should therefore have spin zero and even parity. Measurements of conversion electron intensities (Grant and Richmond 1949) and of the lifetime of the 84 kev excited level (Bell and Graham 1950) have shown that the 84 kev transition is electric quadrupole and consequently the excited level has spin two and even parity. A spin of three or more for ^{170}Tm would make the low energy beta group more favoured than the high energy group and this objection also applies to spin two and even parity.

Spin two and odd parity would make both beta transitions first forbidden but would require the high energy transition to have an α shape. This seems to be excluded by the observations of Fraser (1949). By assuming that the high energy transition was of the allowed shape he was able to distinguish in his complex Kurie plot of ^{170}Tm a lower energy beta group of end point $0{\cdot}900 \pm 0{\cdot}020$ mev which was a straight line. As this result agrees well with our observation of the low energy spectrum one may reverse Fraser's argument and deduce that the high energy transition is in fact of the allowed shape.

Of the remaining possibilities spin zero may be excluded since with odd parity this would lead to an α shape for the low energy spectrum or with even parity to a second forbidden shape. A spin of one and even parity would make both beta transitions allowed in contradiction to their *ft* values and (in the case of the low energy beta group) to the observed beta–gamma angular correlation. ^{170}Tm therefore has spin one and odd parity, as indicated in fig. 1, making both beta transitions first forbidden.

The shell theory of nuclear structure does not seem to be very well established at present for odd odd nuclei. However the stable isotopes ^{169}Tm ($Z=69$) and ^{171}Yb ($N=101$) are both known to have spin $\frac{1}{2}$ (Mack 1950) and therefore ^{170}Tm may well have its odd proton in an $S_{1/2}$ and its odd neutron in a $P_{1/2}$ state. The shell theory definitely predicts odd parity; and the spin would be zero or one for this assignment of orbits. With the 'parallel spins' assumption (Suess, Haxel and Jensen 1949, Nordheim 1950) the total spin would be zero, whereas the observation seems to indicate spin one.

The angular correlation function $W(\theta)$ is of the form $1+R/Q \cos^2 \theta$ for all first forbidden beta transitions followed by a gamma-ray (Falkoff and Uhlenbeck 1950), and Novey (1950) has obtained for ^{170}Tm the correlation function $1-(0{\cdot}259 \pm 0{\cdot}053) \cos^2 \theta$. The beta transition $1(-) \rightarrow 2(+)$ may correspond to any of the nuclear matrix elements $\int r$, $\int \alpha$, $\int \sigma \times r$ and B_{ij} (Konopinski 1943), but of these only $\int \sigma \times r$ would give the negative coefficient R/Q obtained by Novey. The matrix element $\int \sigma \times r$ is associated with the correction factors A_T' (tensor interaction) and A_A' (axial vector interaction). Our results are therefore slightly in favour of the tensor interaction. It is interesting to note that Novey's value of R/Q is in good agreement with the theory (Falkoff and Uhlenbeck

1950) assuming that the beta transition is first forbidden and obeys the tensor form of interaction, but it must be borne in mind that the theoretical value obtained from the figures and tables of Falkoff and Uhlenbeck (1950) is strictly correct only for the case $Z=0$.

We wish to express our thanks to Mr. J. M. C. Scott for many valuable discussions.

REFERENCES

BELL, R. E., and GRAHAM, R. L., 1950, *Phys. Rev.*, **78,** 490.
FALKOFF, D. L., and UHLENBECK, G. E., 1950, *Phys. Rev.*, **79,** 334.
FEINGOLD, A. M., 1951, *Rev. Mod. Phys.*, **23,** 10.
FRASER, J. S., 1949, *Phys. Rev.*, **76,** 1540.
GRANT, P. J., and RICHMOND, R., 1949, *Proc. Phys. Soc.* A, **62,** 573.
KONOPINSKI, E. J., 1943, *Rev. Mod. Phys.*, **15,** 209.
MACK, J. E., 1950, *Rev. Mod. Phys.*, **22,** 64.
NORDHEIM, L. W., 1950, *Phys. Rev.*, **78,** 294.
NOVEY, T. B., 1950, *Phys. Rev.*, **78,** 66.
SUESS, H. E., HAXEL, O., and JENSEN, J. H. D., 1949, *Naturwissenschaften*, **36,** (No. 5), 153.

XXXIII. CORRESPONDENCE

Anomalous Paramagnetism and Exchange Interaction in Copper Acetate

By B. Bleaney and K. D. Bowers
Clarendon Laboratory, Oxford*

[Received January 16, 1952]

The majority of copper salts of reasonable magnetic dilution obey Curie's law with high precision down to very low temperatures. Guha (1951) found, however, that copper acetate, $Cu(CH_3COO)_2$, H_2O had a maximum in its susceptibility (χ) at about room temperature, and at low temperatures χ fell so rapidly that it would reach zero at about 50° K. In view of this paramagnetic resonance measurements at 0·3—0·8 cm^{-1} were undertaken on a single crystal, which showed that the spectrum is quite different from the normal. Soon after we had begun, Lancaster and Gordy (1951) reported resonance measurements on a powder showing similar behaviour, and suggested that a line observed at twice the normal g-value could be explained through interaction between neighbouring copper ions (cf. cobalt (Bleaney and Ingram 1951)). The results of our investigation, and their interpretation, are given below. The measurements have been made principally at 90° K.

Copper acetate grows monoclinic prismatic crystals; the detailed crystallography has not been investigated by X-ray methods. The paramagnetic resonance spectrum is found to resemble that of a nickel Tutton salt (cf. Griffiths and Owen 1951), with two paramagnetic units of apparent spin $S=1$ in unit cell. All our measurements can be fitted to the Hamiltonian

$$\mathscr{H} = DS_z^2+E(S_x^2-S_y^2)+\beta[g_zH_zS_z+g_xH_xS_x+g_yH_yS_y] \quad . \quad . \quad (1)$$

using the values $D=0{\cdot}34$ cm^{-1}, $E=0{\cdot}01$ cm^{-1}, $g_z=2{\cdot}42$, $g_x=g_y=g_\perp=2{\cdot}08$. Thus the z-axis (making an angle $\alpha=\pm 33°$ with the ac-plane) is an axis or nearly tetragonal symmetry, and the g-values are similar to those found in other copper salts. There is a zero field splitting of approximately 0·34 cm^{-1}, and the lines show a curious structure (see Photograph) parallel to the tetragonal axis. This collapses into a single line with no resolved structure perpendicular to this axis.

These results can be satisfactorily explained if strong isotropic exchange forces are postulated between isolated pairs of ions whose individual magnetic axes are parallel to one another. The exchange force is small compared with the crystalline electric field acting on each ion, so that we may take these as orbital singlet states, each with effective spin $\frac{1}{2}$. The exchange couples these spins into a lower antiparallel (and diamagnetic) state with total spin $S=0$, and a higher triplet state with total spin $S=1$, which is paramagnetic. Only the spectrum of this latter state can be observed, of course, and it disappears at 20° K, where substantially all the pairs are in the $S=0$ state.

---

* Communicated by the Authors.

If the exchange interaction is taken to be of the simple form $-J\,S_1 \,.\, S_2$, the Hamiltonian may be written

$$\mathscr{H}=X_1+X_2+\lambda[L_1 \,.\, S_1+L_2 \,.\, S_2]-JS_1 \,.\, S_2+\beta H[(L_1+2S_1)+(L_2+2S_2)]. \quad . \quad . \quad . \quad (2)$$

Here subscripts 1, 2 refer to the two ions ; λ is the spin orbit coupling coefficient. The terms are written in decreasing order of magnitude. Whether the crystalline field (X) is taken either as (cubic+tetragonal) as in the Tutton salts, or as purely tetragonal (corresponding to a likely four planar bonding of copper to the four oxygens of the two acetate groups), the same orbital level will be lowest. The combined effect of the spin-orbit coupling and the exchange gives a singlet state at $\frac{3}{4}J$, plus a triplet at $-\frac{1}{4}J$. The triplet has a small splitting, which, in terms of the Hamiltonian (1) may be written

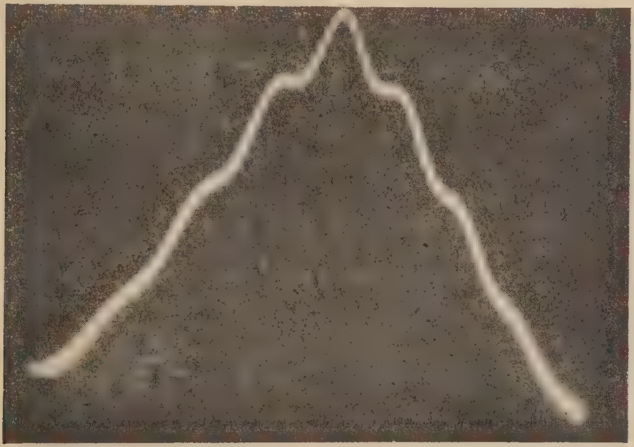

The hyperfine structure of copper acetate.

$$D=-\tfrac{1}{4}J\{\tfrac{1}{8}(g_z-2)^2-(g_\perp-2)^2\}, \quad . \quad . \quad . \quad . \quad . \quad (3)$$

while the formulae for the g-values are the same as for the copper Tutton salts (Abragam and Pryce 1951).

Calculations of the susceptibility shows that our measurements of the g-values and of the angle α give close agreement with the anisotropy observed by Guha. From the temperature variation in his measurements we may obtain the value of J ; a very good fit is obtained if J is assumed to vary slightly with temperature, from -230 cm^{-1} at 80° K to -270 cm^{-1} at

300° K. Such a variation is not improbable, as J varies rapidly with interionic distance, which will change slightly with temperature. This value of J, inserted in (3), gives $D \simeq 1$ cm^{-1}, which is of the same order of magnitude as that observed experimentally. The discrepancy can be explained if J is different for the various orbital levels, since the splitting arises from the small admixture of these into the ground state through the spin-orbit coupling. Since both the splitting and the g-values are related to the crystalline field, the theory shows that both should have the same symmetry axis. This would not necessarily be the case with a splitting due to magnetic dipole–dipole interaction between neighbouring ions, for instance.

Our assumption leads to a natural interpretation of the line structure shown in the photograph. If we add to (1) a term $(S_1 . \tilde{A} . I_1 + S_2 . \tilde{A} . I_2)$ representing the usual magnetic hyperfine structure for the two ions ($\tilde{A}$ being a tensor), each spectral line will be split into several components shifted by $\tilde{A}(m_1+m_2)$ from the centre. Here m_1, m_2 are the nuclear magnetic quantum numbers, which each range from $+3/2$ to $-3/2$ for copper. It is easily seen that this gives seven components with relative intensity 1 : 2 : 3 : 4 : 3 : 2 : 1, which corresponds closely to the observed structure. Parallel to the tetragonal axis, A is approximately 0·008 cm^{-1} while perpendicular it is less than 0·001 cm^{-1}. These values are not greatly different from those in other copper salts.

The mechanism we have postulated is akin to that of antiferromagnetism, except that only pairs of ions are involved, rather than a co-operative effect between many ions. In nuclear paramagnetism it may be likened to the case of ortho- and para-hydrogen. It appears to give a satisfactory explanation of both the fine structure and the hyperfine structure of the paramagnetic resonance spectrum, and of the anomalous variation of the susceptibility.

REFERENCES

ABRAGAM, A., and PRYCE, M. H. L., 1951, *Proc. Roy. Soc.* A, **206,** 164.
BLEANEY, B., and INGRAM, D. J. E., 1951, *Proc. Roy. Soc.* A, **208,** 143.
GRIFFITHS, J. H. E., and OWEN, J., 1951, *Proc. Phys. Soc.* A, **64,** 583.
GUHA, B. C., 1951, *Proc. Roy. Soc.* A, **206,** 353.
LANCASTER, F. W., and GORDY, W., 1951, *J. Chem. Phys.*, **19,** 1181.

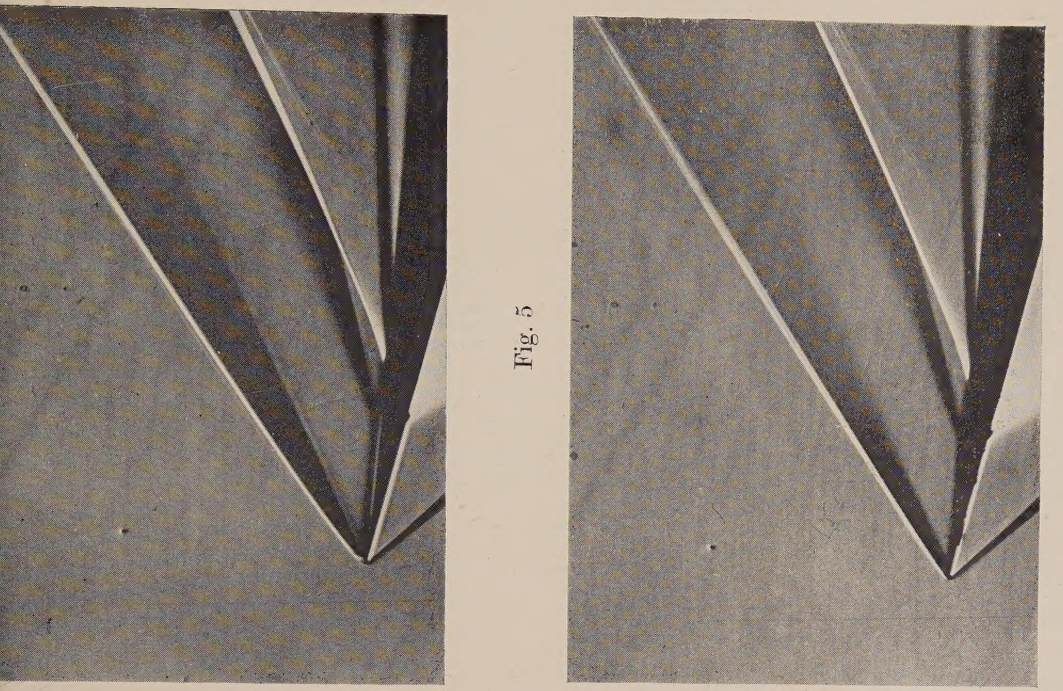

Fig. 5

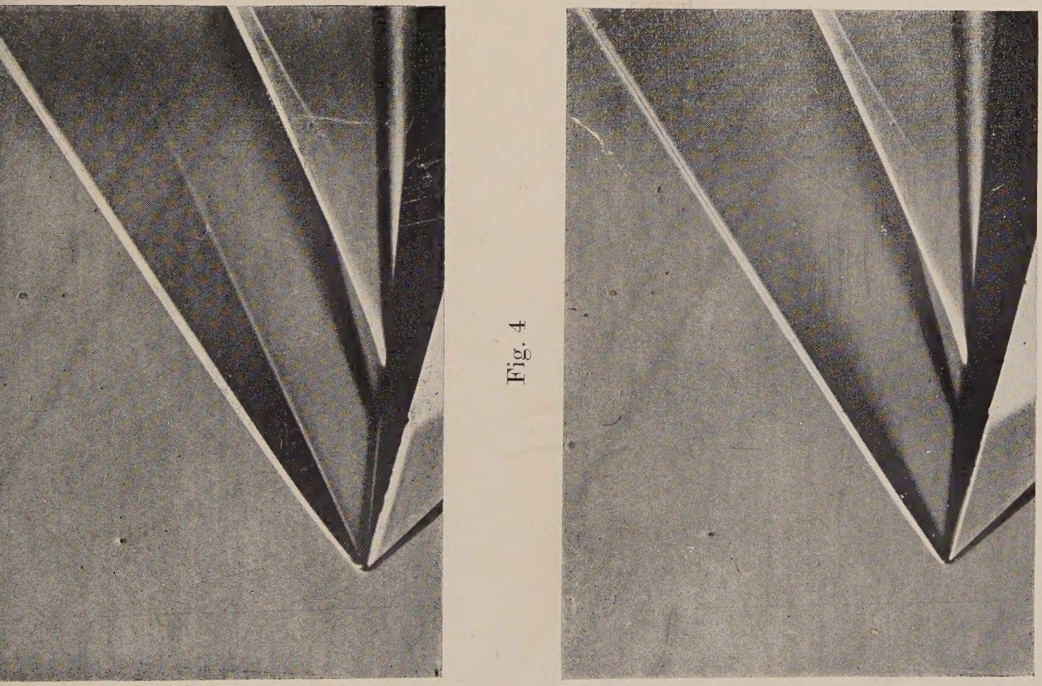

Fig. 4

Fig. 7

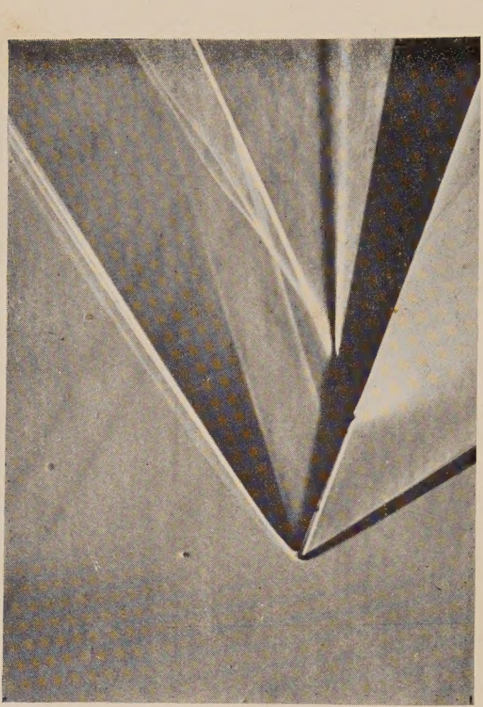

Fig. 9

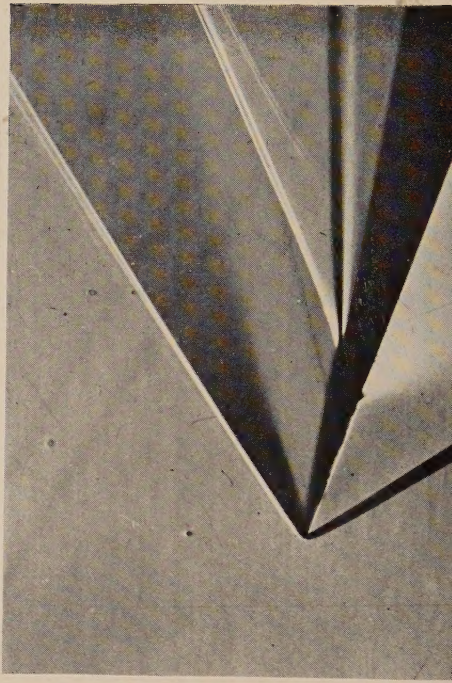

Fig. 6

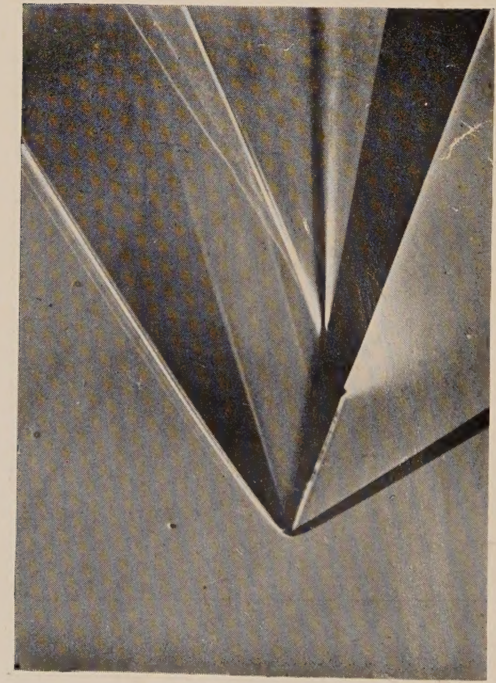

Fig. 8

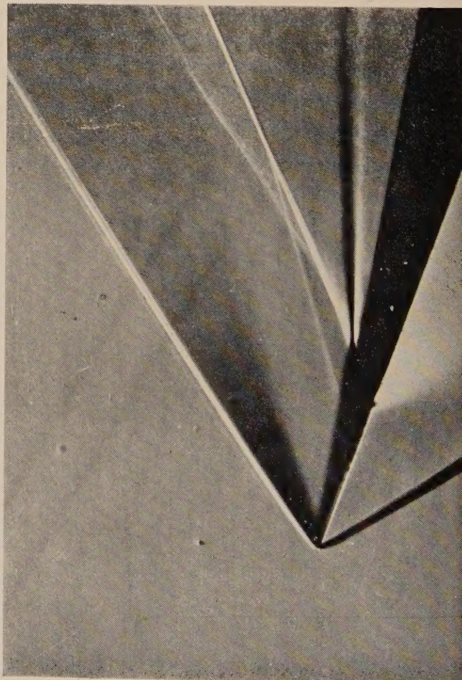

The L *Absorption Spectrum of Nickel. An Anomaly*

By Y. Cauchois
Laboratoire de Chimie Physique, Paris*

[Received January 21, 1952]

The L absorption spectrum of nickel had not been measured previously. In this laboratory we have obtained it with the help of a bent-crystal vacuum spectrograph (Cauchois 1945, 1952) and nickel foils obtained by beating. A gypsum crystal provides, in the experimental device, a dispersion of 1 ev/mm. By registering on the same film, one above the other, the absorption spectrum and the emission spectrum from the same sample when bombarded by electrons, it appears that the L_{III} absorption edge *does not* coincide with the emission edge. The absorption edge is displaced towards lower energies as compared to the emission edge. Discrepancies are of the order of *several times* 0·1 ev.

It is well-known that emission edges and absorption edges of a metal are expected to coincide and in fact do whenever experimental tests could be made (Cauchois 1948). Ni L_{III} seems to be the first and only case when a definite difference is observed.

The measurements of absorption were made on a foil at ordinary temperature, while for emission the foil was heated locally by electron bombardment. This might result in a broadening of the emission edge, together with a mean displacement (due to thermal expansion) towards *low* frequencies ; this is in the opposite direction to the experimental effect reported here.

The observed displacement in our view might well be connected with the magnetic properties of nickel. Further experiments were therefore made with absorbing foils which were heated somewhat above the Curie point. The absorption edge then comes out at higher frequencies than when the metal is ‘ cold ’ ; it is practically at the same position as the emission edge.

The sample used is of somewhat impure nickel whose characteristic data are not precisely known. Its expansion coefficient α may well show some anomalous behaviour at the Curie point, such as is known for some nickel alloys. A sudden decrease in α above the Curie point would displace the edge towards the high energies ; but one would expect the order of magnitude of this displacement to be much smaller than the observed one.

Further experiments are in progress. Tentative explanations will be proposed later.

References

Cauchois, Y., 1945, *Journ. de Phys.*, [8], **6**, 89.
Cauchois, Y., 1952, *Acta Cryst.* (in print).
Cauchois, Y., 1948, Les spectres de rayons X et la structure électronique de la matière. Conférence Rapport, Gauthier Villars. Paris.

---

* Communicated by the Author.

XXXIV. *Notices of New Books and Periodicals received*

Theoretical Physics. By G. Joos. Translated by I. M. Freman. 2nd Edition. (Blackie and Sons, Ltd.) Price 50*s*. net.

A new and up-to-date edition of Professor Joos's well-known book on theoretical physics is very welcome. There have been extensive revisions in the sections on wave mechanics and atomic physics generally, and a new addition of interest is a chapter on various technical problems. It forms a valuable textbook for any student of experimental or theoretical physics, and it is convenient to find mechanics, vibrations, optics, electricity and quantum mechanics treated in the same volume and with consistent notation. N. F. M.

Ferromagnetisme et Antiferromagnetisme. Colloques Internationaux du Centre National de la Recherch Scientifique.

This is the report of the conference on magnetism held at Grenoble in July 1950, under the direction of Professor Neel. Among other interesting papers the reviewer was particularly impressed by the review of antiferromagnetism by Professor Van Vleck. N. F. M.

Modern Magnetism. By L. F. Bates, F.R.S. [Pp. 506.] Third Edition. (Cambridge University Press.) Price 30*s*. net.

It is a tribute to this excellent work which first appeared in 1939 that it should already have reached the stage of a third edition. The clarity of its style and its deliberate, though not undue, emphasis upon the experimental aspects of the subject have appealed to a wide circle of readers.

Though the second edition in 1948 attempted to bring the work up to date by the inclusion of new chapters, it has now been possible to accomplish this far more satisfactorily by recast and rearrangement in appropriate places within the twelve chapters of the book. Many will find special interest in the new material forming much of chapters 10 and 12, where the phenomenon of paramagnetic resonance and the recent development of the domain concept are adequately described ; and in the final section of the volume dealing with the author's own work upon the hysteresis cycle. A. M. T.

The Preparation of Programs for an Electronic Digital Computer. By M. V. Wilkes, D. J. Wheeler and S. Gill. [Pp. 167.] (Addison-Wesley Press, Inc.)

Whilst this book is designed primarily for those directly interested in the operation or construction of electronic computing machines, Parts I. and II. may be profitably read to acquire a general knowledge both of the operation of such machines and, as the authors suggest, the applicability of electronic computers to specific fields. The book, which is confined almost exclusively to the EDSAC, is divided into three parts : Part I. contains a detailed discussion of the framing of orders and their setting in the machine, the design of programmes, and the use of standard 'sub-routines' enabling particular projects to be built up of previously tabulated operations. Part II. gives the specifications of all the sub-routines used in the Cambridge University Mathematical Laboratory, and in Part III. the programme sheets for about one-half of the specified sub-routines are given in full. The second part of the book provides a concise and comprehensive list of the types of operation which may readily be undertaken by electronic machines. J. F. W. B.

[The Editors do not hold themselves responsible for the views expressed by their correspondents.]